ANKARA YILDIRIM BEYAZIT UNIVERSITY

GRADUATE SCHOOL OF NATURAL AND APPLIED SCIENCES

MULTI-ANTENNA COMMUNICATION SYSTEMS WITH SIGNAL SPACE DIVERSITY

Ph.D. Thesis by

Mustafa Anıl REŞAT

Department of Electronics and Communication Engineering

February, 2020

ANKARA

MULTI-ANTENNA COMMUNICATION SYSTEMS WITH SIGNAL SPACE DIVERSITY

A Thesis Submitted to

The Graduate School of Natural and Applied Sciences of

Ankara Yıldırım Beyazıt University

In Partial Fulfillment of the Requirements for the Degree of Philosophy of Doctorate in Electronics and Communication Engineering, Department of Electronics and Communication Engineering

by

Mustafa Anıl REŞAT

February, 2020

ANKARA

Ph.D. THESIS EXAMINATION RESULT FORM

We have read the thesis entitled **"MULTI-ANTENNA COMMUNICATION SYSTEMS WITH SIGNAL SPACE DIVERSITY"** completed by **MUSTAFA ANIL REŞAT** under the supervision of **ASSOC. PROF. DR. SERDAR ÖZYURT** and we certify that in our opinion it is fully adequate, in scope and in quality, as a thesis for the degree of Philosophy of Doctorate.

Assoc. Prof. Dr. Serdar ÖZYURT

Supervisor

Assoc. Prof. Dr. Enver ÇAVUŞ   Assoc. Prof. Dr. Özgür ERTUĞ

Jury Member   Jury Member

Prof. Dr. Fatih Vehbi ÇELEBİ   Asst. Prof. Dr. Selman KULAÇ

Jury Member   Jury Member

Prof. Dr. Ergün ERASLAN

Director

Graduate School of Natural and Applied Sciences

I hereby declare that, in this thesis which has been prepared in accordance with the Thesis Writing Manual of Graduate School of Natural and Applied Sciences,

- All data, information and documents are obtained in the framework of academic and ethical rules,
- All information, documents and assessments are presented in accordance with scientific ethics and morals,
- All the materials that have been utilized are fully cited and referenced,
- No change has been made on the utilized materials,
- All the works presented are original,

and in any contrary case of above statements, I accept to renounce all my legal rights.

Date: 17.02.2020   Signature:…………………………………..

                                       Name & Surname:.Mustafa Anıl REŞAT

ACKNOWLEDGMENTS

2020, 17 February   **Mustafa Anıl REŞAT**

MULTI-ANTENNA COMMUNICATION SYSTEMS WITH SIGNAL SPACE DIVERSITY

ABSTRACT

In this Ph.D. thesis, I studied multiple antenna systems that incorporate signal space diversity (SSD) from a broad perspective. The combination of SSD with multiple antenna systems is shown to be a highly rewarding concept that can provide a reliable and high data rate communication with minimal complexity and cost. The results presented here are very promising for potential future work and system design ideas. The contributions of the thesis cover the journal and conference paper studies that I have done throughout my Ph.D. education. The first chapter is the analysis and field programmable gate array (FPGA) implementation of SSD zero-forcing beamforming with different coordinate interleaving (CI) techniques. The results show that SSD can enhance the error performance of a system significantly and spatial and time CI techniques have various benefits and drawbacks. The performance of zero-forcing multiple-input multiple-output (MIMO) systems with SSD under transmit antenna correlation is also analyzed. It is shown that transmit antenna correlation affects the performance of MIMO SSD systems in a negative way, however different correlation types are less detrimental than others. The second chapter is improving physical layer security in Alamouti orthogonal frequency division multiplexing (OFDM) systems with subcarrier CI. The results show that SSD, when used with subcarrier CI, can be very beneficial to improve the physical layer security of a communication network. Enhancement of the physical layer security of Alamouti OFDM systems is studied under both Rayleigh and Nakagami-m fading channel models. Finally, the third chapter is about the performance of minimum mean-squared error (MMSE) beamforming with time and spatial CI. The results exhibit that SSD technique that is capable of working with different CI strategies can lead up to a huge error performance improvement in MMSE beamforming systems.

Keywords: Multi-antenna systems, signal space diversity, coordinate interleaving, zero-forcing beamforming, minimum mean-squared error beamforming, Alamouti space-time block coding, orthogonal frequency division multiplexing, physical layer security

İŞARET UZAYI ÇEŞİTLEMELİ ÇOKLU-ANTEN SİSTEMLERİ

ÖZ

Bu doktora tezinde işaret uzayı çeşitlemesi (İUÇ) kullanan çoklu-anten sistemlerini geniş bir alanda inceledim. İUÇ'nin çoklu-anten sistemleriyle birleştirilmesinin geniş faydalara sağlayan bir konsept olduğu ve bu sayede güvenilir ve yüksek veri hızlarına sahip bir haberleşmenin oldukça düşük karmaşıklık ve maliyetle gerçekleştirilebileceği gösterilmiştir. Burada sunulan sonuçlar gerçekleştirilebilecek potansiyel çalışmalar ve sistem tasarımı fikirleri açısından oldukça gelecek vaadedicidir. Bu tezin ortaya koyduğu katkılar doktora eğitimim sırasınca üzerinde çalıştığım dergi ve konferans yayınlarını içermektedir. Birinci bölüm, farklı koordinat serpiştirme (KS) teknikleri altında İUÇ sıfıra-zorlayıcı hüzme oluşturma sistemlerinin analizi ve alanda programlanabilir kapı dizilerinde (APKD) gerçeklenmesidir. Sonuçlar göstermektedir ki, İUÇ sistem hata performansını önemli ölçüde geliştirirken uzamsal ve zaman KS teknikleri çeşitli avantaj ve dezavantajlara sahiptir. Bu bölümde verici anten ilintisi altındaki İUÇ kullanan sıfıra-zorlayıcı çoklu-giriş çoklu-çıkış (ÇGÇÇ) sistemlerin performansı da incelenmiştir. Burada verici anten ilintisinin ÇGÇÇ İUÇ sistemlerini olumsuz yönde etkilediği gözlemlenirken farklı ilinti tiplerinin diğerlerine göre daha tercih edilebilir olduğu gösterilmiştir. İkinci bölüm, Alamouti dikgen frekans bölmeli çoğullama (DFBÇ) sistemlerinde alt-taşıyıcı KS kullanarak fiziksel katman güvenliğinin artırılmasıdır. Sonuçlar göstermektedir ki İUÇ alt-taşıyıcı KS ile beraber kullanıldığı zaman ağ fiziksel katman güvenliğine oldukça faydalı olabilmektedir. Alamouti DFBÇ sistemlerde fiziksel katman güvenliğinin geliştirilmesi Rayleigh ve Nakagami-m sönümlemeli kanallar altında çalışılmıştır. Son olarak üçüncü bölüm, zaman ve uzamsal KS minimum ortalama-kare hatası (MOKH) hüzme oluşturma sistemlerinin performansıdır. Ortaya çıkan sonuçların işaret ettiği üzere İUÇ tekniği farklı KS stratejileri kullanarak MOKH hüzme oluşturma sistemlerine yüksek derecede hata performansı iyileştirmesi sağlayabilmektedir.

Anahtar Kelimeler: Çoklu-anten sistemleri, işaret uzayı çeşitlemesi, koordinat serpiştirmesi, sıfıra-zorlayıcı hüzme oluşturma, minimum ortalama-kare hatası hüzme oluşturma, Alamouti uzay-zaman blok kodlama, dikgen frekans bölmeli çoğullama, fiziksel katman güvenliği

CONTENTS

NOMENCLATURE

Roman Letter Symbols

j Imaginary unit, $\sqrt{-1}$

f Frequency, Hz

B Bandwidth, Hz

C Channel capacity, bits/s/Hz

S Signal power, W

N_0 Power spectral density of noise, W/Hz

N_t Number of transmit antennas

N_r Number of receive antennas

N Number of subcarriers

L Number of resolvable paths

Greek Letter Symbols

γ Signal-to-noise ratio, dB

Δ_I Distance between the in-phase components of two symbols

Δ_Q Distance between the quadrature components of two symbols

Θ Constellation diagram rotation angle, $^\circ$

ρ Squared absolute correlation coefficient

φ Correlation coefficient between the true channel coefficient and its error

α Subcarrier index of in-phase component

β Subcarrier index of quadrature component

Subscripts

min Minimum

max Maximum

b Bit

s Symbol

I In-phase component

Q Quadrature component

i Symbol index

n Transmit antenna index

m Receive antenna index

c Carrier signal

Mathematical Operations

$(.)^*$ Complex conjugate

$(.)^T$ Transpose

$(.)^H$ Hermitian transpose (complex conjugate transpose)

$\Re\{.\}$ Real part of a complex number

$\Im\{.\}$ Imaginary part of a complex number

$E\{.\}$ Expected value

$|.|$ Absolute value

$\|.\|$ Eucledian norm

$P(.)$ Probability

$\sum_.$ Summation

LIST OF TABLES

LIST OF FIGURES

CHAPTER 1

INTRODUCTION

1.1 Literature Review

Modern history of multiple antenna telecommunication systems can be traced back to [1], where the theoretical channel capacity of a communication system with multiple transmit and multiple receive antennas was provided. In Telatar's groundbreaking paper [2], the expression of theoretical capacity of a multiple-input multiple-output (MIMO) system was derived based on information theory. Following these pioneer works, there have been numerous studies about multiple antenna system applications in wireless channels and some of them have also been implemented in important standards [3]. IEEE 802.11n standard exploits both MIMO and orthogonal frequency division multiplexing (OFDM) techniques in order to achieve a maximum throughput of 600 Mbps within a 40 MHz channel bandwidth and can attain four spatial streams per channel [4]. IEEE 802.16 can reap the benefits of MIMO systems both in terms of diversity and capacity, and also uses MIMO precoding for spatial multiplexing and space-time block codes to maximize the data rates up to 75 Mbps [5]. One of the most important standards that incorporate MIMO is the 3rd generation partnership project's (3GPP) long term evolution (LTE) where MIMO is joined with orthogonal frequency division multiple access in the downlink and single carrier-frequency division multiple access in the uplink [6]. For downlink 4x2, 2x2 and 1x2 schemes are utilized to achieve a maximum 100 Mbps and for uplink 1x2 scheme is considered to obtain a peak rate of 50 Mbps. Multiple antenna systems are also one of the most important cornerstones of the contemprorary 5th generation (5G) communication systems [7]. 5G systems fully exploit the diversity and spatial multiplexing gains that MIMO offers and also takes a step further by using massive MIMO beamforming communication that enormously improves the spectral efficiency and data rate up to Gbps levels. Other important developments in multiple antenna communication technoogy can be found in the literature surveys such as [8-12].

Another resource that can be used in order to improve the error performance of a system is the signal space. Signal space diversity (SSD) is a technique that utilize the signal space and its dimensions in order to combat the detoriating channel effects. Because that SSD uses just the dimensions of the signal space that is already found in the system itself, it does not require additional resources and brings in a non-significant increment of overall system complexity. SSD has been a very popular research subject since its inception with [13]. The technique then has been put on a more generalized form in [14]. In [15] it has been demonstrated that with a suitable constellation rotation angle it is possible to increase the diversity gain of 8 level phase shift keying (PSK) schemes as much as 8 level PSK trellis coded modulation technique. SSD has been used for frequency-selective channels also, such as in the paper [16]. In [17] SSD has been extended into new system models that incorporate iterative demodulation and decoding using convolutional codes. A technique called bit-interleaved coded-modulation with iterative decoding (BICM-ID) utilizes *N*-dimensional SSD in [18]. BICM-ID and SSD has been also joined with OFDM systems under frequency-selective Rayleigh-fading channels in [19]. In [20] SSD is further extended into low density parity check (LDPC) codes and shown to provide great performance improvement with the selection of a suitable constellation rotation angle.

There have also been some studies on combining multiple antenna systems with SSD from different perspectives. In [21] vertical Bell labs layered space-time scheme is joined with BICM and SSD over frequency selective channels to enhance the diversity gain. A system of high-rate full-diversity space–time–frequency codes is utilized with MIMO structure for frequency-selective block-fading channels in [22]. In [23] space-time, space-frequency and space-time-frequency coding schemes are summarized for MIMO-OFDM systems. SSD is implemented to enhance the performance of MIMO systems in fading channels in [24] and rotated modulation, space-time component interleaving is joined with optimized channel coding. SSD scheme is utilized with receive maximal ratio combining (MRC) to be able to obtain improved diversity gains in fading channels in [25]. A generalized space–frequency block coding structure is shown to be capable of providing full-rate and full-diversity transmission benefits for MIMO-OFDM systems in [26].

1.2 Purpose of the Thesis

The main purpose of this thesis is to investigate the already established schemes that utilize multiple antenna systems and SSD in detail and propose new system models that can reap the benefits of the combination of these two important techniques. Some of the most important goals that are tried to achieve in this thesis can be listed as:

- To demonstrate the benefits of using multiple antenna systems instead of single antenna schemes
- To present the error performance improvement benefits that come along with SSD that also requires little tradeoff in terms of other design criterias
- To exhibit various models of wireless channel medium, their effects on telecommunication signals and propose system models to cope with them
- To provide knowledge about popular techniques that can be found in the literature for wireless telecommunication enviroments and implement them to various system models to improve the overall performance of a system
- To propose different coordinate interleaving techniques that can be employed within SSD applications and show their advantages and disadvantages over each other
- To implement different types of equalizers used with multiple antenna systems in order to eliminate the effects of fading wireless channels
- To show various types of spatial correlation and their distorting effects on the overall system performance
- To provide knowledge about the concept of physical layer security, its importance and propose methods to increase the physical layer security of a communication network
- To present space-time coding methods, motivation behind incorporating them and Alamouti space-time block coding scheme
- To show the importance of OFDM in frequency selective fading channel enviroments
- To demonstrate application of SSD along with different modulation techniques, diversity gains achieved and side benefits that come along with these schemes.

1.3 Original Contributions of the Thesis

The original contributions of the thesis are as follows:

- A journal paper has been published of this thesis [27]. The details of this study are given in Chapter 3. In this work, MIMO zero-forcing receive beamforming (ZFRBF) is joined together with time and spatial component interleaved SSD in order to improve the error performance of the original system. Also the exact average bit error probability expression for BPSK under time interleaving and a close approximation of the average symbol error probability for QPSK are derived. Optimum or sub-optimal constellation diagram rotation angles are accordingly calculated. It is shown that the error performance can be improved significantly by utilizing SSD especially with the time interleaving method. Also, with the implementation of the proposed scheme on FPGA, it is demonstrated that SSD brings in just an insignificant increase to the system complexity.

- One of the conference papers that has been published of this thesis is [28]. The details of this study can be found in Chapter 3. In this work, SSD is incorporated into a zero-forcing MIMO system with various numbers of correlated transmit antennas and uncorrelated receive antennas. A number of different component interleaving strategies are compared for different realistic transmit antenna correlation models.

- In one of the journal papers submitted of this thesis, Alamouti space-time block coded OFDM with SSD is implemented in order to significantly strengthen the physical layer security of a communication network [29]. The details of this study can be found in Chapter 4. The coordinate interleaving step of SSD is performed amongst OFDM subcarriers. Theoretical bit error probability analysis for an authorized user that uses BPSK modulation is also derived. It is shown that with proper coordinate interleaving strategies, it is possible to enhance the physical layer security by guaranteeing a better performance for the legitimate user than an eavesdropper. What is more, it is demonstrated that SSD is also beneficial in terms of improving the immunity against channel estimation errors.

- In one of the conference papers submitted of this thesis, it is shown that coordinate interleaving amongst subcarriers of an Alamouti OFDM system can enhance the physical layer security under Nakagami-m fading channels [30]. The details of this study are given in Chapter 4. The results demonstrate that depending on the knowledge of the CI strategy by the eavesdropper, the performance of the eavesdropper either gets completely destroyed or is always lower than the legitimate user.

- One of the conference papers presented of this thesis is [31]. In this work, minimum mean square error beamforming (MMSE BF) is utilized along with various number of transmit antennas with SSD. Coordinate interleaving is performed in the spatial and time domains. It is demonstrated that by using time or spatial CI, it is possible to highly improve the error performance of a MMSE BF system without needing extra bandwidth, time slots or significant complexity increment. Different CI strategies used in this work present alternative solutions for different system design criteria in terms of error performance and latency. The details of this study can be found in Chapter 5.

CHAPTER 2

FUNDAMENTALS

2.1 Introduction

Modern telecommunication technologies try to exploit almost every kind of medium that it can in order to provide reliable and fast services for the ever increasing user number from all around the world. Despite some great developments in the traditional wireline mediums, such as the great brekathroughs within fibre optoelectronic tech, most influential innovations still appear for wireless communication systems. Mobile phone standards continue to achieve expectional standards and still has a huge potential waiting to be explored. Similarly, wireless local area networks continue to be implemented instead of the traditional wired networks in many places. Other wireless services, such as wireless sensor networks, wireless communication between vehicles and infrastructure, smart homes and workplaces, wireless biomedical implementions, are becoming a part of our daily lives. Thus, wireless telecommunication engineers should overcome lots of challenges that gets in the way of meeting the huge demands from the users. In order to obtain a reliable communication system, one of the most popular techniques is to use diversity techniques such as SSD. Another groundbreaking innovation is the utilization of multiple antennas instead of single antennas at the terminals. With the help of multiple antenna configurations, greater data rates and improved reliablity can be achieved. However, the most important obstacle that stands in the way of achieving higher performance systems is the wireless channel medium itself [32,33].

2.2 Wireless Channel Effects

Wireless communication medium is a lot more challenging than wired systems, as it is vulnerable to stochastically time-varying noise, interference and fading. The continuous movement of terminals bring new problems to combat against. The main distorting component in wireless channels is path loss that is is caused by the weakening of the transmitted power throughout the medium. Path loss stays the same

for very large distances between the transmitter and receiver. The second important deterioting component is shadowing which is caused by obstacles along the communication medium that absorb the transmitted signal power. Unlike path loss, the shadowing effect changes within smaller distances that are proportional to the length of the obstacles. These two effects are also called as large-scale propagation effects as they stay constant through large distances. On the contrary, the third effect which is called multipath occurs over very short distances that is proportional to the signal wavelength. Thus, multipath effects are also termed as small-scale propagation effects (or multipath fading).

Multipath fading is the channel effect that has the strength of varying the channel characteristics most in a short time period. The multipath fading effect can be modeled deterministically such as ray-tracing models, however in reality multipath fading channels are stochastic almost every time. Thus, it is reasonable to model multipath channels as randomly varying impulse responses in time, where a single pulse transmitted will be received as a pulse train at the receiver. Time delay spread is an important metric used to define multipath channels, where delay spread is defined as the time delay between the first and last received signal components of the original transmitted signal. If time delay is larger than the inverse of the signal bandwidth, the received signal will be spreaded in time significantly, resulting in distortions and errors. The other important aspect of the multipath channel is its time-varying nature, that occurs because of the constantly moving terminals and the location of reflectors in the transmission path.

The received signal after passing through a time-varying multipath channel can be defined as:

$$r(t)=R\left\{\sum_{n=0}^{N(t)}\alpha_n(t)u\left(t-\tau_n(t)\right)e^{j2\pi\left[f_c\left(t-\tau_n(t)\right)+\left(\phi_{D_n}+\phi_0\right)\right]}\right\} \tag{2.1}$$

where, $n = 0$ represents the line of sight path and $N(t)$ is the total number of resolvable multipaths. $\alpha_n(t)$ is the amplitude, $\tau_n(t)$ is the delay component and ϕ_{D_n} is the Doppler phase shift of each multipath. The received signal is the result of convolution of the

baseband input signal u(t) and the lowpass time-varying channel impulse response c(τ,t):

$$r(t)=R\left\{\left(\int_{-\infty}^{\infty} c(\tau,t)u(t-\tau)d\tau\right)e^{j2\pi f_c t}\right\} \tag{2.2}$$

It can be seen that c(τ,t) has two parameters to consider, where t is the observation time of the impulse response at the receiver and τ is the delay between the transmit and receive times of the impulse response. The channel impulse response is given by:

$$c(\tau,t)=\sum_{n=0}^{N(t)} \alpha_n(t)e^{-j\phi_n(t)}\delta(t-\tau_n(t)) \tag{2.3}$$

where $\delta(t)$ is the transmitted impulse and $\phi_n(t)=2\pi f_c\tau_n(t)-\phi_{D_n}-\phi_0$.

Two zero-mean Gaussian random variables X and Y with variance σ^2, it can be shown that $Z=\sqrt{X^2+Y^2}$ is Rayleigh-distributed and Z^2 is exponentially distributed. Because that r_I and r_Q are both zero-mean Gaussian random variables with a variance of σ^2, then the signal envelope $z(t)=|r(t)|=\sqrt{r_I^2(t)+r_Q^2(t)}$ has a Rayleigh distribution with:

$$p_Z(z)=\frac{z}{\sigma^2}\exp\left[\frac{-z^2}{2\sigma^2}\right] \tag{2.4}$$

Rayleigh and Rician distributions are two of the most commonly used channel models, especially within the theoretical literature. Despite the fact that they are successful at practically modeling most of the properties of real channels they do not thoroughly cover all the aspects of them. Nakagami-m fading distribution is one of the oftenly utilized channel models that is more capable of covering the properties of real channels that are acquired from real-time experimental measurements as a whole:

$$p_Z(z)=\frac{2m^m x^{2m-1}}{\Gamma(m)P_r^m}\exp\left[\frac{-mz^2}{P_r}\right] \tag{2.5}$$

for fading parameter m being greater than or equal to 0.5 and P_r is the average power of the received signal. It should be noted that for m = 1 Nakagami-m distribution turns into Rayleigh fading, whereas when m gets closer to infinity no fading will occur, thus a Nakagami-m channel will turn into an AWGN channel. On the contrary the more m

gets smaller than one the more distorting the effect of the channel will be, even worse than Rayleigh fading.

One of the most important parameters of a wideband multipath fading channel is the power delay profile which is defined as the average power associated with a given multipath delay. Coherence bandwidth is the frequency spectrum where two frequency components of a signal are likely to experience correlated fading. If a narrowband signal with a bandwidth that is much smaller than the coherence bandwidth is transmitted, the fading will be almost equal through all of the signal spectrum, which is the case of flat fading. The opposite case is called as frequency-selective, where the channel amplitude changes across the signal spectrum significantly. Similarly, channel coherence time is the duration where the channel impulse response stays almost the same. The cases where the signal duration is smaller and bigger than the coherence time are called as slow and fast fading, respectively [33].

2.3 Capacity of Wireless Channels

Channel capacity defines the limit of maximum data rate that can be achieved within a communication channel without the addition of encoding techniques. The concept of channel capacity was proposed by Claude Shannon who defined capacity in terms of the maximum mutual information between the input and output of a channel. It has been shown that with various encoding techniques it is possible to obtain a reliable communication with a data rate very close to the Shannon capacity.

Shannon channel capacity is the mutual information of the channel maximized over all possible input distributions:

$$C = \max_{p(x)} I(X;Y) = \max_{p(x)} \sum_{x,y} p(x,y) \log\left(\frac{p(x,y)}{p(x)p(y)}\right) \tag{2.6}$$

Assuming the received signal of through an AWGN channel with a bandwidth of B is shown as $y(t)=x(t)+n(t)$, where $x(t)$ is the input signal with a power of S and $n(t)$ is the AWGN. The signal-to-noise ratio can be defined as the power of the transmitted signal divided by the power of the noise $\gamma = \frac{S}{N_0 B}$, where N_0 is the power spectral density

of n(t). For the AWGN channel, the maximizing input distribution is Gaussian, which results with the channel capacity in terms of bits per second:

$$C = B \log_2 (1+\gamma) \tag{2.7}$$

Shannon capacity of a fading channel with CSI known at the receiver is given as:

$$C = \int_0^\infty B \log_2 (1+\gamma)\, p(\gamma)\, d\gamma \tag{2.8}$$

The Shannon capacity of a fading channel with receiver CSI only is always less than the capacity of an AWGN channel with the same average SNR. What is more, if the CSI of the receiver is imperfect, the capacity decreases even further [33].

2.4 Diversity

In order to combat the effects of fading diversity is one of the most important techniques to consider. With diversity statistically independent replicas of the same transmitted signal that travel among different paths are combined at the receiver. Diversity aims to exploit the low probability of deep fades existing and affecting the transmitted copies in all the diversity branches. As a result, the error rate can be decreased, because of the fact that the probability of each independent signal path to experience bad fading gets lower as the number of paths increase. The receiver combines the replicas in a way that the received signal experience a fading that is much lower than a single path. The simplest form of diversity is to choose the strongest of all the replicas received, which is termed as selection combining technique. Other popular methods incude threshold combining, equal gain combining and maximal ratio combining.

In order to achieve diversity gain we need independent fading paths. To obtain these paths various methods can be used such as:

- Space (antenna) diversity: Multiple receive antennas that are seperated with a distance big enough to make the signals transmitted from the antennas uncorrelated are utilized. With uniform antennas, the minimum distance between the antennas should be at least equal to half of the wavelength. On the

other hand, for directional antennas a larger seperation is needed. The diversity gain will be less if there is correlation amongst the antennas.

- Antenna polarization diversity: Another method is to use transmit and receive antennas with cross-polarizations. Although the waves are transmitted through same paths, the power is distributed equally to the polarization dimensions so that the error performance will roughly be equal to the first technique. The drawbacks of this method are there are only two dimensions that the polarization space can use (horizontal and vertical) and we need double of the actually needed transmit power because the power is divided into two of the dimensions.

- Antenna direction diversity: The angle of the antennas can be made so small that, the multipath effect for each single antenna can be eliminated. The disadvantages of this method is that it can need a high number of antenna to cover the communication range.

- Frequency diversity: By using multiple (carrier) frequency channels whose separation is larger than the coherence bandwidth of the channel. Frequency hopping and multicarrier systems are suitable to obtain this kind of diversity.

- Time diversity: The same signal is transmitted at different time periods that are seperated by the coherence time of the channel.

- Multipath diversity: With resolution of multiple paths that have different transmission times from the transmitter to the receiver.

- Transmit diversity: Achieved by using multiple antennas at the transmitter and sending the same signal from them with a predefined coefficient. The technique is the same as receiver diversity, where the diversity is implemented at the transmitter instead of the receiver and has the same gain as receiver diversity. The hard part of the transmit diversity design is to acquire the information of channel phase and channel gain at the transmitter. While, it is easier to do this with receive diversity where these values can be measured at the receiver with the help of pilot or trainer symbols and then fed back to the transmitter, there is no such chance with transmit diversity. Thus, transmit diversity requires high computational power transmitters such as base stations that can measure the channel values. Another technique of obtaining transmit diversity is utilizing a

space-time code. The simplest but still one of the most important schemes is the Alamouti STBC. Alamouti STBC uses two transmit antennas that transmits the same symbols in two seperate time periods. The diversity gain will be less if there is correlation amongst the transmit antennas.

- Signal space (modulation) diversity: SSD is achieved by sending the symbol components that are mapped from a multidimensional signal constellation diagram over independent fading channels.

2.4.1 Signal Space Diversity

Utilization of rotated signal constellation diagrams date back to [13]. SSD, which is based on this idea of constellation diagram rotation, has an old background being proposed first in [14] and generalized in [15]. There has been a huge interest towards SSD throughout the years and a fine amount of literature about the subject has been formed. The studies about SSD still continues, whether it is about offering new developments about the technique or implementing it to the already existing systems for improving the performance of these schemes, such as the optimum rotation angle calculations, applying SSD with different modulation schemes (possibly with as many dimensions as can be came up with), effect of channel impairments on SSD and integrating SSD with multiple antenna systems.

SSD is capable of providing great performance enhancements over fading channels and does it so without the requirement of additional bandwidth or power expediture [16]. There would be no performance improvement with rotated constellation diagrams under an AWGN channel transmission [34]. On contrast, with the signal constellations designed for Rayleigh fading AWGN channel performances suffer because of the low packing density of the lattices [35]. SSD comes up as a good alternative herein. The main idea behind SSD is transforming a modulation scheme into signal points with distinct multidimension components and sending these components from independent paths (which provides the diversity gain). The first case is achieved by constellation diagram rotation and the second is obtained by coordinate interleaving. Consequently, we can say that SSD exploits the potential diversity that is in the nature of signal constellations themselves. As the diversity gain increases one

more degree of freedom is added to the system. Figure 2.1 shows the application of constellation rotation on the conventional BPSK diagram.
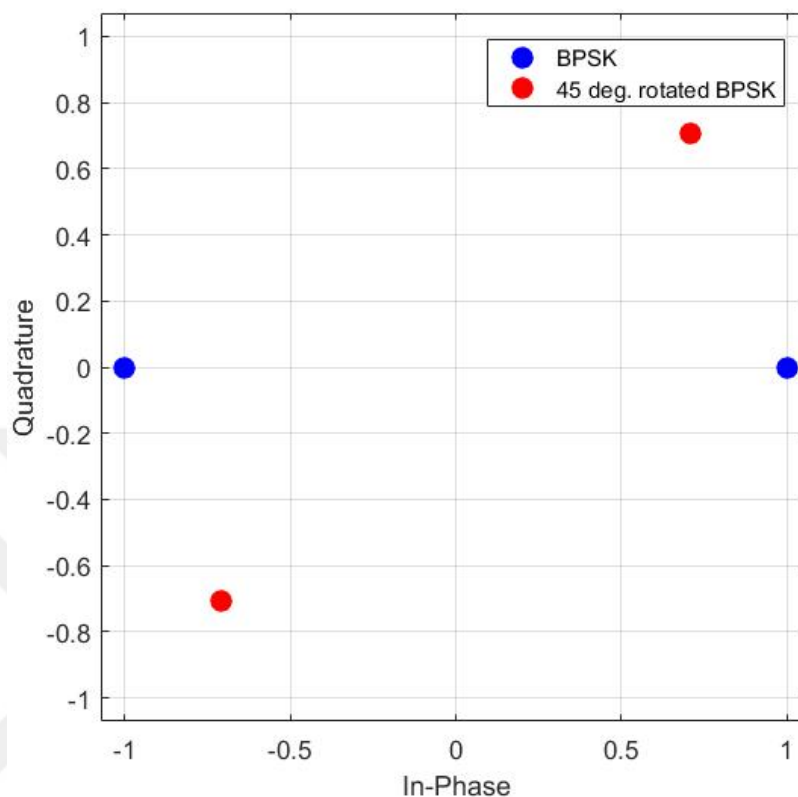
Figure 2.1 Rotation of BPSK constellation diagram

As we rotate the diagram we should arrange the rotation angle in such a way that any two points are distinguishable in the maximum number of distinct components. With the help of rotation, the probability of two points experiencing deep fading at the same time gets drastically reduced. In the original diagram if a deep fade hits even only one of the components of the transmitted sginal point, two points may collapse together due to the effect of noise. It can be seen from Figure 1 that even if fading hits the transmitted signal, unlike the non-rotated constellation, the rotated constellation points each have distinct I and Q components, which increases the immunity against channel distortions.The signal constellation rotation operation for 4-ASK (amplitude shift keying) modulation scheme, with an angle of 45 degree counter clock-wise just like BPSK, is shown in Figure 2.2.
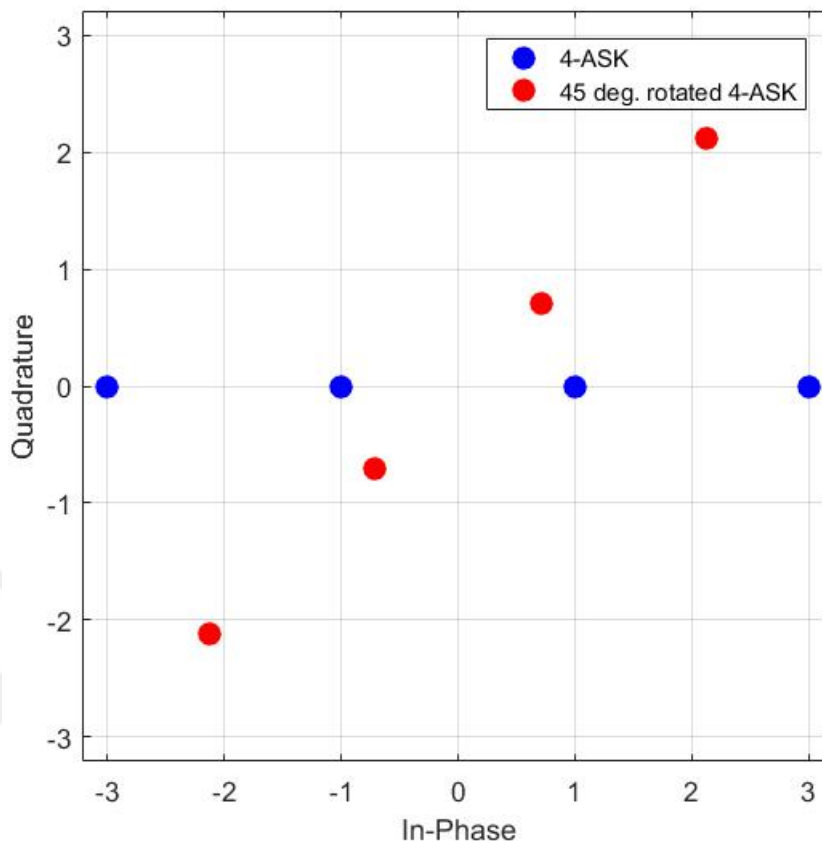
Figure 2.2 Rotation of 4-ASK constellation diagram

For one-dimensional modulation schemes such as BPSK or ASK the optimum rotation angle that provides the best diversity gain will be the same. For a two-dimensional constellation diagram such as QPSK we can rotate the original diagram to obtain distinct I and Q components for all the signal points as in Figure 2.3.

Two dimensional modulation schemes with SSD has a maximum achievable diversity order of two [36]. This diversity gain can be achieved with the second step of SSD, component interleaving which is reversed at the receiver with the component deinterleaving operation [37]. If the fading paths that I and Q components are transmitted from are uncorrelated the maximum attainable diversity gain is achieved [38]. The realization of independently fading paths for the interleaving step can be done in different domains such as spatial paths, time slots, frequency bands and subcarriers.
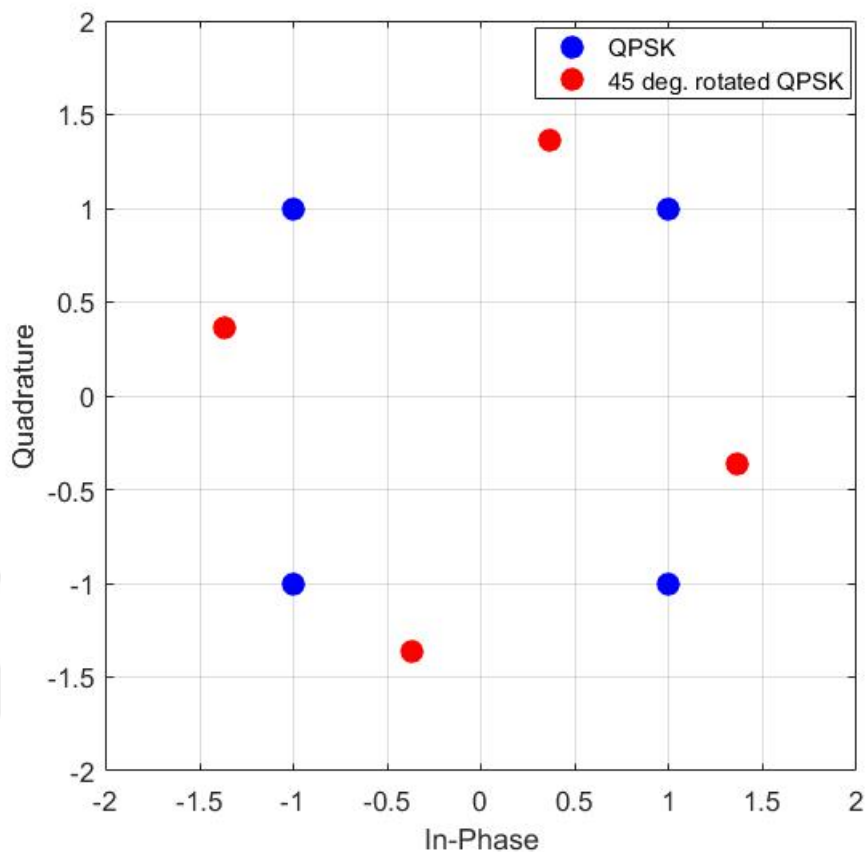
Figure 2.3 Rotation of QPSK constellation diagram

Besides the benefit of diversity gain, SSD is attractive also because of the fact that it does not need extra bandwidth or power resources. Also it does add a non-significant complexity to the system, mostly a slightly more complex ML detector than the original one. In [14], it is demonstrated that to reduce the error probability of multi-dimensional signal sets that use SSD, there are four factors to be considered:

1. Minimizing the average energy per constellation point.

2. Maximizing the diversity order.

3. Maximizing the minimum-product distance between the transmitted and received set of signal constellations.

4. Minimizing the total number of points at the minimum-product distance.

Some of the important telecommunication standards has also exploited the advantages of SSD by making it a part of them, such as the digital terrestrial video broadcasting system (DVB-T2) [39]. The rotation number can even be increased to get more gain

out of SSD, with a tradeoff requiring a more complicated interleaver and detector structure as the number increases [13]. The attainable diversity of digital terrestrial video next generation handheld (DVB-NGH) standard is increased up to four with the help of a second rotation and interleaving process. It has been shown in [40] that the traditional approach which try to maximize the minimum Eculidean distance does not always minimize the error probability with fading channels, unlike AWGN channels. As a result different modulation approaches may be needed for fading channels. The studies in [14] show that diversity of a system under a block fading channel can be enhanced by interleaving I and Q components of QPSK symbols, and the rotation angle of the constellation diagram will determine the error performance, which is not the case with AWGN channels. The signal constellation rotation operation can be represented with a rotational matrix. An exemplary rotational matrix, where θ represents the rotation angle can be shown as:

$$\mathbf{R} = \begin{bmatrix} \cos(\theta) & \sin(\theta) \\ -\sin(\theta) & \cos(\theta) \end{bmatrix} \tag{2.9}$$

The optimum rotation angles should be determined according to the modulation schemes used and the characteristics of the channel that the transmission takes place in [33,41]. In [42], it is tried to find the optimum angle that maximizes the minimum Euclidean distance. Another method is to find the angle that maximizes the minimum product distance [43].

2.5 Multiple Antenna Systems

Multiple antenna systems defines the signal processing methods that use multiple antennas at either the transmitter or receiver only or both the transmitter and receiver in order to improve the performance of telecommunication systems for specific goals. To do so, multiple antenna systems either try to eliminate the effects of multipath scattering or use them in favor of its own advantages. The first one is called the spatial diversity methods and the second is referred as the spatial multiplexing techniques. Diversity methods improve error performance, whereas spatial multiplexing techniques increase data rate. There is a tradeoff between these two gains. The more diversity gain acquired the less spatial multiplexing gain we can have, and vice versa.

Two common performance criterias to define diversity within a MIMO system are diversity order and diversity gain. Diversity order (N_d), is the number of independent copies of a transmitted signal. As an $N_t \times N_r$ MIMO system may have a maximum of $N_t N_r$ independent paths between the transmitter and the receiver, with MIMO diversity it is possible to achieve a maximum N_d of $N_t N_r$. The slope of a MIMO system's BER vs SNR graph is the diversity gain (G_d). In the linear region (high SNR region), we can write:

$$P_b = K(G_c \hat{\gamma})^{-G_d} \qquad\qquad (2.10)$$

where K is a constant dependent on the modulation scheme, G_c is the coding gain constant and $\hat{\gamma}$ is the average SNR. Diversity gain is much more than often equal to the diversity order with Rayleigh fading. In order to achieve the maximum possible diversity gain, MIMO systems utilize space-time coding coding techniques.

The maximum maximum number of data streams that a spatial multiplexing MIMO system can have is $N_s = \min(N_t, N_r)$. Thus, it can be deduced that for a NxN MIMO system the throughput increases linearly with the number of antennas $C_{NxN} = NC_N$. Similarly, spectral efficiency also increases as the bandwidth does not change.

For a flat-fading channel a MIMO system with n transmit and m receive antennas can be represented by:

$$\begin{bmatrix} y_1 \\ \vdots \\ y_m \end{bmatrix} = \begin{bmatrix} h_{11} & \cdots & h_{1n} \\ \vdots & \ddots & \vdots \\ h_{m1} & \cdots & h_{mn} \end{bmatrix} \begin{bmatrix} x_1 \\ \vdots \\ x_n \end{bmatrix} + \begin{bmatrix} n_1 \\ \vdots \\ n_m \end{bmatrix} \qquad\qquad (2.11)$$

or $\mathbf{y} = \mathbf{Hx} + \mathbf{n}$, where $\mathbf{x}$ is the n-dimensional transmitted symbol, $\mathbf{n}$ is the m-dimensional AWGN vector, and the channel matrix $\mathbf{H}$ consists of zero mean Rayleigh fading complex circular Gaussian random variables h_{ij} representing the channel gain from transmit antenna j to receive antenna i.

When both transmitter and receiver have perfect knowledge of the channel matrix $\mathbf{H}$, the channel capacity is given by:

$$C= \max_{\mathbf{Q}:\text{Tr}(\mathbf{Q})\leq P} \log\left|\mathbf{I}+\mathbf{HQH}^{+}\right| = \max_{\{P_i\}: \sum_i P_i \leq P} \sum_i B \log\left(1+\frac{\lambda_i^2 P_i}{N_0 B}\right) \qquad (2.12)$$

where the maximum is taken over all matrices $\mathbf{Q}$ (instantaneous input covariance matrix) that satisfy the average power constraint P. Here, $\mathbf{I}$ is the instantaneous identity matrix. The optimal power allocation for MIMO systems is the same with SISO, water-filling. The capacity is then given by for a cutoff value of γ_0 and $\gamma_i = \frac{\lambda_i^2 P_i}{N_0 B}$:

$$C= \sum_{i=1\left(\gamma_i \geq \gamma_0\right)} B \log\left(\gamma_i/\gamma_0\right). \qquad (2.13)$$

For a MISO system that has the CSI at the receiver, because that $\|\mathbf{H}\|^2 = N_t$, the capacity can be written as:

$$C= \log_2(1+\text{SNR}). \qquad (2.14)$$

Thus, the capacity of a MISO system with CSI at the receiver is the same with a SISO one. Multiple transmit antennas only provides a capacity improvement if the transmitter has the CSI knowledge that it can use this knowledge to adjust the transmitted signal. Thus, MISO systems with only CSI at the receiver often integrate space-time coding to achieve transmit spatial diversity. On the contrary, for MISO systems with CSI knowledge both at the transmitter and receiver the capacity enhances into [33]:

$$C= \log_2(1+N_t\text{SNR}). \qquad (2.15)$$

2.5.1 Alamouti Space-Time Block Coding

Alamouti space-time coding was one of the first space-time codes to be developed and it is widely used in MIMO techniques to achieve transmit diversity. Alamouti coding has some advantages over other transmit diversity schemes. Firstly, it requires CSI at the receiver only. It does not need any extra bandwidth and finally, it has a low complexity thanks to its simplicity.

The most basic form of the Alamouti scheme is the 2x1 type. This model has the following steps: space-time coding, diversity combining, CSI estimation at the

receiver and maximum likelihood detection. Alamouti space-time coding is shown in Table 2.1.

Table 2.1 Alamouti space-time block coding

Time period	Antenna 1	Antenna 2
T	s_1	s_2
$t+T_s$	$-s_2^*$	s_1^*

Table 2.1 table shows that Alamouti coding is applied both in the spatial and time domains. Hence, as the name suggests it is a space-time code.

The estimation of the transmitted symbols at the receiver is done with the decoding operations:

$$\tilde{s}_1 = \left(\sum_{i=1}^{2} \left| h_{1,i} \right|^2 \right) s_1 + h_{11}^* z_1(1) + h_{12} z_1^*(2) \tag{2.16}$$

$$\tilde{s}_2 = \left(\sum_{i=1}^{2} \left| h_{1,i} \right|^2 \right) s_2 + h_{12}^* z_1(1) - h_{11} z_1^*(2) \tag{2.17}$$

Thus, 2×1 Alamouti coding has the same performance with 1×2 MRRC, which shows that it can achieve transmit diversity with optimum performance without a reduction in the data rate or the requirement for CSI at the transmitter. Alamouti method can also be generalized to multiple number of receive antennas without changing the space-time coding performed by the transmitter.

2.5.2 Spatial Multiplexing

Spatial multiplexing is achieved by utilizing layered space-time (LST) coding, where a layer describes a data stream from a single transmit antenna. LST techniques can be classified as: vertical Bell Laboratory layered space-time (V-BLAST), horizontal BLAST (H-BLAST), diagonal BLAST (D-BLAST), multi-group space-time coding (MGSTC), threaded space-time coding (TSTC). In addition to LST techniques, spatial multiplexing can also be achieved with beamforming.

With V-BLAST, the bit stream is split into N_t streams and each stream is separately modulated before being transmitted from their antennas. It is called vertical because that the input stream is split into parallel streams that are often shown vertically to describe. Each layer can be adjusted to have different modulation schemes and data rates where the overall bandwidth used by the antennas does not change. The overall space-time code rate of the V-BLAST method is $r_s = N_t$ and the spectral efficiency is accordingly $N_t r_t \log_2(M)$ bps/Hz; where M is the modulation level, if the same order is used on all layers. The diversity gain of spatial multiplexing changes along with the layers. For V-BLAST, the diversity order changes amongst the layers in the range of $(N_r - N_t + 1)$ to N_r. The overall performance on the other hand is mostly affected by the layer with the least spatial diversity. Thus, it can be said that the overall spatial diversity of V-BLAST is approximately equal to $(N_r - N_t + 1)$ [3].

2.6 Orthogonal Frequency Division Multiplexing

With multicarrier modulation the spectrum is divided into several subchannels and transmission of symbols are done via these subcarriers instead of the whole frequency band. If the subchannels are orthogonal it is called as orthogonal frequency division multiplexing (OFDM). The important thing to consider is to attain each subchannel a bandwidth that is smaller than the coherence bandwidth in order to have flat fading with each of them. By adding a cyclic prefix (CP), OFDM systems are able to completely remove ISI.

Multicarrier modulation has been very popular with contemprorary standards although it has been around for a long time. In 1950s multicarrier systems were used within military high frequency radios. Now it is a big part of wireless LANs. There is still a race between single carrier transmission and multicarrier systems. It has been shown that for mobile radio, single carrier equalization has almost the same performance with some supportive techniques such as interleaving. On the other hand, with the help of other methods such as adaptive loading multicarrier system performance can be highly improved. Multicarrier systems are sensitive against frequency or timing offset, as they can distort the orthogonality. What is more, the peak-to-average power ratio of multicarrier systems is a big problem as nonlinear amplifiers are commonly used.

Orthogonal frequency division multiplexing (OFDM) transmission scheme is a type of multi-carrier modulation. It divides the total spectral bandwidth into smaller portions of subcarrier bandwidths and also overlaps them for greater bandwidth efficiency. The overlapping process is realized according to the Nyquist criterion. To produce these orthogonal signals discrete Fourier transform (DFT) and inverse DFT (IDFT) are used. DFT and IDFT are in practice implemented efficiently with fast Fourier transform (FFT) and inverse fast Fourier transform (IFFT), respectively. In OFDM the N-point IFFT of the modulated symbols is taken firstly, which are indeed the samples for the sum of N orthogonal subcarrier signals. After the addition of a CP transmission is realized. CP is important in order to eliminate or mitigate the effects of inter-symbol interference (ISI) between consecutive OFDM symbols. The receiver removes the CP and takes the N-point FFT of the received samples. The spectrum of an OFDM signal consists of the sum of the frequency shifted versions of sinc functions in the frequency domain seperated by a bandwidth of 1/T. The subcarrier bandwidth should be less than the channel coherence bandwidth in order to remove ISI and experience flat-fading for each subchannel. For nonoverlapping channels, $f_n = f_c+n(2B_N)$ for n=0,1,2,…,N-1, where f_n is the frequency of the nth subcarrier and f_c is the central frequency. The subcarrier bandwidth is $B_N = B/N$, for B being the baseband bandwidth and N being the total subcarrier number. For each subcarrier transmission the data rate is $R_N=R/N$ for a total data rate of R. The transmitted signal during one symbol period T_N is:

$$s(t)=R\left\{\sum_{n=0}^{N-1} s_n g(t) e^{j2\pi f_n t}\right\} \qquad (2.18)$$

where, s_n is the symbol transmitted via the nth subcarrier and g(t) is the transmitted pulse.

OFDM with nonoverlapping subchannels is a technique that is not very sensitive against small frequency offsets and timing jitters but its spectral efficiency is also low. By overlapping the subcarriers, spectral efficiency can be enhanced. The subcarrier set of $\{\cos(j2\pi f_n)\,,j=1,2,…,N\}$ form a set of orthonormal basis functions. The minimum frequency seperation that must be preserved for the subcarriers to be orthogonal is f_n. For overlapping channels, $f_n=f_c+nB_N$ for n=0,1,2,…,N-1. The spectral efficiency is

improved to twice but the system is more vulnerable against distorting effects that can destroy the orthogonality and cause high error numbers.

Despite being invented in the 1950s, implementation of modulators and demodulators for each subchannel was too complex for the era. What made OFDM popular was the development of FFT and IFFT algorithms in the 1970s, that enabled the OFDM scheme to be implemented with much less complexity and cost. This discrete implementation of OFDM with FFT algorithms is also called discrete multitone modulation (DMT).

After modulation, the symbol stream is divided into N parallel streams via a serial-to-parallel converter. An inverse DFT is applied on these N symbols, which can be efficiently implemented using the IFFT algorithm. After IFFT the set of $\{x_0, x_1, x_2, \ldots, x_{N-1}\}$ is obtained:

$$x_n = \frac{1}{\sqrt{N}} \sum_{k=0}^{N-1} X_k e^{j2\pi nk/N} \;,\; n=0,1,2,\ldots,N-1 \tag{2.19}$$

After the cyclic prefix addition and parallel-to-serial converter and digital to analog converter blocks the baseband OFDM signal is obtained. In the receiver the reverse of the transmitter operations are employed.

With DMT it is possible to remove all ISI if the maximum delay spread of the channel is known. In order to do this, we can add a guard time between two symbol transmissions that is equal to the channel delay spread. Another popular method is adding a cyclic prefix after the IFFT, that will be removed in the receiver. For a channel delay spread with a maximum value of $\mu T_N/N$, the channel delay spread has a maximum duration of μ additional samples. The CP $\{x_{N-\mu}, \ldots, x_{N-1}\}$ consists of the last μ values of the IFFT symbols set and attached to the beginning of the set [33].

For a channel impulse response of c(t), the received signal without AWGN will be y(t)=x(t)*c(t). In the receiver cyclic prefix is removed with the last μ samples of $\{y_n\}$. The input to the FFT block is equal to the circular convolution of $\{x_n\}$ and $\{c_n\}$. By doing so, adding the cyclic prefix at the transmitter effectively converts the circular convolution of the FFT to a linear convolution. The FFT output without AWGN is

$\widehat{X}_k = C_k X_k$. As a result, the effects of the channel can be completely removed by frequency equalization [33,44].

2.7 Physical Layer Security

Because of its broadcasting nature that makes every receiver able to capture the signals within the communication range, wireless systems have always been prone against dangerous security risks. It is not safe anymore to just rely on cryptography based security systems that have been the security standard for years because of the everlong increasing wireless connectivity. Crypto based systems that forms a secret key between the terminals follow the basic Shannon security model. For large wireless networks that does not have a centralized structure, formation, management and trafficking the keys are very demanding processes. Also, long key lengths that are neccesarry for increased security require more resources. Most importantly, computing process of modern machines, with especially the newly emerging quantum computing technology is able to decypher keys that assume the eavesdropper will have limited computational capabilities which is no more true. What is more, new technologies such as internet of things, vehicular communication and remote surgery are prone to latencies and power limitations which make encryption based techniques not compatible. Finally, privacy sensitive services such as financial or personal secret information can not rely on any discovery of their datas which can happen frequently with traditional techniques. In order to prevent these unwanted eavesdropping, physical layer security (PLS) is a new concept proposed that is not prone to much of these traditional security system problems.

Shannon was the first one that defined the fundamentals of secrecy concept. Applications that are based on Shannon techniques however use crypto based keys that assume the existence of a noiseless channel which is not the case with wireless systems. Wyner was the initiator of PLS who showed that secure communication is possible without the utilization of keys, when the unauthorized receivers' channel has a much worse performance than the legitimate ones'. As a result codes that try to achieve this feature have been started to use instead of secret keys. However Wyner approaches may have some problems too, such as the legitimate user's signal-to noise

ratio must always be lower than that of an eavesropper. But we know that this is not always maintable with wireless communication medium as there are many random elements. What is more, in order to increase secrecy it is usually necessary to sacrifice capacity. There have been lots of PLS studies that is based on Wyner's original work throughout the years that are considered for different enviroments and scenarios.

Generally, with PLS approaches it is assumed that three terminals exist: the legitimate transmitter node (Alice), the legitimate receiver node (Bob) and the eavesdropper (Eve). Alice sends her private data to Bob, while Eve tries to capture the information. In order to achieve PLS, system models are used between Alice and Bob that can obtain benefits from the physical enviroment such as noise, fading diversity. The models also use already existing signal processing methods that will ensure security between the legitimate terminals.

In order to show the level of security of a system certain secrecy performance metrics are used. There are two subgroups of these metrics: SNR based and complexity based. Some SNR based metrics are the secrecy rate, capacity, outage probability, throughput. Secrecy capacity is the difference between the authorized user's and illegitimate user's channel capacities. It represents the maximum rate of secure communication avaliable between Alice and Bob. Complexity based metrics are utilized with key based methods that are defined as the measurement of the length of the key extracted from the channel.

Some of the most important PLS techniques utilize signal processing techniques that are already found in the literature such as: polar coding, adaptive modulation, OFDM subcarrier-based power allocation, beamforming, artificial noise addition, space-time coding and signal space diversity [45].

CHAPTER 3

ANALYSIS AND FPGA IMPLEMENTATION OF ZERO-FORCING RECEIVE BEAMFORMING WITH SIGNAL SPACE DIVERSITY UNDER DIFFERENT INTERLEAVING TECHNIQUES

This chapter is based on [27] and [28], where multiple-input multiple-output zero-forcing receive beamforming (ZFRBF) is combined with time and spatial component interleaved signal space diversity (SSD) and the system's error performance and implementation complexity are analyzed. A transceiver system with two transmit and M ($M \geq 2$) receive antennas is considered where the number of simultaneous substreams equals two. The error performance of the proposed scheme with binary phase-shift keying (BPSK) and quadrature phase-shift keying (QPSK) modulations is studied. Under the time component interleaved SSD case, an exact average bit error probability expression for BPSK and a tight approximation on the average symbol error probability for QPSK are derived. The signal constellation rotation angles are accordingly computed. Using a similar approach, the signal constellation rotation angles are also determined for the scenario of spatial component interleaved SSD. It is demonstrated that the performance of the original ZFRBF model can be improved significantly by utilizing SSD especially with the time interleaving method. Another contribution to the literature is to study hardware complexity of the proposed scheme on FPGA. It is shown that while achieving considerable performance gain, SSD introduces only an insignificant increase to the system complexity without any extra bandwidth or time slot usage. Finally, spatial interleaving is incorporated into a zero-forcing multiple-input multiple-output system with various numbers of correlated transmit antennas and uncorrelated receive antennas. Different realistic transmit antenna correlation models are adopted. A number of different component interleaving strategies are compared for these correlation models.

3.1 Introduction

Multiple-input multiple-output (MIMO) systems have been attracting huge attention thanks to their potential for high data rate transmission without any need for extra bandwidth or time slots. Provided rich enough scattering, a MIMO system with respectively t and r antennas at the transmitter and receiver enables a linear increase in the channel capacity with the minimum of t and r ($\min(t,r)$). The amount of the channel state information (CSI) knowledge at the transmitter also plays an essential role in determining the channel capacity. If there is no CSI knowledge at the transmitter side, the optimal strategy is to send the data through independent streams over all the transmit antennas [2].

Zero-forcing beamforming (ZFBF) is a spatial multiplexing technique with low-complexity that removes interference among different substreams of a MIMO system by coding each of $\min(t,r)$ substreams independently and employing a linear processing (spatial filtering) operation on the substreams either at the transmitter (zero-forcing precoding) or at the receiver (zero-forcing receive beamforming, ZFRBF). For the linear processing step, beamforming weight vectors acquired from the pseudo-inverse of the channel matrix can be used [46]. Another approach is to use the null space bases of a linear space spanned by the transmission streams [47]. With the help of ZFBF method, we can split a $t \times r$ MIMO channel (assuming a full-rank channel matrix) into $\min(t,r)$ independent parallel subchannels. Thus, ZFBF can be utilized to achieve the full spatial multiplexing gain [48-52]. ZFBF can be used with both single and multi-user MIMO schemes. Low-complexity of implementation and no possibility error propagation among substreams are the two most significant benefits of ZFBF. Contrarily, the selection of the beamforming weight vectors may boost the noise power at the receiver significantly in a ZFBF system, which in return reduces the error performance specifically in low signal-to-noise ratio (SNR) region.

In this chapter, signal space diversity (SSD) (also known as modulation diversity) is resorted to enhance the error performance of ZFRBF system with negligible complexity while requiring no additional bandwidth or time slots. The SSD concept was first presented in [53] and achieves diversity by ensuring two conditions for two

dimensional signal constellations. The first requirement is that no two symbols in the signal constellation share identical in-phase (I) or quadrature (Q) components. This criterion can be met by properly rotating the signal constellation [13]. The second condition is making sure that both I and Q components of a transmitted symbol are affected by different fading characteristics which is accomplished by utilizing component interleaving at the transmitter and deinterleaving at the receiver [13-15]. It has been shown that the diversity level can be doubled with SSD for two dimensional signal constellations. SSD has been a widely researched subject for single-input single-output systems so far. It has been demonstrated that for a two-dimensional modulation scheme, SSD introduces no increment in the decoding complexity.

Recent studies about SSD also include MIMO systems [54-68]. In some of these works, the component interleaving/deinterleaving is performed in the time domain, which is referred to as the time interleaving method hereafter. With time interleaving, I and Q components of a symbol are transmitted at different time slots so that they can pass through different paths with possibly different fading states. This method uses independent component interleaving/deinterleaving blocks at the transmitter and receiver, respectively. Since the subchannel gains become uncorrelated in time interleaving (assuming an interleaving depth greater than channel coherence time) under ZFBF, it has a considerably low bit error rate. This technique on the other hand may necessitate a long interleaving depth which can cause problems for latency-sensitive applications. In [54], a concept called coordinate interleaved spatial multiplexing (CISM) is presented. Assuming availability of CSI at both the transmitter and receiver, component interleaved data streams are transmitted over the different eigenmodes of the channel to increase the diversity order. The performance of precoded bit-interleaved coded modulation (BICM) spatial multiplexing MIMO system with spatial component interleaver is inspected in [55]. For Nakagami-m fading channels, the performance of orthogonal space-time block codes with SSD is investigated in [56]. SSD is combined with Vertical Bell Labs Layered Space-Time (V-BLAST) and orthogonal frequency-division multiplexing (OFDM) techniques in [57] and the system performance is analyzed for Rayleigh fading channels. SSD is utilized with BICM and spatial division multiplexing over frequency selective Rayleigh fading channels in [21].

The component interleaving can also be realized by means of transmitting distinct components of a symbol from different transmit antennas, [58-63] which is called as spatial interleaving in this chapter. For spatial interleaving, I and Q components of a transmitted symbol are sent over different transmit antennas. This strategy prevents the extra time latency caused by the interleaver and deinterleaver blocks. In [59], coordinate interleaved orthogonal design is introduced and shown to achieve full-diversity, full-rate, and single-symbol maximum likelihood (ML) decodability for complex signal constellations. Its performance is assessed over quasi-static flat Nakagami-m fading channels in [59]. In [60], SSD is combined with V-BLAST method in order to improve the diversity gain of the original V-BLAST technique. A coded MIMO system with SSD is introduced for block-fading channels and found to achieve full spatial multiplexing and diversity gains [61]. A closed-loop scheme with full CSI at the transmitter is considered in [62] where SSD is coupled with zero-forcing precoding. In [63], SSD is integrated with maximal ratio combining and transmit antenna selection under correlated receive antennas. M-ary quadrature amplitude modulation (QAM) with SSD and generalized selection combining is studied in [64], where the system error performance under Rayleigh fading channels is presented. Coordinate interleaving is utilized in a diagonal fashion across the space-time axes for a 2×2 MIMO-OFDM scheme in [65]. The study in [66] proposes a space-time signaling scheme that encodes data along multiple dimensions and applies interleaving to the components of the symbols over all the layers such that the diversity gains of the weak layers are improved. In [67], a coded SSD scheme that uses space-time-frequency component interleavers is proposed to improve the performance of MIMO–OFDM systems in frequency-selective and time-varying fading channels. The study in [68] adds SSD into multi-antenna models and extends the coordinate interleaved non-orthogonal amplify and forward method for multi-antenna relay scenarios.

In this chapter, SSD is integrated with ZFRBF in an open-loop (full CSI knowledge available only at the receiver side) MIMO scenario. It is demonstrated that the performance of ZFRBF systems can be improved by utilizing SSD with time or spatial component interleaving. It turns out that the time interleaving approach yields much higher error performance as compared to the spatial interleaving method. Hence, there exists a trade-off between the time and spatial interleaving approaches in terms of error

performance and latency. The error performances of the presented schemes are analyzed over slow flat Rayleigh fading channels. An exact expression on the average bit error probability (ABEP) for time-interleaved binary phase shift keying (BPSK) with SSD is presented. The union bound is exploited to approximate the average symbol error probabilities (ASEP) for both the time and spatial-interleaved quadrature phase shift keying (QPSK) with SSD. The optimum signal constellation rotation angle value for the time-interleaved BPSK and the near-optimum signal constellation rotation angle values under the QPSK scenarios with two and three receive antennas are derived. The proposed schemes are implemented on field-programmable gate array (FPGA) and the implementation complexities of the studied schemes are illustrated. The results indicate that SSD introduces an insignificant amount of complexity increase while obtaining considerable performance gains. Finally, the performance of transmit antenna correlated ZF MIMO systems with SSD is investigated for slow flat Rayleigh fading channels under the assumption of different models of transmit antenna correlation. For each type of correlation model, bit error rate (BER) performance is illustrated for three, four and five transmit/receive antennas.

3.2 System Model

In this chapter, a single-user $2 \times M$ MIMO system with two simultaneous substreams is considered. Figure 1 shows the block diagram of the proposed ZFRBF with SSD model.
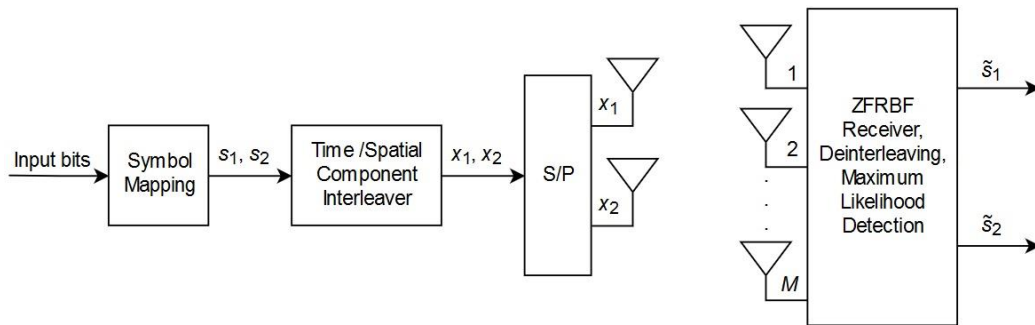
Figure 3.1 Block diagram of the system model

The received complex baseband signal can be formulated as

$$\mathbf{y} = \mathbf{Hx} + \mathbf{n} = \mathbf{h}_1 x_1 + \mathbf{h}_2 x_2 + \mathbf{n} \tag{3.1}$$

where $\mathbf{h}_1$ and $\mathbf{h}_2$ represent the first and second columns of the Mx2 channel matrix $\mathbf{H}$, respectively. Here, the vector $\mathbf{x} \in C^{2 \times 1}$ shows the transmitted baseband signal. The end goal is to transmit two independently modulated symbols $s_i = s_{iI} + j s_{iQ}$, $i \in \{1,2\}$, where the subscripts I and Q refer to the I and Q components of the corresponding symbol, respectively.

3.2.1 Transmitter

The modulated symbols are formed with using rotated BPSK or QPSK modulators. The modulated symbols are arranged according to the per-symbol (per-bit) power constraint of $|s_i|^2 = E_s$ ($|s_i|^2 = E_b$) where E_s (E_b) shows the energy per-symbol (per-bit). The vector $\mathbf{n} \in C^{M \times 1}$ represents the additive white Gaussian noise (AWGN) where $E[\mathbf{nn}^H] = N_0 \mathbf{I}$ with $\mathbf{I}$ denoting the identity matrix. Also, N_0 stands for the one-sided power spectral density of AWGN at the receiver. The $(m,i)^{th}$ element of $\mathbf{H}$, i.e., $[\mathbf{H}]_{mi} \in C$, symbolizes the fading coefficient of the path between the ith transmit antenna and m^{th} receive antenna. The existence of a rich enough scattering environment and a homogeneous network with enough spacing among the antennas are assumed. Therefore, the elements of $\mathbf{H}$ are independent and identically distributed (IID) zero-mean complex Gaussian random variables with unit variance, i.e., a Rayleigh fading scenario. The fading coefficients remain constant during the time slot of one codeword transmission and independently change between transmissions. The complete CSI is only available at the receiver side.

The formation of the interleaved vector $\mathbf{x}$ changes according to the adopted interleaving strategy. For the scheme with time interleaving, the vector $\mathbf{x}$ is obtained by applying time interleaving to I and Q components of each of s_1 and s_2 in an independent and parallel manner. Hence, two independent time domain component interleavers are required in this case. Additionally, the depth of the time domain component interleavers must be at least as large as the channel coherence time to

benefit from independent fading. On the other hand, for the spatial interleaving method, the vector **x** is formed as

$$\mathbf{x} = \begin{bmatrix} x_1 \\ x_2 \end{bmatrix} = \begin{bmatrix} s_{1I}+js_{2I} \\ s_{1Q}+js_{2Q} \end{bmatrix}. \tag{3.2}$$

As the preceding expression indicates, interleaving is performed in the spatial domain independently of the channel coherence time under spatial interleaving.

3.2.2 Zero-Forcing Receive Beamforming with Signal Space Diversity

ZFRBF with Spatial Interleaving

In this case, I components of s_1 and s_2 are orthogonally combined and transmitted from the first transmit antenna as $x_1 = s_{1I}+js_{2I}$. Within the same time period, Q components of s_1 and s_2 are sent from the second transmit antenna as follows $x_2 = s_{1Q}+js_{2Q}$. Representing the received baseband symbol vector as **y** and the (M-1) dimensional orthogonal projection matrices on the null spaces of $\mathbf{h}_1$ and $\mathbf{h}_2$ respectively by $\mathbf{P}_{\mathbf{h}_1}^{\perp}$ and $\mathbf{P}_{\mathbf{h}_2}^{\perp}$, the ZFRBF receiver first projects **y** onto the vector $\mathbf{h}_1^H \mathbf{P}_{\mathbf{h}_2}^{\perp}$. This yields

$$\frac{\mathbf{h}_1^H \mathbf{P}_{\mathbf{h}_2}^{\perp}}{\left\| \mathbf{h}_1^H \mathbf{P}_{\mathbf{h}_2}^{\perp} \right\|} \mathbf{y} = \left\| \mathbf{h}_1^H \mathbf{P}_{\mathbf{h}_2}^{\perp} \right\| x_1 + \frac{\mathbf{h}_1^H \mathbf{P}_{\mathbf{h}_2}^{\perp}}{\left\| \mathbf{h}_1^H \mathbf{P}_{\mathbf{h}_2}^{\perp} \right\|} \mathbf{n} =$$
$$\left\| \mathbf{h}_1^H \mathbf{P}_{\mathbf{h}_2}^{\perp} \right\| s_{1I} + R\left\{ \frac{\mathbf{h}_1^H \mathbf{P}_{\mathbf{h}_2}^{\perp}}{\left\| \mathbf{h}_1^H \mathbf{P}_{\mathbf{h}_2}^{\perp} \right\|} \mathbf{n} \right\} + j\left(\left\| \mathbf{h}_1^H \mathbf{P}_{\mathbf{h}_2}^{\perp} \right\| s_{2I} + I\left\{ \frac{\mathbf{h}_1^H \mathbf{P}_{\mathbf{h}_2}^{\perp}}{\left\| \mathbf{h}_1^H \mathbf{P}_{\mathbf{h}_2}^{\perp} \right\|} \mathbf{n} \right\} \right). \tag{3.3}$$

Then, by projecting **y** onto $\mathbf{h}_2^H \mathbf{P}_{\mathbf{h}_1}^{\perp}$

$$\frac{\mathbf{h}_2^H \mathbf{P}_{\mathbf{h}_1}^{\perp}}{\left\| \mathbf{h}_2^H \mathbf{P}_{\mathbf{h}_1}^{\perp} \right\|} \mathbf{y} = \left\| \mathbf{h}_2^H \mathbf{P}_{\mathbf{h}_1}^{\perp} \right\| x_2 + \frac{\mathbf{h}_2^H \mathbf{P}_{\mathbf{h}_1}^{\perp}}{\left\| \mathbf{h}_2^H \mathbf{P}_{\mathbf{h}_1}^{\perp} \right\|} \mathbf{n} =$$
$$\left\| \mathbf{h}_2^H \mathbf{P}_{\mathbf{h}_1}^{\perp} \right\| s_{1Q} + R\left\{ \frac{\mathbf{h}_2^H \mathbf{P}_{\mathbf{h}_1}^{\perp}}{\left\| \mathbf{h}_2^H \mathbf{P}_{\mathbf{h}_1}^{\perp} \right\|} \mathbf{n} \right\} + j\left(\left\| \mathbf{h}_2^H \mathbf{P}_{\mathbf{h}_1}^{\perp} \right\| s_{2Q} + I\left\{ \frac{\mathbf{h}_2^H \mathbf{P}_{\mathbf{h}_1}^{\perp}}{\left\| \mathbf{h}_2^H \mathbf{P}_{\mathbf{h}_1}^{\perp} \right\|} \mathbf{n} \right\} \right) \tag{3.4}$$

is obtained. If we define $\gamma_1 = \mathbf{h}_1^H \mathbf{P}_{\mathbf{h}_2}^{\perp} \mathbf{h}_1$, $\gamma_2 = \mathbf{h}_2^H \mathbf{P}_{\mathbf{h}_1}^{\perp} \mathbf{h}_2$ and the noise components as

$$n_{1I} = R\left\{ \frac{\mathbf{h}_1^H \mathbf{P}_{\mathbf{h}_2}^{\perp}}{\left\| \mathbf{h}_1^H \mathbf{P}_{\mathbf{h}_2}^{\perp} \right\|} \mathbf{n} \right\}, \ n_{1Q} = I\left\{ \frac{\mathbf{h}_1^H \mathbf{P}_{\mathbf{h}_2}^{\perp}}{\left\| \mathbf{h}_1^H \mathbf{P}_{\mathbf{h}_2}^{\perp} \right\|} \mathbf{n} \right\}, \ n_{2I} = R\left\{ \frac{\mathbf{h}_2^H \mathbf{P}_{\mathbf{h}_1}^{\perp}}{\left\| \mathbf{h}_2^H \mathbf{P}_{\mathbf{h}_1}^{\perp} \right\|} \mathbf{n} \right\}, \ n_{2Q} = I\left\{ \frac{\mathbf{h}_2^H \mathbf{P}_{\mathbf{h}_1}^{\perp}}{\left\| \mathbf{h}_2^H \mathbf{P}_{\mathbf{h}_1}^{\perp} \right\|} \mathbf{n} \right\},$$ the

decision variables for the two transmitted symbols (s_1 and s_2) at the receiver are

subsequently given by $d_1 = \sqrt{\gamma_1}s_{1I}+j\sqrt{\gamma_2}s_{1Q} + n_{1I} + jn_{2I}$ and $d_2 = \sqrt{\gamma_1}s_{2I}+j\sqrt{\gamma_2}s_{2Q} + n_{1Q} + jn_{2Q}$, respectively [69]. Note that γ_1 and γ_2 are identically distributed correlated random variables.

ZFRBF with Time Interleaving

Suppose that two time-domain component interleavers function in an independent manner at the transmitter, i.e., the components of s_1 and s_2 are independently interleaved. Also, assume that interleaving depths in the two interleavers are greater than the channel coherence time. Consequently, after the application of deinterleaving at the receiver, it can be concluded that I and Q components of both s_1 and s_2 are affected by independent fades through the channel. ZFRBF operation is carried out in the same manner as in the spatial interleaving scenario. It can be shown that the decision variables in this case have the following form

$$d_1=\sqrt{\gamma_{11}}s_{1I}+j\sqrt{\gamma_{21}}s_{1Q}+n_{1I}+jn_{1Q} \tag{3.5}$$

$$d_2=\sqrt{\gamma_{12}}s_{2I}+j\sqrt{\gamma_{22}}s_{2Q}+n_{2I}+jn_{2Q} \tag{3.6}$$

where γ_{11}, γ_{21}, γ_{12}, γ_{22} are IID random variables denoting the squared signal gains. It can be shown that the distribution of γ_{ij} for $\{i,j\}\in\{1,2\}$ is identical to that of γ_1 and γ_2 [56]. Additionally, the noise components n_{1I}, n_{1Q}, n_{2I}, n_{2Q} are IID zero-mean Gaussian random variables each with a variance of $N_0/2$. This is a direct consequence of the employed interleaving structure.

3.2.3 Transmit Antenna Correlation

In this scenario, a spatially interleaved single-user MIMO transmission system with t transmit antennas and r receive antennas with t = r is assumed. The goal is to simultaneously transmit t independently modulated symbols in a parallel fashion from the transmitter to the receiver. In the transmitter, a rotated binary phase shift keying (BPSK) signal constellation is first employed to map the (possibly coded) data bits into the modulated symbols (s_i, (i $\in$ {1, 2, . . . , t})). As the rotation angle for the BPSK signal constellation, 45 degree counter-clockwise is used [62]. Then, the component

interleaving is applied to the t modulated symbols. The component interleaving is implemented over transmit antennas. Hence, the used component interleaving technique is not as troublesome as the component interleaving in time domain, which requires time domain interleaving depths greater than the channel coherence time. The entries of the transmitted baseband signal **x** for a certain interleaving strategy are given by $s_{aI}+js_{bQ}$, $(a, b \in \{1, 2, \ldots , t\})$. Here, the choice of a and b depends on the interleaving strategy used. A set of digital-to-analog conversion (DAC) operations are used to transmit the baseband signal **x** from the transmit antennas. The received complex baseband signal **y** is:

$$\mathbf{y}=\mathbf{Hx}+\mathbf{n}=\mathbf{h}_1 x_1+\mathbf{h}_2 x_2+\ldots+\mathbf{h}_t x_t+\mathbf{n} \qquad (3.7)$$

where **H** is the r-by-t channel matrix with its (i, k) entry, i.e., $[\mathbf{H}]_{ik} \in C$, denoting the fading coefficient between the kth transmit antenna and i^{th} receive antenna. Also, $\mathbf{h}_1$, $\mathbf{h}_2$,..., $\mathbf{h}_t$ denote the columns of the matrix **H**. Additionally, the vector $\mathbf{x} \in C^{t\times 1}$ denotes the transmitted baseband signal. Also, x_1, x_2,..., x_t denote the elements of the vector **x**. Additionally, $\mathbf{n} \in C^{r\times 1}$ represents additive white Gaussian noise at the receiver such that $E\{\mathbf{nn}^H\} = N_0\mathbf{I}$ with **I** denoting the identity matrix. A slow flat Rayleigh fading scenario with rich scattering and enough antenna spacing only at the receive side is assumed. Hence, the scenario of interest involves uncorrelated receive antennas and correlated transmit antennas. We have:

$$\mathbf{H}=\widetilde{\mathbf{H}}\mathbf{R}^{1/2} \qquad (3.8)$$

where the t-by-t matrix **R** is the correlation matrix capturing the effect of the correlation among the transmit antennas. The elements of the matrix $\widetilde{\mathbf{H}}$ are independent and identically distributed (IID) zero-mean complex Gaussian random variables with unit variance. In this chapter three types of correlation matrix structures **R** are used namely uniform, dual, and exponential correlation models. All of these models have practical applications.

The entries of the uniform correlation matrix are given by $[\mathbf{R}]_{ik}=1$ for $i = k$ and $[\mathbf{R}]_{ik}=\rho$ for $i \neq k$, where $[\mathbf{R}]_{ik}$ represents the ith row k^{th} column element of **R**. Also, ρ $(0 < \rho < 1)$ denotes the correlation coefficient between any two transmit antennas. We have:

$$R=\begin{bmatrix} 1 & \rho & \rho & \rho & \dots & \rho & \rho \\ \rho & 1 & \rho & \rho & \dots & \rho & \rho \\ \vdots & \vdots & \vdots & \vdots & \ddots & \vdots & \vdots \\ \rho & \rho & \rho & \rho & \dots & \rho & 1 \end{bmatrix} \quad (3.9)$$

For an antenna array, the uniform correlation matrix is applicable when all the transmit antennas are separated with the same distance from each other.

The elements of the dual correlation matrix are given by $[\mathbf{R}]_{ik}=1$ for $i = k$, $[\mathbf{R}]_{ik}=\rho$ for $|i-k|=1$, and $[\mathbf{R}]_{ik}=0$ for the remaining entries. We have:

$$R=\begin{bmatrix} 1 & \rho & 0 & 0 & \dots & 0 & 0 \\ \rho & 1 & \rho & 0 & \dots & 0 & 0 \\ \vdots & \vdots & \vdots & \vdots & \ddots & \vdots & \vdots \\ 0 & 0 & 0 & 0 & \dots & \rho & 1 \end{bmatrix} \quad (3.10)$$

For an antenna array, the dual correlation matrix provides a more realistic model as compared to the uniform correlation matrix. The reason behind this can be explained based on the fact that the correlation between two antennas reduces when the distance between them increases and when separated far enough the correlation may be equal to zero.

The entries of the exponential correlation matrix are given by $[\mathbf{R}]_{ik}=\rho^{|i-k|}$. We have:

$$R=\begin{bmatrix} 1 & \rho & \rho^2 & \rho^3 & \dots & \rho^{t-2} & \rho^{t-1} \\ \rho & 1 & \rho & \rho^2 & \dots & \rho^{t-3} & \rho^{t-2} \\ \vdots & \vdots & \vdots & \vdots & \ddots & \vdots & \vdots \\ \rho^{t-1} & \rho^{t-2} & \rho^{t-3} & \rho^{t-4} & \dots & \rho & 1 \end{bmatrix} \quad (3.11)$$

For an antenna array, the exponential correlation matrix provides a more realistic model as compared to the other discussed correlation models. The reason behind this can be explained again by the fact that the correlation between two antennas reduces when the distance between them increases.

The receiver uses ZF equalization to suppress the intersymbol interference, under the assumption of full CSI being only available at the receiver. For equalization, the received complex baseband signal $\mathbf{y}$ is projected onto the vector $\mathbf{h}_i^H \mathbf{P}_i^\perp$, for all i, where

$i \in \{1, 2, \ldots, t\}$ and $\mathbf{P}_i^\perp$ denotes the projection matrix onto the null space of the vectors $\mathbf{h}_1, \mathbf{h}_2, \ldots, \mathbf{h}_{i-1}, \mathbf{h}_{i+1}, \mathbf{h}_{i+2}, \ldots, \mathbf{h}_t$. This yields:

$$\frac{\mathbf{h}_i^H \mathbf{P}_i^\perp}{\|\mathbf{h}_i^H \mathbf{P}_i^\perp\|}\mathbf{y} = \|\mathbf{h}_i^H \mathbf{P}_i^\perp\|x_i + \frac{\mathbf{h}_i^H \mathbf{P}_i^\perp}{\|\mathbf{h}_i^H \mathbf{P}_i^\perp\|}\mathbf{n}$$

$$= \|\mathbf{h}_i^H \mathbf{P}_i^\perp\|s_{aI} + R\left\{\frac{\mathbf{h}_i^H \mathbf{P}_i^\perp}{\|\mathbf{h}_i^H \mathbf{P}_i^\perp\|}\mathbf{n}\right\} + j\left(\|\mathbf{h}_i^H \mathbf{P}_i^\perp\|s_{bQ} + I\left\{\frac{\mathbf{h}_i^H \mathbf{P}_i^\perp}{\|\mathbf{h}_i^H \mathbf{P}_i^\perp\|}\mathbf{n}\right\}\right) \tag{3.12}$$

for $i \in \{1,2,\ldots,t\}$. Suppose that I and Q components of the ith symbol s_i ($i \in \{1,2,\ldots,t\}$) are sent from the αth and β^{th} transmit antennas, respectively. The maximum likelihood detector at the receiver forms the decision variable for the ith symbol (s_i) as:

$$d_i = R\left\{\frac{\mathbf{h}_\alpha^H \mathbf{P}_\alpha^\perp}{\|\mathbf{h}_\alpha^H \mathbf{P}_\alpha^\perp\|}\mathbf{y}\right\} + jI\left\{\frac{\mathbf{h}_\beta^H \mathbf{P}_\beta^\perp}{\|\mathbf{h}_\beta^H \mathbf{P}_\beta^\perp\|}\mathbf{y}\right\} \text{ for } i \in \{1, 2, \ldots, t\}.$$

3.3 Performance Analysis

This section provides BPSK ABEP and QPSK ASEP expressions under time and spatial-interleaved ZFRBF. Optimum and near-optimum signal constellation rotation angles are derived.

3.3.1 ABEP & optimum rotation angle for BPSK under time interleaving

The pairwise error probability (PEP) is the probability of detecting a transmitted symbol erroneously at the receiver. Let $P(s_i \rightarrow \tilde{s}_i)$ be the probability that the transmitted symbol s_i is erroneously detected as $\tilde{s}_i$. Because of the symmetry, we have the relationship between the two conditional PEP expressions as $P(s_1 \rightarrow \tilde{s}_1 | \gamma_{11}, \gamma_{21}) = P(s_2 \rightarrow \tilde{s}_2 | \gamma_{12}, \gamma_{22})$. Using the ML decision rule, the conditional PEP can be written as

$$P(s_1 \rightarrow \tilde{s}_1 | \gamma_{11}, \gamma_{21}) = P\left(\left|d_1 - \left(\sqrt{\gamma_{11}}\tilde{s}_{1I} + j\sqrt{\gamma_{21}}\tilde{s}_{1Q}\right)\right|^2 < \left|d_1 - \left(\sqrt{\gamma_{11}}s_{1I} + j\sqrt{\gamma_{21}}s_{1Q}\right)\right|^2\right)$$

$$= P\left(2\sqrt{\gamma_{11}}\Delta_I n_{1I} + 2\sqrt{\gamma_{21}}\Delta_Q n_{1Q} < -\gamma_{11}\Delta_I^2 - \gamma_{21}\Delta_Q^2\right) \tag{3.13}$$

where, $\Delta_I = s_{1I} - \tilde{s}_{1I}$ and $\Delta_Q = s_{1Q} - \tilde{s}_{1Q}$ represent the distances between I and Q components of the two rotated BPSK signal constellation points, respectively. Here, conditioned on the squared channel gains γ_{11} and γ_{21}, the sum

$2\sqrt{\gamma_{11}}\Delta_I n_{1I} + 2\sqrt{\gamma_{21}}\Delta_Q n_{1Q}$ is a zero-mean Gaussian random variable with a variance of $2N_0(\gamma_{11}\Delta_I^2 + \gamma_{21}\Delta_Q^2)$. Using this information, we can write [62]

$$P(s_1 \to \tilde{s}_1 | \gamma_{11}, \gamma_{21}) = Q\left(\sqrt{\frac{\gamma_{11}\Delta_I^2 + \gamma_{21}\Delta_Q^2}{2N_0}}\right) \tag{3.14}$$

where $Q(.)$ is the Q-function formulated as $Q(x) = \frac{1}{\sqrt{2\pi}}\int_x^\infty \exp(-u^2/2)\,du$. In order to determine the unconditional PEP, the joint probability density function of independent random variables γ_{11} and γ_{21} is required. It can be shown that γ_{11} and γ_{21} are chi-squared random variables each with (2M-2) degrees of freedom [70]. Hence, we can write

$$f(\gamma_{11}, \gamma_{21}) = \frac{\gamma_{11}^{M-2}\gamma_{21}^{M-2}}{\left((M-2)!\right)^2}\, e^{-\gamma_{11}-\gamma_{21}} \tag{3.15}$$

for $\gamma_{11} \geq 0$ and $\gamma_{21} \geq 0$.

Using Craig's formula [71] the conditional PEP expression in (3.9) can be rewritten as

$$P(s_1 \to \tilde{s}_1 | \gamma_{11}, \gamma_{21}) = \frac{1}{\pi}\int_0^{\pi/2} \exp\left(-\frac{\gamma_{11}\Delta_I^2 + \gamma_{21}\Delta_Q^2}{4N_0 \sin^2\phi}\right)d\phi. \tag{3.16}$$

The unconditional PEP is then given by

$$P(s_1 \to \tilde{s}_1) = \frac{1}{\pi}\int_0^{\pi/2}\int_0^\infty\int_0^\infty \exp\left(-\frac{\gamma_{11}\Delta_I^2 + \gamma_{21}\Delta_Q^2}{4N_0 \sin^2\phi}\right) f(\gamma_{11}, \gamma_{21})d\gamma_{11}d\gamma_{21}d\phi. \tag{3.17}$$

For BPSK modulation, the ABEP P_b and PEP are identical. Consequently, the PEP formula can directly be used to find the optimum rotation angle. For BPSK, we have $\Delta_I = 2\sqrt{E_b}\cos(\theta)$ and $\Delta_Q = 2\sqrt{E_b}\sin(\theta)$ where θ refers to the rotation angle counter-clockwise. It can mathematically be shown that the optimum rotation angle minimizing (3.17) is 45-degree counter-clockwise [62, Theorem 2].

When the optimum rotation angle value of 45-degree is used, we have $\Delta_I = \Delta_Q = \sqrt{2E_b}$ and we can accordingly write

$$P_b = \frac{1}{\pi} \int_0^{\pi/2} \int_0^\infty \int_0^\infty \exp\left(-\frac{E_b(\gamma_{11}+\gamma_{21})}{2N_0\sin^2\phi}\right) \frac{\gamma_{11}^{M-2}\gamma_{21}^{M-2}}{\left((M-2)!\right)^2} e^{-\gamma_{11}-\gamma_{21}} d\gamma_{11} d\gamma_{21} d\phi. \tag{3.18}$$

Using the following integral identity

$$P_b = \int_0^\infty \exp(-ax)x^c dx = c!/a^{c+1} \tag{3.19}$$

where a is a positive real number and c is an integer such that $c \geq 2$, we can write

$$P_b = \frac{1}{\pi} \int_0^{\pi/2} \left(\frac{\sin^2\phi}{\sin^2\phi+\frac{E_b}{2N_0}}\right)^{2M-2} d\phi. \tag{3.20}$$

Using [72, Eq. (5A.4b)], the preceding integral can be solved in an exact closed-form as

$$P_b = \left(\frac{1-\sqrt{\frac{E_b/2N_0}{1+E_b/2N_0}}}{2}\right)^{2M-2} \sum_{k=0}^{2M-3} \binom{2M-3+k}{k} \left(\frac{1+\sqrt{\frac{E_b/2N_0}{1+E_b/2N_0}}}{2}\right)^k. \tag{3.21}$$

3.3.2 ABEP & near-optimum rotation angle for BPSK under spatial interleaving

In this case, an approximation on the unconditional PEP is provided in [69] as follows

$$P(s_1 \rightarrow \tilde{s}_1) \approx \frac{1}{\pi} \int_0^{\frac{\pi}{2}} \int_0^\infty \int_0^\infty \exp\left(-\frac{\gamma_1\Delta_I^2+\gamma_2\Delta_Q^2}{4N_0\sin^2\phi}\right) \frac{\gamma_1^{M-1}\gamma_2^{M-1}\Gamma(M+1,\gamma_1+\gamma_2)}{(M-1)!(M-2)!\left(\gamma_1+\gamma_2\right)^{M+1}} d\gamma_1 d\gamma_2 d\phi. \tag{3.22}$$

Here, $\Gamma(s,x)$ represents the upper incomplete gamma function [73]. It is also known from [69] that the near-optimum value for θ is 45-degree counter-clockwise for spatial-interleaved BPSK. With the condition of $\theta = 45°$, the ABEP expression for BPSK under spatial interleaving is approximated as [69]

$$P_b \approx \frac{M!(M-1)!}{(2M-1)!} \sum_{i=0}^M \binom{M+i-2}{M-2} \left[\frac{1}{2}-\sqrt{\frac{E_b/N_0}{2+E_b/N_0}} \sum_{k=0}^{M+i-2} \frac{(2k)!}{2^{k+1}(k!)^2(2+E_b/N_0)^k}\right] \tag{3.23}$$

where the expansion $\Gamma(M+1,x)=M!e^{-x}\sum_{i=0}^M x^i/i!$ is exploited.

3.3.3 ASEP & near-optimum rotation angles for QPSK

To find the ASEP for QPSK with time interleaving, we need to find the PEP expression as a function of the rotation angle θ. Let $P(s_a \to s_b)$ be the probability that the detector erroneously decides in favor of s_b when the transmitted symbol is s_a. Substituting (3.15) into (3.17) and using (3.19) yields $P(s_a \to s_b)$ as

$$P(s_a \to s_b) = \frac{1}{\pi} \int_0^{\pi/2} \int_0^\infty \int_0^\infty \exp\left(-\frac{\gamma_{11}\Delta_I^2 + \gamma_{21}\Delta_Q^2}{4N_0 \sin^2 \phi}\right) \frac{\gamma_{11}^{M-2} \gamma_{21}^{M-2}}{((M-2)!)^2} e^{-\gamma_{11} - \gamma_{21}} d\gamma_{11} d\gamma_{21} d\phi. \qquad \textbf{(3.24)}$$

Taking the integral with respect to γ_{11} and γ_{21} yields

$$P(s_a \to s_b) = \frac{1}{\pi} \int_0^{\pi/2} \left(\frac{\sin^2 \phi}{\sin^2 \phi + \frac{\Delta_I^2}{4N_0}}\right)^{M-1} \left(\frac{\sin^2 \phi}{\sin^2 \phi + \frac{\Delta_Q^2}{4N_0}}\right)^{M-1} d\phi. \qquad \textbf{(3.25)}$$

Assuming $\Delta_I \neq \Delta_Q$ and using [72, (5A.58-60)], we can further evaluate the expression as

$$P(s_a \to s_b) = \frac{\left(\frac{\Delta_I}{\Delta_Q}\right)^{2M-4}}{2\left(1 - \left(\frac{\Delta_I}{\Delta_Q}\right)^2\right)^{2M-3}} \left[\sum_{k=0}^{M-2} \left(\left(\frac{\Delta_Q}{\Delta_I}\right)^2 - 1\right)^k B_k I_k \left(\frac{\Delta_Q^2}{4N_0}\right) - \left(\frac{\Delta_I}{\Delta_Q}\right)^2 \sum_{k=0}^{M-2} \left(1 - \right. \right.$$

$$\left. \left. \left(\frac{\Delta_I}{\Delta_Q}\right)^2\right)^k C_k I_k \left(\frac{\Delta_I^2}{4N_0}\right)\right] \qquad \textbf{(3.26)}$$

where

$$B_k \triangleq (-1)^{M-2+k} \binom{2M-4-k}{M-2}, \qquad \textbf{(3.27)}$$

$$C_k \triangleq \sum_{n=0}^{M-2} \binom{k}{n} \frac{(2M-4-n)!(-1)^{M-2+n}}{(M-2-n)!(M-2)!}, \qquad \textbf{(3.28)}$$

$$I_k(c) = 1 - \sqrt{\frac{c}{1+c}} \left[1 + \sum_{n=1}^{k} \frac{(2n-1)!!}{n! 2^n (1+c)^n}\right]. \qquad \textbf{(3.29)}$$

Here, the double factorial notation (2n-1)!! represents the product of only odd integers from 1 to (2n-1). (3.26) can be taught as the exact generalized PEP expression between

any two symbols in the generalized PSK signal constellation under time interleaving. The requirement $\Delta_I \neq \Delta_Q$ must be satisfied for (3.26) to be valid. This condition is satisfied for any pair of signal points by the appropriate signal constellation rotation.

To approximate the exact ASEP (P_s) expression of a generalized PSK modulation with an order that is equal to or greater than 4, the union bound can be used [70]. For QPSK modulation, the following union bound is utilized

$$P_s \leq \frac{1}{4} \sum_{a=1}^{4} \sum_{\substack{b=1 \\ a \neq b}}^{4} P(s_a \rightarrow s_b) \tag{3.30}$$

where s_a and s_b show the symbols of the rotated QPSK signal constellation such that a $\neq$ b.

Within a rotated QPSK signal constellation, for any two symbols s_a and s_b (({a,b} $\in$ {1,2,3,4}, a $\neq$ b)), Δ_I and Δ_Q are given by

$$\Delta_I = \sqrt{E_s}(\cos(\theta_a + \theta) - \cos(\theta_b + \theta)), \tag{3.31}$$

$$\Delta_Q = \sqrt{E_s}(\sin(\theta_a + \theta) - \sin(\theta_b + \theta)), \tag{3.32}$$

where θ ($0° < \theta < 45°$) is the counter-clockwise rotation angle and, θ_a and θ_b represent the phases of s_a and s_b in the original (non-rotated) signal constellation, respectively.

To be able to derive the near-optimum rotation angles for QPSK modulation, the union bound method is utilized. For time interleaving, Δ_I and Δ_Q expressions are substituted into the generalized PEP expression for every symbol pair of the constellation diagram and the rotation angles that minimize the union bound are obtained by using the "NMinimize" function of the Mathematica software package for different E_s/N_0 and M values. The angle optimization search space is constrained within the range of ($0°$, $45°$). Table 3.1 shows the obtained rotation angles for different E_s/N_0 values when M = 2 and M = 3 under time interleaving.

Table 3.1 Near-optimum rotation angle values for 2×2 and 2×3 QPSK time-interleaved SSD scheme

M = 2		M = 3	
E_s/N_0	Θ	E_s/N_0	θ
0	32.119°	0	44.966°
5	33.037°	3	42.797°
10	31.475°	6	37.495°
15	30.321°	9	34.245°
20	29.862°	12	32.391°
25	29.706°	15	31.397°
30	29.656°	18	30.881°

In order to find the near-optimum rotation angles for spatial interleaving, Δ_I and Δ_Q expressions are implemented into the generalized PEP expression in (3.26) for every symbol pair of the constellation diagram. Then, Mathematica is used (with a step size of 1°) to determine the rotation angles. The near-optimum rotation angle is found to be equal to 44° for all the E_s/N_0 values between 0 and 30 dB when M = 2 and for all the E_s/N_0 values between 0 and 15 dB when M = 3.

3.4 Results

Using the optimum and near-optimum angle values of Section 3.3, performance of the proposed schemes under different scenarios is demonstrated. In addition, FPGA implementations of the relevant methods are presented in order to compare complexities of the different techniques.

3.4.1 Simulation Results

In this section, the proposed time and spatial-interleaved schemes are compared with the standard ZFRBF with no SSD model under BPSK and QPSK modulations. SSD

simulations use the derived optimum or near-optimum rotation angle values as given in Section 3.3.

In Figure 3.2, 2×2 time and spatial-interleaved BPSK models are compared against ZFRBF without SSD. It is clear that SSD yields major gains when incorporated into the standard ZFRBF. It can also be seen that time interleaving provides much more performance gain as compared to spatial interleaving. For instance, for an ABEP of 10^{-4}, the time interleaving method provides 14.7 dB gain whereas the spatial interleaving method has just a benefit of 2 dB when compared with the no SSD counterpart. This significant performance gap between the two interleaving approaches can be attributed to the degree of the correlation between the channel gains which suggests that the performance of the studied ZFRBF scheme significantly benefits from uncorrelated channel gains. Looking from a designer perspective, it can be proposed that it would be much better to use time interleaving instead of spatial interleaving with BPSK whenever latency does not cause a serious problem. The trade-off between these two methods in terms of latency and error performance can be exploited according to the need. The strong match between the analytical curves and their simulated counterparts in Figure 3.2 validates the analytical derivations. In addition, the similar trend between the theoretical and simulation results for spatial interleaving method shows the correctness of approximation under this case.

In Figure 3.3, the error performances of 2×3 BPSK models are demonstrated. It is again obvious that time interleaving outperforms spatial interleaving technique. For an ABEP of 10^{-4}, the time interleaving method is capable of providing a 6.35 dB gain, whereas the spatial interleaving method supplies a gain of 1.23 dB beyond ZFRBF with no SSD. These results reveal that the gains attained by SSD decrease with higher number of receive antennas. Moreover, increasing the number of receive antennas has the effect of reducing the difference between the SSD gains of the two interleaving techniques (12.7 dB in 2×2 case and 5.12 dB in 2×3 case). The main reason behind this is that the two substreams tend to become less correlated with spatial interleaving method as the number of receive antennas gets larger [62]. Hence, the performance of spatial interleaving approaches to the performance of time interleaving as M increases. The analytical derivation regarding to the time interleaving method is also justified in

Figure 3 by the strong correlation between the analytical and simulation curves. Comparing Figure 3.2 and Figure 3.3 at an ABEP of 10^{-4}, one can observe that the performance of time interleaving in 2×2 case gets close as near as 1 dB to that of no SSD scenario in 2×3 case.

In Figure 3.4, 2×2 time and spatial-interleaved QPSK models are compared against the ZFRBF model without SSD. It is one more time clear that SSD helps in improving the system performance of ZFRBF significantly. It can also be seen that time interleaving provides higher performance gain as compared to spatial interleaving. For instance, for an ASEP of 10^{-4}, the time interleaving method provides a 14.24 dB gain whereas the spatial interleaving method has a gain of 1.06 dB. From a design point of view, again there exists a trade-off between latency and error performance. The analytical and simulation curves have a high degree of matching between each other; thus confirming the correctness of the analytical results. Also, Figure 3.4 reveals that the union bound approximation in the theoretical ASEP expressions for both time and spatial interleaving methods follows a similar trend with the simulated results and the match with the exact simulation results gets better as SNR increases.

In Figure 3.5, 2×3 QPSK schemes are compared. It is demonstrated that for an ASEP of 10^{-4}, the time interleaving method provides a 6.1 dB gain whereas the spatial interleaving method has a gain of 0.9 dB when compared to no SSD case. Similar to the BPSK case, increasing the receive antenna number highly improves the error rate performance for QPSK. Finally, for the spatial interleaving method, as the number of receive antennas increases, the degree of match between the union bound approximation and the simulation results gets better.

3.4.2 FPGA implementation results

In order to assess the additional hardware complexity introduced due to SSD, two versions of a 2×2 MIMO ZFRBF system (one version without SSD and second version with SSD under spatial interleaving) are implemented on an FPGA. As the hardware

Figure 3.2 Performance comparison of different schemes with 2×2 BPSK system.

Figure 3.3 Performance comparison of different schemes with 2×3 BPSK system.

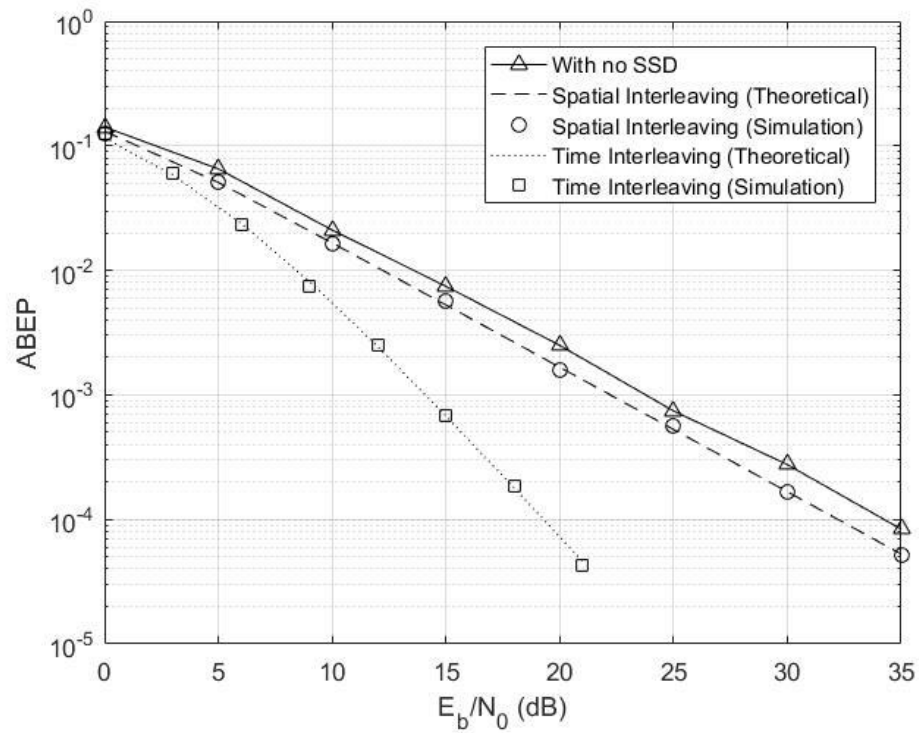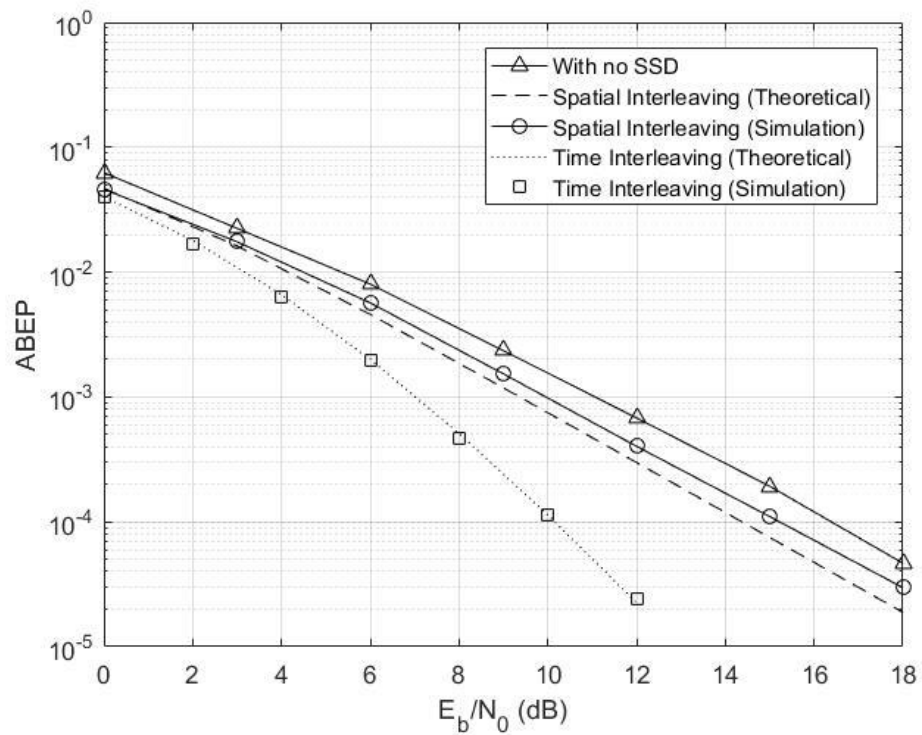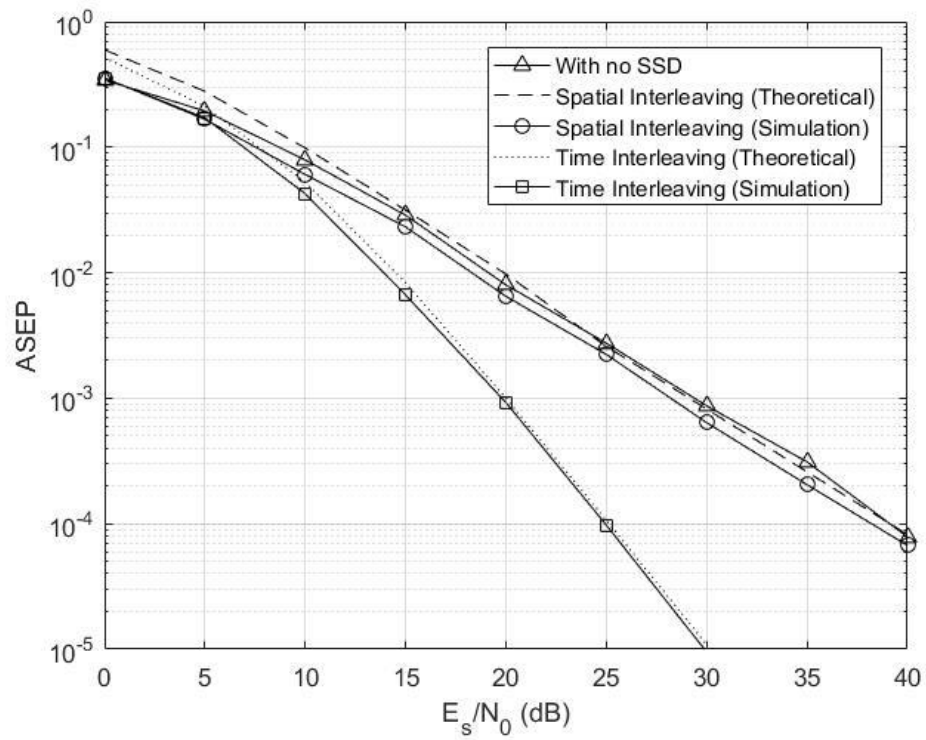**Figure 3.4** Performance comparison of different schemes with 2×2 QPSK system.
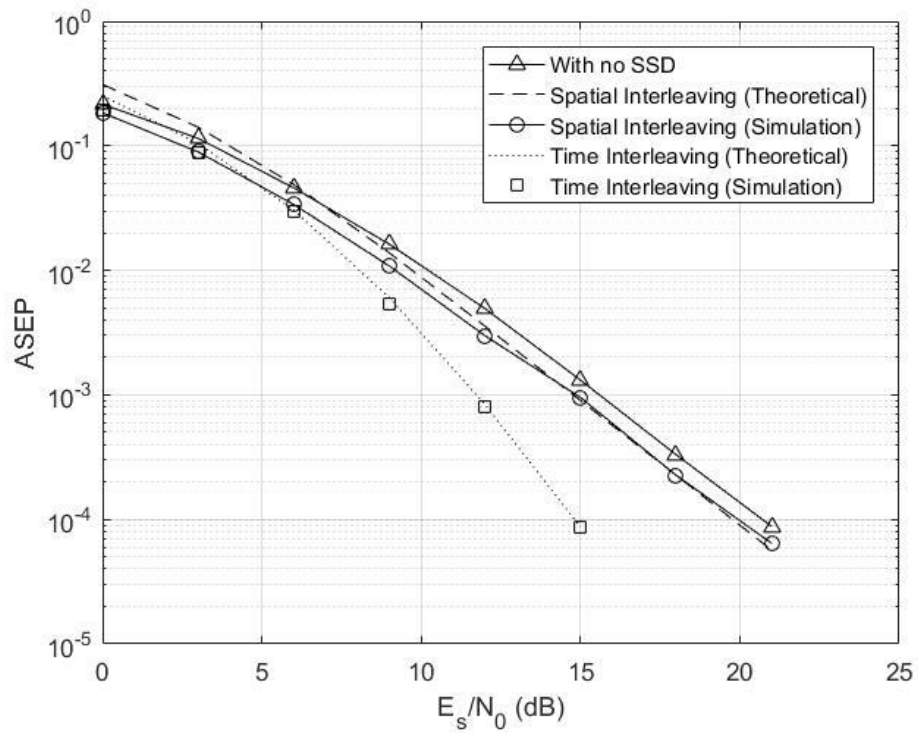
Figure 3.5 Performance comparison of different schemes with 2×3 QPSK system.
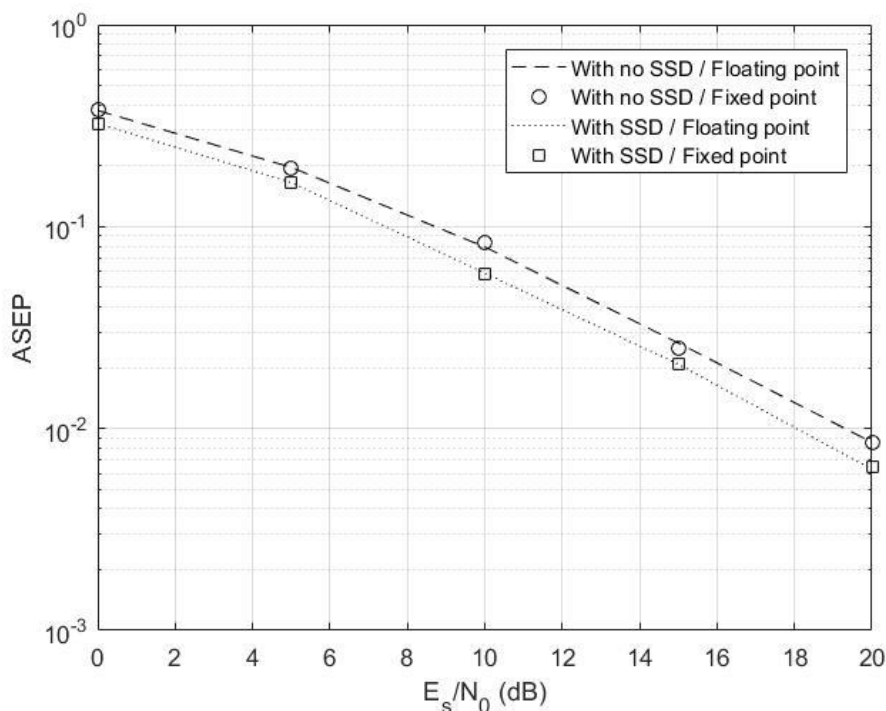
Figure 3.6 Performance comparison of the fixed point and floating point models.

complexities of spatial interleaving and time interleaving methods are similar, only spatial interleaving technique is implemented with BPSK and QPSK modulations.

As a first step for the FPGA implementation, the 32-bit float variables and 32-bit floating point arithmetic operations in simulation model are converted to a fixed point model. Compared to a floating point model, a fixed point implementation entails less hardware complexity and lower power consumption while achieving a faster clock speed or higher throughput. In fixed point model of 2×2 system, all the variables are represented in a 20-bit 2's complement format and all arithmetic operations are carried out in 20-bit. This bit-width value of 20 is determined after extensive performance simulations, where negligible or no performance degradation in average error probability simulations is aimed. Figure 3.6 shows that performance of 2×2 system with 20-bit fixed point closely matches to the floating point performance for all SNR values.

As a second step for the FPGA implementation, the fixed point designs of 2×2 MIMO system are modelled in Verilog Hardware Description Language (HDL) for SSD and

with no SSD cases. Xilinx Vivado Design Suite is used for functional verification, synthesis, and place and route design steps. Both architectures are implemented on Xilinx Virtex-7 VC709 FPGA where 100 MHz clock speed and 400 Mbps throughput are attained in both designs. The Verilog design of transmitter section consists of modulation, signal rotation, and component interleaving modules where ZFRBF, deinterleaving, and detector modules are included at the receiver side. Figure 3.7 demonstrates the schematic diagram of the synthesized design of the receiver. Here, (3.3) is implemented on FPGA. In this scheme, firstly the projection matrices are formed (N_F1 and N_F2) and channel fading coefficients are estimated (F_C1 and F_C2). Next, beamforming matrices (BF1 and BF2) are constructed for ZFRBF and spatial deinterleaving operation (ZFRBF_SDI) is performed onto the received baseband signal y. Finally, symbol estimation (S_E) is done according to the Euclidean distances. The N_F blocks calculate $\mathbf{P}_{\mathbf{h}_1}^\perp$ and $\mathbf{P}_{\mathbf{h}_2}^\perp$, while F_C yields the values of $\sqrt{\gamma_1}$, $\sqrt{\gamma_2}$, $\mathbf{h}_1^H \mathbf{P}_{\mathbf{h}_2}^\perp$ and $\mathbf{h}_2^H \mathbf{P}_{\mathbf{h}_1}^\perp$. Outputs of BF1 and BF2 are $\frac{\mathbf{h}_1^H \mathbf{P}_{\mathbf{h}_2}^\perp}{\left\| \mathbf{h}_1^H \mathbf{P}_{\mathbf{h}_2}^\perp \right\|}$ and $\frac{\mathbf{h}_2^H \mathbf{P}_{\mathbf{h}_1}^\perp}{\left\| \mathbf{h}_2^H \mathbf{P}_{\mathbf{h}_1}^\perp \right\|}$, respectively. These architectures employ full pipelining to achieve higher clocking speed on FPGA. In the implementations, Xilinx IP cores are used for division and square root operations.

N_F: Projection matrix formation
F_C: Fading coefficient calculation
BF: Beamforming
ZFRBF_SDI: ZFRBF spatial deinterleaving

S_E: Symbol estimation
y: Received baseband signal
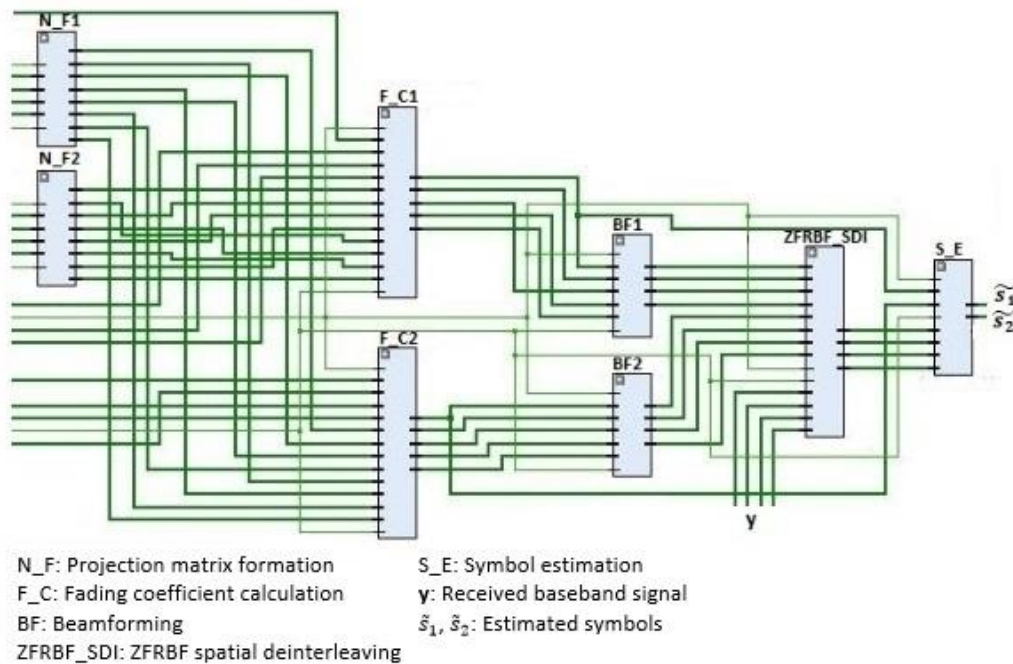$\hat{s}_1, \hat{s}_2$: Estimated symbols

Figure 3.7 Schematic of the synthesized ZFRBF design.

Table 2 gives transmitter and receiver resource usages of FPGA implementations for SSD and with no SSD. In contrast to no SSD design, SSD design introduces additional 10 Flip-Flops (FFs) at the transmitter, which is due to the interleaving operation. As for the receiver side, integration of SSD technique to the ZFRBF system adds only 1.25% more FF and 1.77% more look-up table (LUT) while it uses 2.6% less memory LUT modules compared to ZFRBF with no SSD. In addition, two extra DSP48 modules are used with SSD design to perform the additional operation resulting from decision stage. Considering the significant performance advantage of SSD approach, this extra implementation complexity is highly tolerable. To be more practical and accurate in terms of real systems, the complexity of SSD system is also analyzed in a complete receiver system where more complicated blocks such as symbol time synchronization, LDPC decoder, and channel estimator blocks are included. Table 3 shows the resource usage of a complete receiver system with SSD and no SSD. When the comparison is performed for an entire receiver, the extra complexity introduced by SSD technique turns out to be at most 0.71% which is highly negligible.

Table 3.2 Resource utilization for ZFRBF

| | Transmitter | | Receiver | | |
	No SSD	With SSD	No SSD	With SSD	Increment
FF	136	146	47680	48265	1.23
LUT	69	69	47668	48513	1.77
MLUT	-	-	269	262	-2.6
DSP48	-	-	72	74	2.78

Table 3.3 Resource utilization for the complete receiver

	No SSD	With SSD	Increment
FF	111819	112404	0.52
LUT	119112	119957	0.71
MLUT	6203	6196	-0.11
DSP48	639	641	0.31

3.4.3 Results of transmit antenna correlation scenarios

The scenario of three transmit / receive antennas

For the scenario with three transmit and receive antennas, there are two different interleaving strategies to test. These two strategies are labeled as Strategy 1 and Strategy 2. For the sake of comparison, the original ZF scheme without SSD is also shown. This is called as Strategy 3. The baseband transmit vectors for these strategies are respectively given as:

$$\mathbf{x}=\begin{bmatrix} s_{1I}+js_{2I} \\ s_{1Q}+js_{3Q} \\ s_{3I}+js_{2Q} \end{bmatrix}, \mathbf{x}=\begin{bmatrix} s_{1I}+js_{2I} \\ s_{3I}+js_{3Q} \\ s_{1Q}+js_{2Q} \end{bmatrix}, \mathbf{x}=\begin{bmatrix} s_{1I}+js_{1Q} \\ s_{2I}+js_{2Q} \\ s_{3I}+js_{3Q} \end{bmatrix} \tag{3.33}$$

The correlation coefficient ρ is chosen to be equal to 0.85 in all simulations. It can be seen from Figure 3.8 that under uniform correlation, Strategy 1 and Strategy 2 (both with SSD) yield better performance as compared to Strategy 3 which has no SSD. For a BER of 10^{-2}, Strategy 1 and Strategy 2 provide about 2.8 and 2 dB gains. It can be seen from Figure 3.9 that under dual correlation, Strategy 1 outperforms Strategy 2 and Strategy 3. For a BER of 10^{-2}, Strategy 1 provides almost 2.2 dB gain as compared to the other schemes which perform very close to each other for this scenario. It can be seen from Figure 3.10 that under exponential correlation, Strategy 1 again performs better than Strategy 2 and Strategy 3. For a BER of 10^{-2}, Strategy 1 provides about 2.3 dB gain as compared to Strategy 3. In this case, Strategy 2 attains around 0.6 dB gain

as compared to Strategy 3. Hence, Strategy 1 yields the best performance in all the considered correlation models when t = r = 3.

Figure 3.8 The comparison of the BER performances for the relevant strategies with three transmit and receive antennas under uniform correlation.

Figure 3.9 The comparison of the BER performances for the relevant strategies with three transmit and receive antennas under dual correlation.

Figure 3.10 The comparison of the BER performances for the relevant strategies with three transmit and receive antennas under exponential correlation.

The scenario of four transmit / receive antennas

There exist three different interleaving strategies for the case of four transmit and receive antennas. These strategies are labeled as Strategy 1, Strategy 2, and Strategy 3. Here, the original ZF scheme without SSD is called Strategy 4. The baseband transmit vectors for these strategies are respectively given as:

$$
\mathbf{x}=\begin{bmatrix} s_{1I}+js_{2I} \\ s_{3I}+js_{4I} \\ s_{1Q}+js_{2Q} \\ s_{3Q}+js_{4Q} \end{bmatrix},\mathbf{x}=\begin{bmatrix} s_{1I}+js_{2I} \\ s_{3I}+js_{4I} \\ s_{3Q}+js_{4Q} \\ s_{1Q}+js_{2Q} \end{bmatrix},\mathbf{x}=\begin{bmatrix} s_{1I}+js_{2I} \\ s_{1Q}+js_{2Q} \\ s_{3I}+js_{4I} \\ s_{3Q}+js_{4Q} \end{bmatrix},\mathbf{x}=\begin{bmatrix} s_{1I}+js_{1Q} \\ s_{2I}+js_{2Q} \\ s_{3I}+js_{3Q} \\ s_{4I}+js_{4Q} \end{bmatrix} \tag{3.34}
$$

The correlation coefficient ρ is chosen to be equal to 0.85 in all simulations. It can be seen from Figure 3.11 that under uniform correlation, the Strategies 1, 2 and 3 perform very similarly and all outperforms Strategy 4 by around 3.3 dB gain at a BER of 2×10^{-2}.
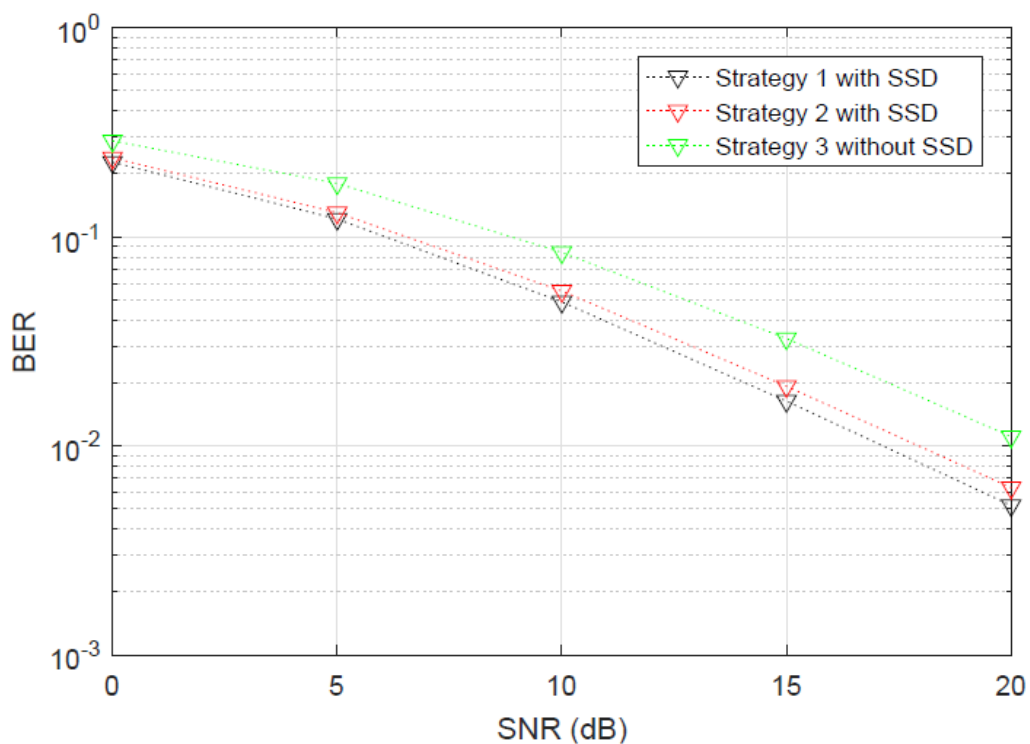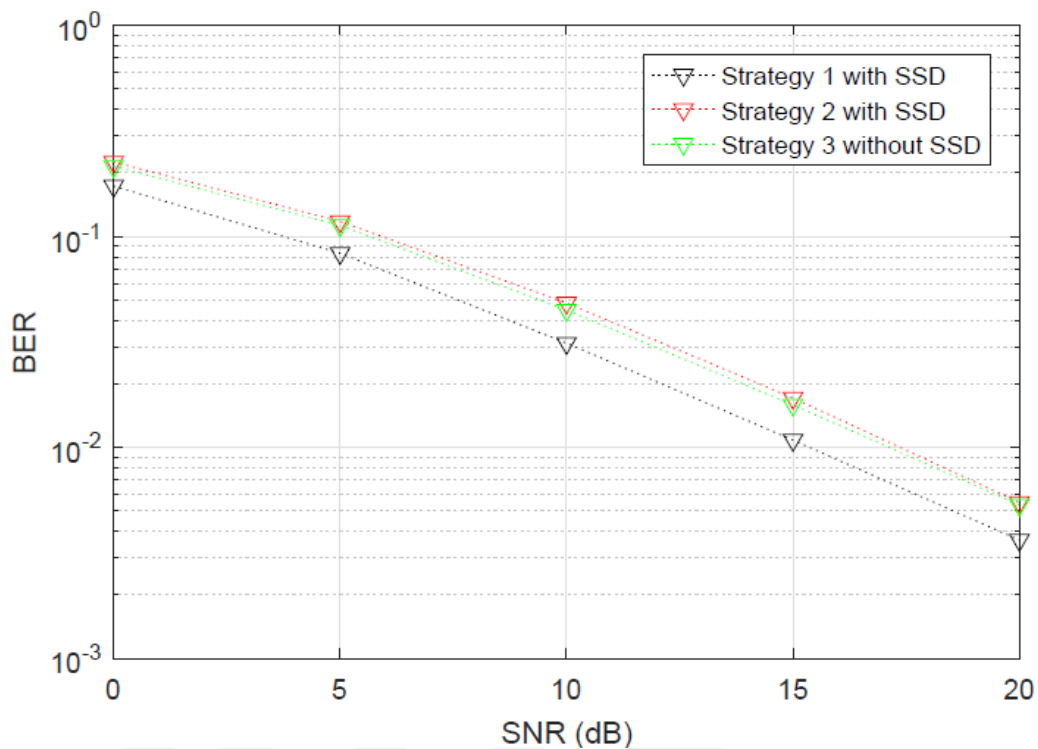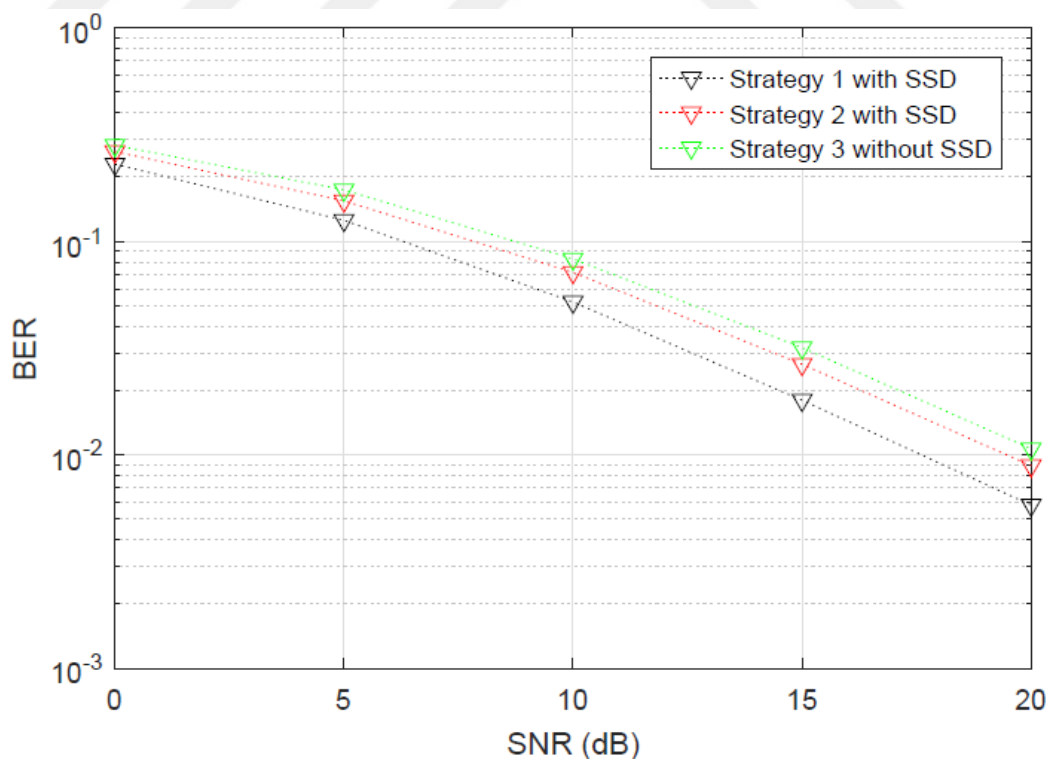

Figure 3.11 The comparison of the BER performances for the relevant strategies with four transmit and receive antennas under uniform correlation.

Figure 3.12 The comparison of the BER performances for the relevant strategies with four transmit and receive antennas under dual correlation.

It can be seen from Figure 3.12 that under dual correlation, Strategy 3 outperforms all the other strategies. For a BER of 10^{-2}, Strategy 3 produces more than 5.2 dB gain as compared to Strategy 4 without SSD. It can be seen from Figure 3.13 that under exponential correlation, Strategy 3 performs better than all the other strategies as before.

Figure 3.13 The comparison of the BER performances for the relevant strategies with four transmit and receive antennas under exponential correlation.

In this case, for a BER of 2×10^{-2}, Strategy 3 yields about 6 dB gain as compared to Strategy 4. It can be deduced from the results that Strategy 3 has a more beneficial CI strategy than the other strategies for the considered correlation models.

The scenario of five transmit / receive antennas

There are four distinct interleaving strategies for the scenario with five transmit and receive antennas. These strategies are labeled as Strategy 1, Strategy 2, Strategy 3, and Strategy 4. In this case, the original ZF scheme without SSD is represented as Strategy 5. The baseband transmit vectors for these strategies are respectively given as:

$$\mathbf{x}=\begin{bmatrix} s_{1I}+js_{2I} \\ s_{3I}+js_{4I} \\ s_{5I}+js_{5Q} \\ s_{3Q}+js_{4Q} \\ s_{1Q}+js_{2Q} \end{bmatrix},\mathbf{x}=\begin{bmatrix} s_{1I}+js_{2I} \\ s_{3I}+js_{4I} \\ s_{5I}+js_{5Q} \\ s_{2Q}+js_{4Q} \\ s_{1Q}+js_{3Q} \end{bmatrix},\mathbf{x}=\begin{bmatrix} s_{1I}+js_{2I} \\ s_{3I}+js_{5I} \\ s_{4I}+js_{5Q} \\ s_{2Q}+js_{3Q} \\ s_{1Q}+js_{4Q} \end{bmatrix},\mathbf{x}=\begin{bmatrix} s_{1I}+js_{1Q} \\ s_{3I}+js_{4I} \\ s_{2Q}+js_{5I} \\ s_{3Q}+js_{4Q} \\ s_{1Q}+js_{5Q} \end{bmatrix},\mathbf{x}=\begin{bmatrix} s_{1I}+js_{1Q} \\ s_{2I}+js_{2Q} \\ s_{3I}+js_{3Q} \\ s_{4I}+js_{4Q} \\ s_{5I}+js_{5Q} \end{bmatrix} \quad \textbf{(3.35)}$$

The correlation coefficient ρ is chosen to be equal to 0.85 in all simulations. It can be seen from Figure 3.14 that under uniform correlation, all the strategies with SSD performs very similarly.
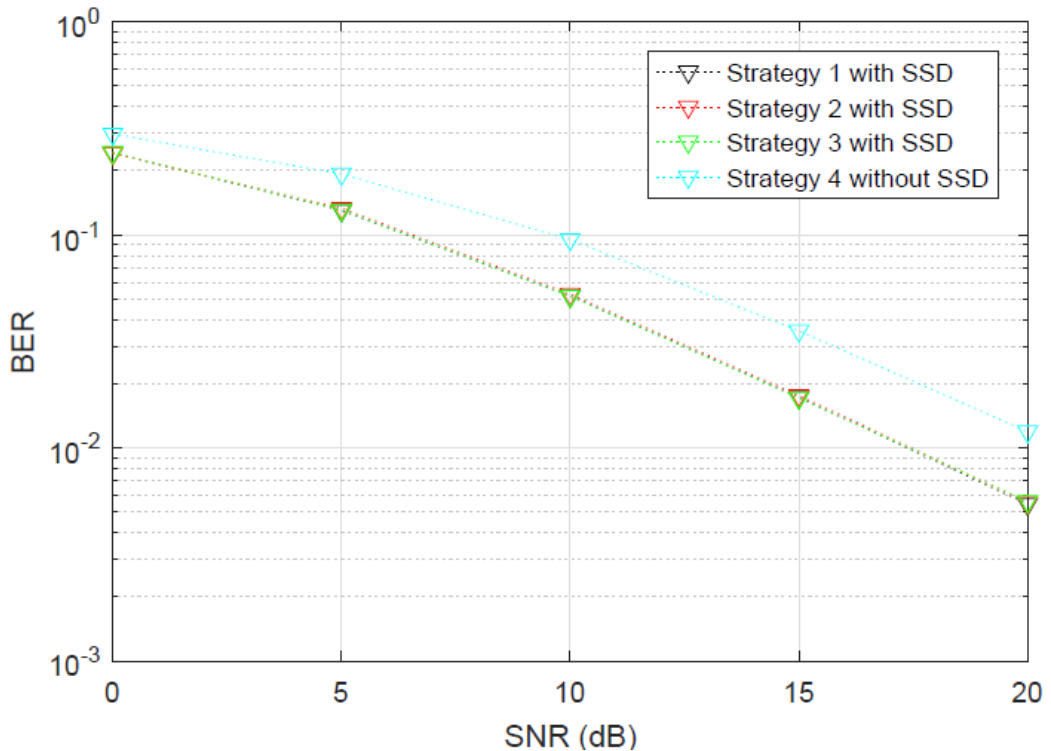

Figure 3.14 The comparison of the BER performances for the relevant strategies with five transmit and receive antennas under uniform correlation.
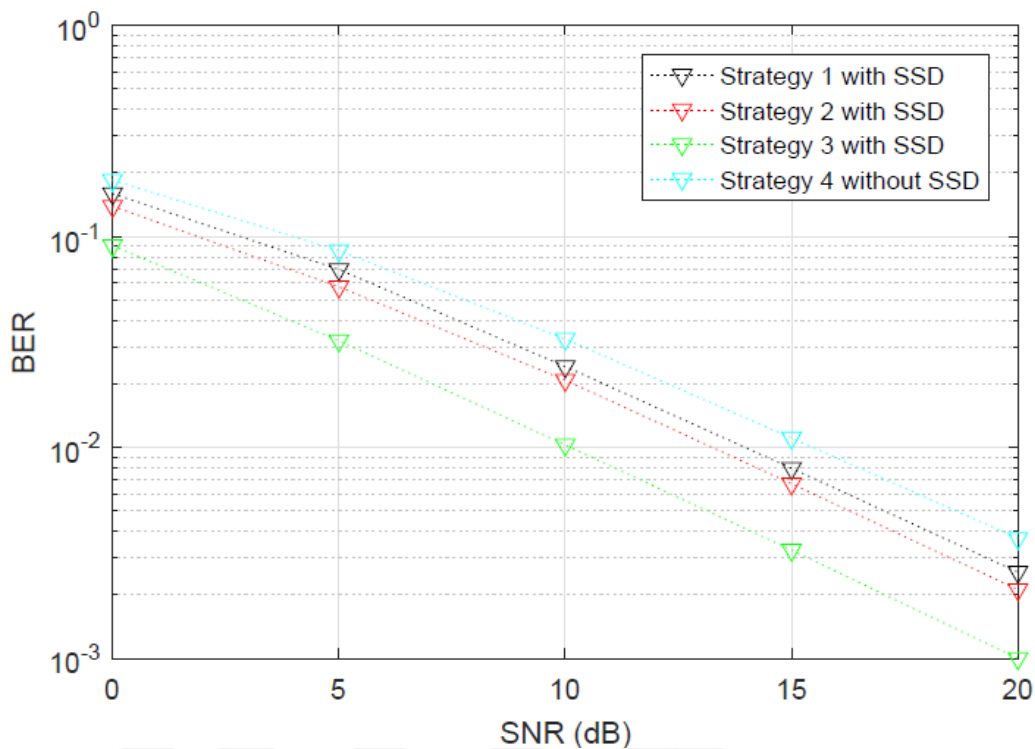
The four strategies with SSD yield about 2.7 dB gain for a BER of 2×10^{-2} as compared to Strategy 5 without SSD. It can be seen from Figure 3.15 that under dual correlation, Strategy 3 outperforms other strategies. Strategy 3 produces around 2.5 dB gain as compared to Strategy 5 at a BER of 2×10^{-2}. It can be seen from Figure 3.16 that under exponential correlation, Strategy 1 performs better than other strategies. Strategy 1 produces around 4.3 dB gain as compared to Strategy 5 at a BER of 10^{-2}.

Figure 3.15 The comparison of the BER performances for the relevant strategies with five transmit and receive antennas under dual correlation.
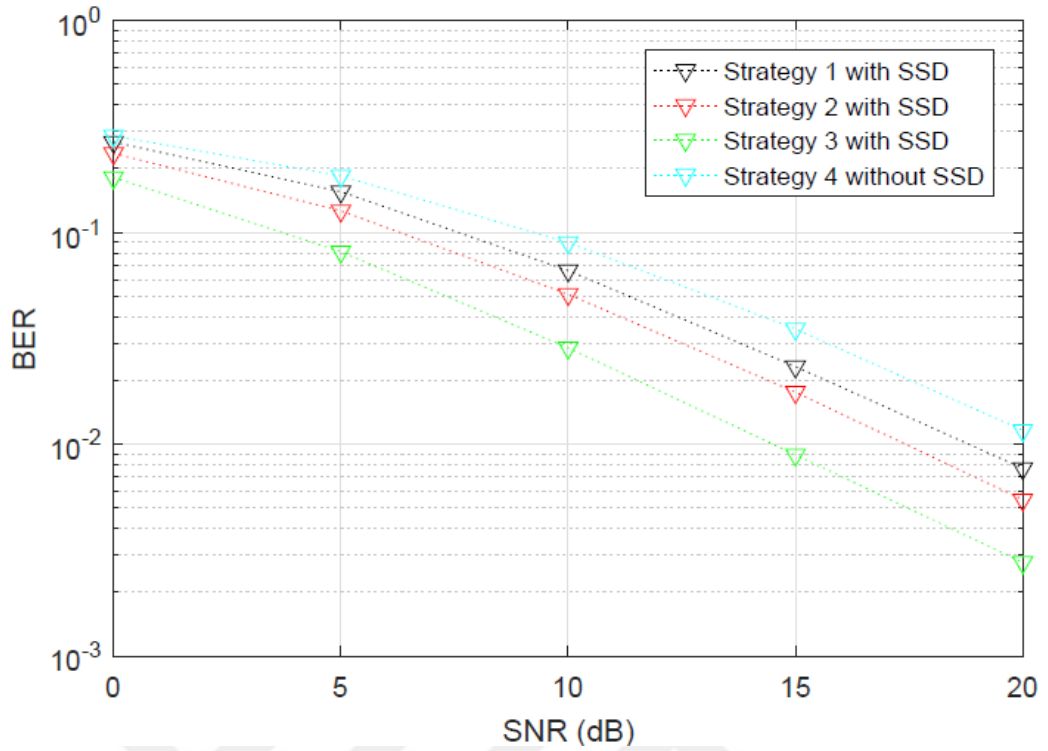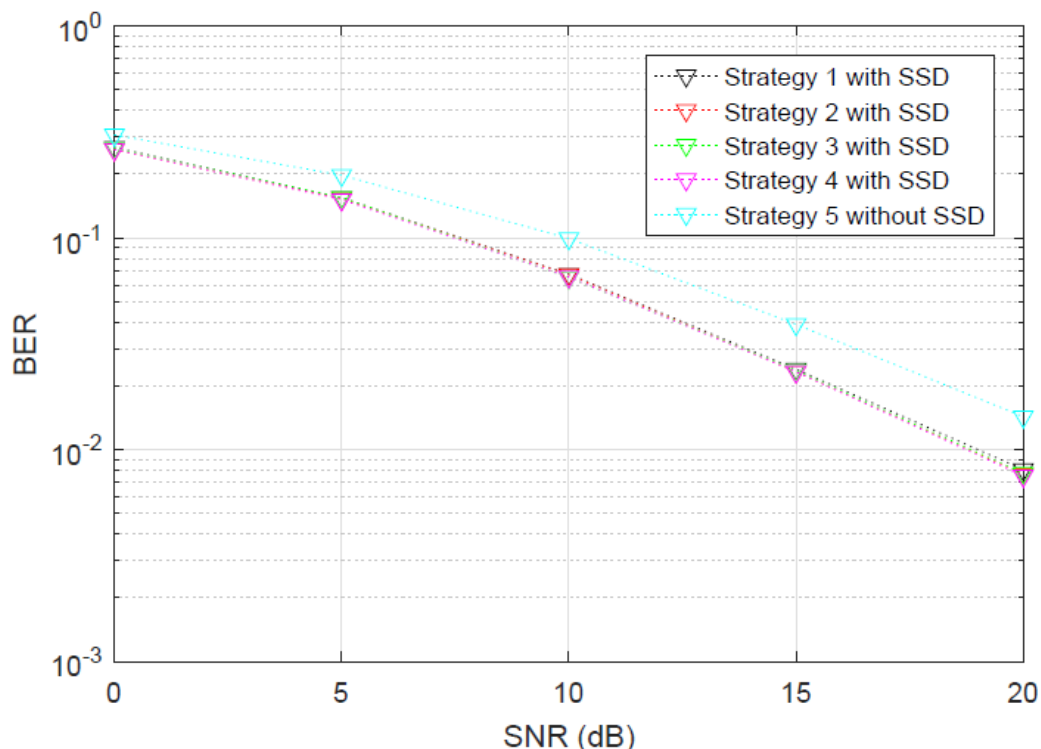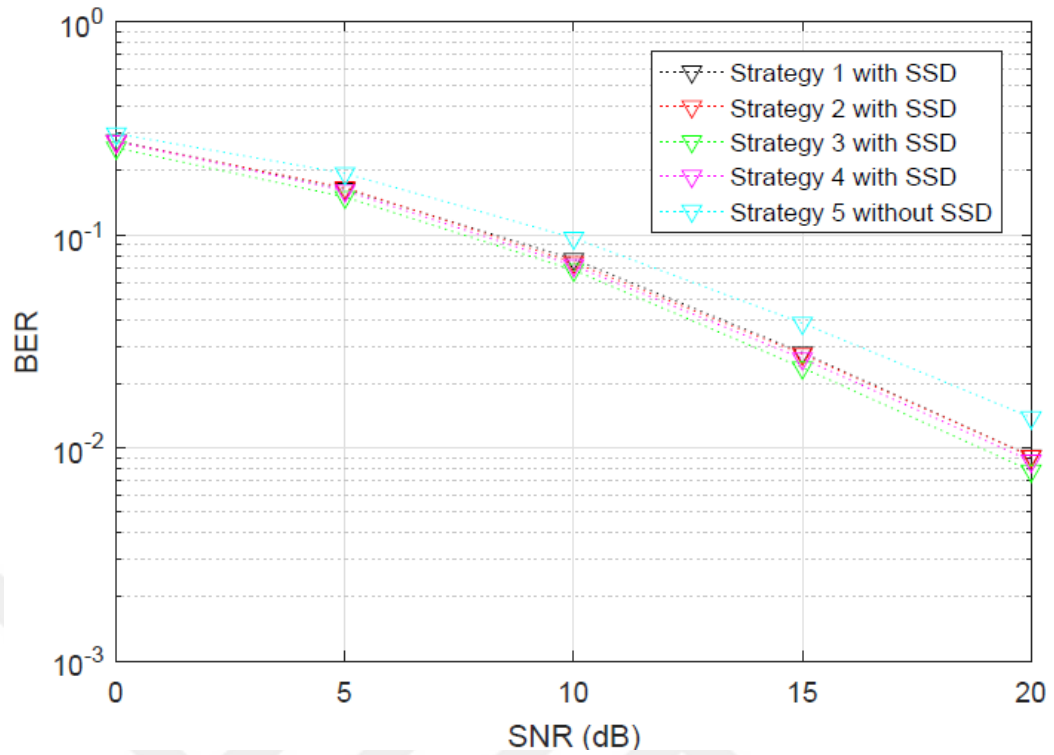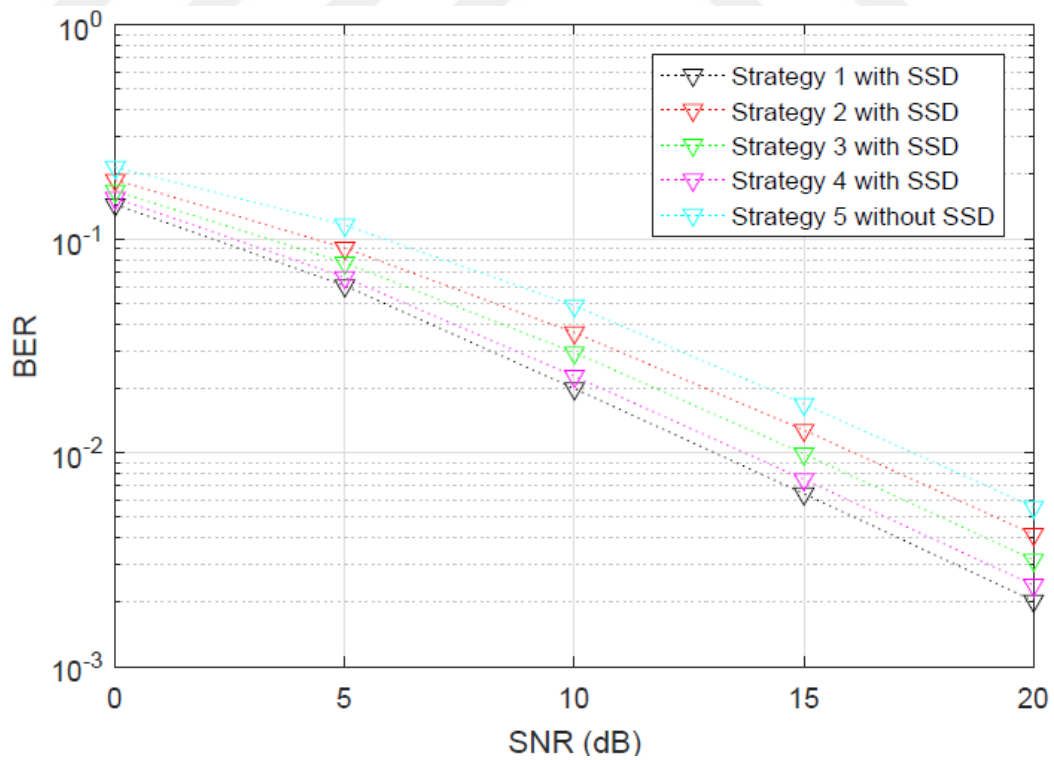

Figure 3.16 The comparison of the BER performances for the relevant strategies with five transmit and receive antennas under exponential correlation.

3.5 Conclusion

In this chapter, the performance of ZFRBF with SSD for two different (time and spatial) interleaving techniques has been analyzed and its hardware complexity has been studied by means of FPGA implementation. The exact ABEP expression and the optimum rotation angle value of time-interleaved BPSK have been derived. Union bound is used to find the approximate ASEP expression of QPSK with SSD. The near-optimum rotation angles for QPSK with SSD have also been determined. The simulations show that the error performance of ZFRBF can be improved highly by utilizing SSD especially under the time interleaving method. There is a trade-off between the time and spatial interleaving approaches in terms of latency and error performance. It has been shown that with a bit-width value of 20, the performance of the fixed point model approximately matches the floating point model. It has also been demonstrated with the FPGA implementation that SSD causes only a slight increase in complexity whilst using no extra bandwidth or time slots. SSD brings in 0.71% extra complexity at most for a complete receiver, which is highly negligible and tolerable regarding the huge error performance increment that comes along with it. Finally, spatial interleaving is implemented into a ZF MIMO system over slow flat Rayleigh fading channels with BPSK modulation for correlated transmit antennas and uncorrelated receive antennas. Assuming three models for transmit antenna correlation, bit error rate performances of the different component interleaving strategies have been examined. It is shown that the performance of the system depends on the used component interleaving strategy as different interleaving strategies perform differently under distinct types of correlation models. The presented method in this chapter can also be applied to other two-dimensional modulation schemes. The optimal rotation angles under these schemes can also be derived based on the PEP expressions presented in this chapter.

CHAPTER 4

IMPROVING PHYSICAL LAYER SECURITY IN ALAMOUTI OFDM SYSTEMS WITH SUBCARRIER COORDINATE INTERLEAVING

This chapter is based on [29] and [30], where Alamouti space-time block coded OFDM is incorporated with signal space diversity (SSD) in order to significantly strengthen the physical layer security of the communication network. The coordinate interleaving step of SSD is performed amongst OFDM subcarriers. Based on the correlation coefficients between the subcarrier channel gains, distinct coordinate interleaving strategies are used and compared in terms of bit error rate. The proposed system model is able to improve the security by enabling a legitimate user to have much less error than an eavesdropper, even under the worst-case scenario where the unauthorized receiver somehow captures the interleaving strategy compromised by the transmitter and legitimate receiver. An exact closed-form expression of the bit error rate is derived for the legitimate user and shown to match with the simulation results. Finally, it is demonstrated that the system is also capable of enhancing the resistance against channel estimation errors at the receiver. The proposed system does not require high complexity or additional bandwidth or time resources.

4.1. Introduction

Security has always been one of the most important challenges regarding wireless communications. Due to its broadcasting structure, any receiver in the coverage area of the transmitter can access wireless channels. Thus, wireless links are vulnerable against illegitimate eavesdropping threatening the privacy of legitimate users. Many traditional upper layer security solutions that have been proposed are either not capable enough or require high computational complexity and cost. The most common method using secret keys between the transmitter and receiver is becoming more vulnerable against security threats with the tremendous increment of computational power [73]. Physical layer security (PLS) is being considered as a better alternative or a

performance booster of traditional security methods that rely on encryption and secret keys. In order to achieve this type of security, key traits of a wireless communication environment, such as fading, interference, and path diversity are generally utilized [74]. There are two main benefits of PLS over the encryption techniques. First, it does not depend on computational complexity and secondly it does not have a centralized structure [75]. Various PLS capacity studies have been applied for wireless fading channels where both the transmitter and receiver are equipped with a single antenna [76-81]. Recently, PLS of multiple antenna schemes are also investigated [82-90].

Alamouti space-time block coding (STBC) scheme is one of the most utilized techniques to attain transmit diversity without the requirement for channel state information (CSI) at the transmitter. With Alamouti STBC, multiple transmit antennas provide space diversity by sending two signals over two distinct time periods. Another commonly used technique is the orthogonal frequency division multiplexing (OFDM), which has become a part of contemporary standards throughout the years. It is well known that frequency selective fading channels can be converted into several narrowband flat fading channels by exploiting OFDM. Thus, Alamouti scheme and OFDM can be jointly used in order to attain a good performance/complexity tradeoff in frequency selective fading environments [90-97]. OFDM is also frequently used along with other multiple-input multiple-output techniques in order to improve PLS [98-102].

Signal space diversity (SSD), known for its bandwidth and power efficiency, increases the diversity of a communication system by utilizing the orthogonal dimensions already within the signal space [14]. In order to achieve this with two-dimensional signal constellations, such as phase shift keying (PSK) and quadrature amplitude modulation (QAM), SSD first applies signal constellation rotation in such a way that every point in the signal constellation has distinct in-phase (I) and quadrature (Q) components. Following that, coordinate interleaving (CI) operation takes place so that the I and Q components of each symbol is transmitted via independent paths. With multiple antennas and multi carrier systems, the latter condition can be realized by sending the components of the transmitted signal from different antennas, time slots or subcarrier channels.

The concept of coordinate interleaved orthogonal design has been proposed in [58], which is demonstrated to be able to achieve full-rate, full-diversity and single-symbol maximum likelihood (ML) decodability for complex signal constellation diagrams. STBC and SSD are integrated in [56] and the error performance of the system is presented under Nakagami-m fading environments. A combination of SSD and Alamouti STBC is proposed in [103] to boost the diversity order. Similarly, in [104] SSD has been combined with Alamouti scheme and new full-rate STBCs that can attain full diversity for QAM are constructed. To obtain more diversity gain in fading environments, SSD with Alamouti STBC is considered in [105] and the effect of constellation rotation angle on the performance is demonstrated.

In [106], OFDM is used with SSD in such a way that the constellation rotation angle is optimized for every subcarrier. A grouped linear constellation precoded (GLCP) OFDM technique is analyzed in [107] and it is found out that it can achieve maximum multipath diversity with subcarrier grouping. The optimal subcarrier grouping for GLCP OFDM is derived in [108] by taking the correlation structures of subcarriers into consideration. In [109], different CI approaches that try to minimize the correlation coefficient between the fading coefficients affecting the components of a transmitted symbol have been offered for various scenarios. The studies [110-112] mainly focus on the OFDM-SSD schemes for security purposes. Dynamic subcarrier CI is applied for OFDM in [110]. The case for imperfect channel reciprocity is considered in [111] and a compensation model based on minimum mean square prediction is proposed. With an adaptive interleaving scheme that is based on the CSI between the transmitter and legitimate receiver, the study in [112] attains security enhancement. Here, the components affected from fading badly are interleaved with those having less fading.

In this chapter, a novel technique that applies a CI strategy similar to the one in [109] for Alamouti OFDM SSD systems is offered in order to highly improve the PLS of the network. The method enhances the error performance of a legitimate user without serious complexity increase. Even in the worst-case scenario, where the unauthorized user somehow discovers the CI strategy of the transmitter, it experiences a significantly lower error performance than the legitimate user. The reason behind this

is that the CI approaches used in the system are dependent on the main communication link between the transmitter and the legitimate receiver. Furthermore, it is shown that the proposed model significantly increases the immunity against channel estimation errors (CEE) at the receiver. Rotated binary phase shift keying (BPSK) modulation for symbol mapping is used. In order to apply CI, only **Q** components of two different symbols are swapped by taking the correlation coefficient between the subcarrier gains into consideration. Thus, different CI approaches are used for distinct communication scenarios in which it is tried to make the correlation coefficients between the subcarrier gains affecting the symbol components equal to zero. An exact closed-form bit error rate (BER) expression for the legitimate user is derived and demonstrated to be compatible with the simulation results.

4.2. System Model

In this chapter, a three node wireless network is considered. Alice is the transmitter and communicates with an authorized user Bob through the main channel **H**. An unauthorized user Eve tries to eavesdrop the transmission channel between Alice and Bob. The channel between Alice and Eve is represented with **H'**. The eavesdropper is of passive type, which implies that it just attempts to tap the main channel but does not transmit anything to distort the communication between Alice and Bob. For both of the transmissions between Alice and Bob, and between Alice and Eve, a multiple-input single-output system with two transmit antennas under a frequency selective channel is considered. OFDM is utilized in order to transform the frequency selective fading channel into a series of parallel flat fading channels. In addition, it is assumed that the channel characteristics do not change during the transmission of one Alamouti OFDM period and alter independently between two transmission periods. Full CSI is known only at the receivers, i.e., Bob (Eve) has knowledge of **H** (**H'**).

4.2.1 Transmitter

Let 2N be the total number of symbols transmitted over an Alamouti OFDM period. Note that N represents the number of OFDM subcarriers (assumed a power of two) and L denotes the number of resolvable transmission paths for the both channels. Suppose that the length of the CP (in terms of symbol number) equals L. Each of the

OFDM subcarriers carries one modulated symbol coming from a $\pi/4$-rotated BPSK signal constellation. Note that, the system can also be used with other $\pi/4$-rotated one-dimensional modulation schemes (such as amplitude shift keying or pulse amplitude modulation) optimally. The transmitter block diagram is given in Figure 4.1.
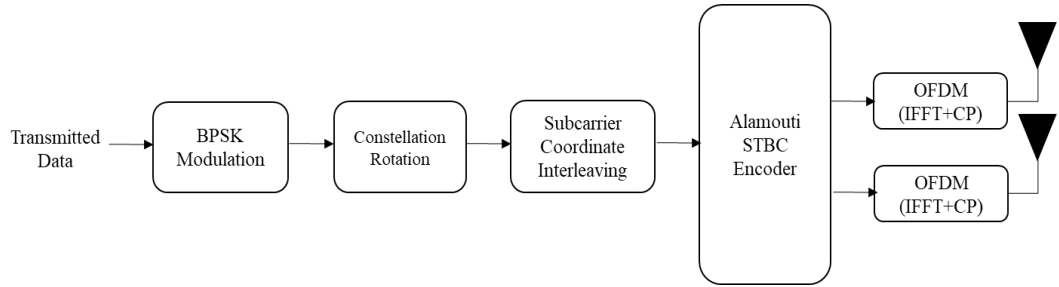

Figure 4.1 Block diagram of the transmitter.

The modulator produces an independent modulated symbol sequence $\{s_1,s_2,\ldots,s_{2N}\}$, where E_b represents the energy per bit and $|s_\alpha|^2=E_b(N/(2N+2L))$ for $\alpha\in\{1, 2,\ldots,2N\}$. The coefficient $N/(2N+2L)$ is needed in order to normalize the symbol power by taking the power loss caused by the cyclic prefix symbols during an Alamouti OFDM transmission. The symbols can be further decomposed as $s_\alpha=s_{\alpha I}+ js_{\alpha Q}$, where $s_{\alpha I}$ and $s_{\alpha Q}$ show the αth symbol's I and Q components, respectively. CI is applied on the symbol sequence $\{s_1,s_2, \ldots,s_{2N}\}$ by interleaving Q components only according to the interleaving strategy. The interleaved sequence of symbols is denoted as $\{X_1,X_2,\ldots,X_{2N}\}$. We can express X_α as $X_\alpha=s_{\alpha I}+js_{\beta Q}$ for $\alpha,\beta\in\{1, 2,\ldots,2N\}$ with $\alpha\neq\beta$. Alamouti STBC is applied on $\{X_1,X_2,\ldots,X_{2N}\}$. In this sense, four sequences each of which contains N elements are produced. These four sequences are given by $\{X_1,X_3,\ldots,X_{2N-1}\}$, $\{X_2,X_4,\ldots,X_{2N}\}$, $\{-X_2^*,-X_4^*,\ldots,-X_{2N}^*\}$, and $\{X_1^*,X_3^*,\ldots,X_{2N-1}^*\}$. In the first time period, $\{X_1,X_3,\ldots,X_{2N-1}\}$ and $\{X_2,X_4,\ldots,X_{2N}\}$ are fed to two independent N-IFFT blocks, output of which are respectively transmitted (after CP addition) from the first and second transmit antennas. Note that this operation (called transmission of an OFDM frame) requires a duration of N symbol time slots. The same process takes place in the second time period where two independent IFFT operations are applied on $\{-X_2^*,-X_4^*, \ldots,-X_{2N}^*\}$ and $\{X_1^*,X_3^*,\ldots,X_{2N-1}^*\}$.

4.2.2 Channel models

Rayleigh fading channel

Under the Rayleigh fading channel scenario, the channel has a multipath structure that can be modelled as a finite impulse response filter with L taps. The tap coefficients are independent and identically distributed (IID) zero-mean complex Gaussian random variables each having an average power of 1/L. Assume that $h_{v,l}$ denotes the lth ($l \in \{1,2,\dots,L\}$) tap of the channel between the vth ($v \in \{1,2\}$) transmit antenna and the receive antenna for the main channel.

Nakagami-m fading channel

It is assumed that, when shown in the polar coordinate system for $h_{v,l} = |h_{v,l}| e^{j\theta_{v,l}}$, $|h_{v,l}|$ and $\theta_{v,l}$ are independent random variables. Following that, $|h_{v,l}|$ magnitudes has Nakagami-m probability distribution function (pdf) for r≥0 as shown below:

$$f_{|h_{v,l}|}(r) = \frac{2m^m r^{2m-1} \exp(-mr^2)}{\Gamma(m)}. \qquad (4.1)$$

Here, m is the parameter that defines the shape of the pdf. Additionally, $E\{|h_{v,l}|^2\} = 1$ thus all of the channel coefficients have identical average power (uniform power delay profile). The effect of the fading will decrease as m increases. Also, all of the $\theta_{v,l}$ values have a uniform distribution between 0 and 2π. It is assumed that all channel coefficients have the same m value. It can be shown that the elements $H_{v,k}$ are identically distributed and correlated between each other Gaussian random variables and they are also equal to the summation of L IID Nakagami-m random phase vectors.

4.2.3 Receiver

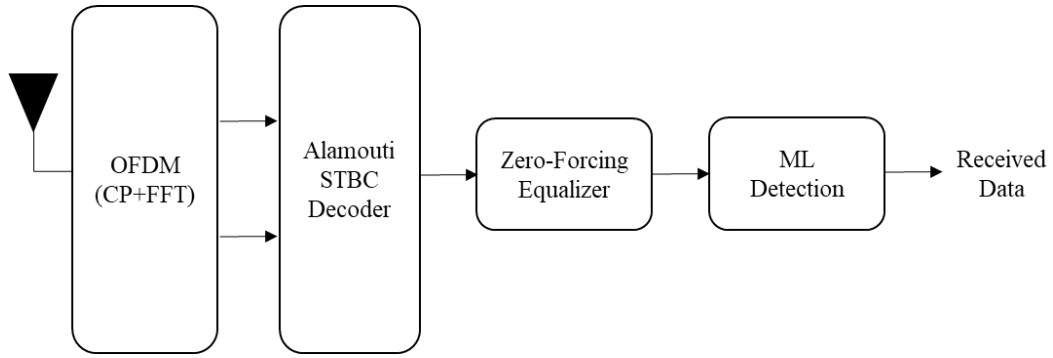The block diagram of the receiver is given in Figure 4.2.

Figure 4.2 Block diagram of the receiver.

At the receiver, CP removal and N-FFT operations are respectively applied on the first received frame to yield $\{Y_{1,1}, Y_{1,2}, \ldots, Y_{1,N}\}$. The same procedure is repeated on the second received frame and $\{Y_{2,1}, Y_{2,2}, \ldots, Y_{2,N}\}$ is obtained. Alamouti decoding is subsequently performed N times. The Alamouti decoding process can be explained for the kth step ($k \in \{1,2,\ldots,N\}$) as follows: Let $\mathbf{X}_k = [X_{2k-1}\ X_{2k}]^T$, and $\mathbf{Y}_k = \left[Y_{1,k}\ Y_{2,k}^*\right]^T$, and

$$\mathbf{H}_k = \begin{bmatrix} H_{1,k} & H_{2,k} \\ H_{2,k}^* & -H_{1,k}^* \end{bmatrix}$$ where $H_{v,k}$ for $v \in \{1,2\}$ represents the kth element of the vector obtained by applying N-point FFT on $\{h_{v,1}, h_{v,2}, \ldots, h_{v,L}\}$. It can be shown that $H_{v,k}$'s are identically distributed zero-mean complex Gaussian random variables with $E\{|H_{v,k}|^2\}=1$. We can write:

$$\mathbf{Y}_k = \mathbf{H}_k \mathbf{X}_k + \mathbf{Z}_k \tag{4.2}$$

where $\mathbf{Z}_k$ is a noise vector with IID zero-mean complex Gaussian noise components each with a variance of $N_0/2$ per dimension. A zero-forcing (ZF) equalizer is utilized to recover $\mathbf{X}_k$ where the left-hand side of (4.2) is multiplied with $\mathbf{A}_k \mathbf{H}_k^{-1}$ where $\mathbf{H}_k^{-1}$ represents the inverse of $\mathbf{H}_k$ and the matrix $\mathbf{A}_k$ is given by $\mathbf{A}_k = \sqrt{|H_{1,k}|^2 + |H_{2,k}|^2}\, \mathbf{I}_2$ ($\mathbf{I}_2$ is a 2x2 identity matrix). The equalization procedure can be shown as $\widetilde{\mathbf{Y}}_k = \mathbf{A}_k \mathbf{H}_k^{-1} \mathbf{Y}_k = \mathbf{A}_k \mathbf{X}_k + \widetilde{\mathbf{Z}}_k$ with $\widetilde{\mathbf{Y}}_k = \left[\widetilde{Y}_{1,k}\ \widetilde{Y}_{2,k}\right]^T$ and $\widetilde{\mathbf{Z}}_k = \mathbf{A}_k \mathbf{H}_k^{-1} \mathbf{Z}_k$. Assume that the ML detector forms the decision variables d_{2k-1} and d_{2k} to recover the $(2k-1)^{th}$ and $2k^{th}$ modulated symbols (s_{2k-1} and s_{2k}) by applying coordinate deinterleaving (CD) in accordance with the CI process applied at the transmitter for $k \in \{1,2,\ldots,N\}$. We have

$$d_{2k-1}=R\{\widetilde{Y}_{1,k}\}+jI\{\widetilde{Y}_{1,m}\}$$

$$=\sqrt{\left|H_{1,k}\right|^2+\left|H_{2,k}\right|^2}s_{2k-1,I}+j\sqrt{\left|H_{1,m}\right|^2+\left|H_{2,m}\right|^2}s_{2k-1,Q}+\breve{Z}_{2k-1} \qquad (4.3)$$

and

$$d_{2k}=R\{\widetilde{Y}_{2,k}\}+jI\{\widetilde{Y}_{2,m}\}$$

$$=\sqrt{\left|H_{1,k}\right|^2+\left|H_{2,k}\right|^2}s_{2k,I}\quad+j\sqrt{\left|H_{1,m}\right|^2+\left|H_{2,m}\right|^2}s_{2k,Q}+\breve{Z}_{2k} \qquad (4.4)$$

where the value of m (m $\in$ {1,2,...,N} and k $\neq$ m) is determined by the CI strategy. Also, $\breve{Z}_{2k-1}$ and $\breve{Z}_{2k}$ are the noise components after CD and their real and imaginary parts are IID zero-mean Gaussian random variables each with a variance of $N_0/2$.

In order to determine the interleaving strategy, the approach in [109, Section IV.B] is utilized. Using this method, it is ensured that $H_{1,k}$ and $H_{1,m}$ ($H_{2,k}$ and $H_{2,m}$) are uncorrelated for all k and m values, where k,m $\in$ {1,2,...,N} and k$\neq$m. It is assumed that N and L have multiple common factors such that more than one CI strategies making $H_{1,k}$ and $H_{1,m}$ ($H_{2,k}$ and $H_{2,m}$) uncorrelated exist.

4.3 Bit Error Rate Analysis

In this section, a bit error rate analysis of the proposed system under Rayleigh fading channel is performed, where perfect CSI at the receiver is assumed, i.e., $\varphi=1$. Let the channel gains affecting the I and Q components of the $(2k-1)^{th}$ and $(2k)^{th}$ modulated symbols be denoted by $\{\gamma_{2k-1}, \psi_{2k-1}\}$ and $\{\gamma_{2k}, \psi_{2k}\}$ respectively. Then, it can be written that $\gamma_{2k-1}=\gamma_{2k}=\sqrt{\left|H_{1,k}\right|^2+\left|H_{2,k}\right|^2}$ and $\psi_{2k-1}=\psi_{2k}=\sqrt{\left|H_{1,m}\right|^2+\left|H_{2,m}\right|^2}$ (k,m $\in$ {1, 2, ..., N} and k$\neq$m). Let e_α ($\alpha\in$ {1,2,...,2N}) be the event that the αth modulated symbol is erroneously detected at the receiver. Note that e_α ($\alpha\in$ {1,2,...,2N}) are equiprobable. Thus, the conditional BER (instantaneous BER) is given by:

$$P\left(e|\gamma_1, \gamma_2, \ldots \gamma_{2N}, \psi_1, \psi_2, \ldots, \psi_{2N}\right)=$$

$$\frac{P(e_1|\gamma_1, \psi_1) + P(e_2|\gamma_2, \psi_2) + P(e_3|\gamma_3, \psi_3) + \ldots + P(e_{2N}|\gamma_{2N}, \psi_{2N})}{2N}. \qquad \textbf{(4.5)}$$

Assuming ML decision rule and utilizing the symmetry among the unconditional error probabilities, the unconditional BER can be written as $P(e)=E\left\{P\left(e_1|\gamma_1, \psi_1\right)\right\}$ where the expectation is taken over γ_1 and ψ_1. Using the approach in [109], we can write:

$$P(e) = \frac{1}{\pi} \int_0^{\pi/2} \int_0^\infty \int_0^\infty \exp\left(-\frac{N}{2N+2L}\frac{\gamma_1^2 E_b + \psi_1^2 E_b}{2N_0 \sin^2(\emptyset)}\right) f(\gamma_1) f(\psi_1) d\gamma_1 d\psi_1 d\emptyset. \qquad \textbf{(4.6)}$$

Applying change of variables as $x_1 = \gamma_1^2$ and $x_2 = \psi_1^2$, we can write:

$$P(e) = \frac{1}{\pi} \int_0^{\pi/2} \int_0^\infty \int_0^\infty \exp\left(-\frac{N}{(2N+2L)}\frac{E_b}{2N_0}\frac{x_1+x_2}{\sin^2(\emptyset)}\right) x_1 x_2 \exp\left(-(x_1+x_2)\right) dx_1 dx_2 d\emptyset \qquad \textbf{(4.7)}$$

where x_1 and x_2 are IID chi-squared random variables each with four degrees of freedom. Integrating (4.7) with respect to x_1 and x_2 leads to:

$$P(e) = \frac{1}{\pi} \int_0^{\pi/2} \frac{16}{\left(2 + \frac{N}{(2N+2L)N_0 \sin^2(\emptyset)}\right)^4} d\emptyset. \qquad \textbf{(4.8)}$$

It is given in [72, 5A.4b] that the definite integral $I_m = \frac{1}{\pi} \int_0^{\pi/2} \left(\frac{\sin^2\theta}{\sin^2\theta + c}\right)^m d\theta$ can be evaluated as $J_m(c) = \left(\frac{1-\mu(c)}{2}\right)^m \sum_{k=0}^{m-1} \binom{m-1+k}{k} \left(\frac{1+\mu(c)}{2}\right)^k$, where $\mu(c) = \sqrt{\frac{c}{1+c}}$ and m is an integer. Using this result, we can evaluate (4.8) as:

$$P(e) = \left(\frac{1-\rho}{2}\right)^4 \sum_{z=0}^{3} \binom{3+z}{z} \left(\frac{1+\rho}{2}\right)^z \qquad \textbf{(4.9)}$$

where $\rho = \sqrt{\frac{E_b/2N_0}{2 + 2\frac{L}{N} + \frac{E_b}{2N_0}}}$. For sufficiently high E_b/N_0 values, we can neglect the term "2". In such a case, the diversity order of the system can be shown to be equal to 4.

4.4. Numerical Results

In this section, some numerical results regarding the system model's error performance under different scenarios and channel models are presented.

4.4.1 Scenarios under Rayleigh fading channel model

Firstly, how the usage of CI affects the error performance for both a random CI scheme and the optimum CI strategy proposed in this chapter is shown. Secondly, a scenario as follows is considered. A transmitter (named Alice) communicates with an authorized (legitimate) receiver (named Bob) while an unauthorized (illegitimate) receiver (named Eve) tries to eavesdrop the conversation. The performances of Bob and Eve are compared and how the suggested technique can improve the PLS is demonstrated. Finally, it is illustrated how the system model can also be useful for enhancing resistance against CEE.

In the first scenario, the performances of the proposed CI method, a random CI scheme, and no CI case for N = 32 and L = 4 are compared. The random CI technique randomly interleaves Q components (without any consideration on the correlation between the channel gains affecting any modulated symbol) as in [109]. In Figure 4.3, the error performances of the relevant models for the first scenario are compared. It can be clearly seen that when CI is used, a significant improvement can be achieved even with the random CI method. Approximately 2.13 dB gain can be attained at a BER of 10^{-3} with the random CI strategy as compared to the standard Alamouti OFDM model without CI. The performance gain is even greater with the proposed scheme as it outperforms the no CI case by approximately 4 dB. Moreover, the total match between the analytical and simulation results under the proposed optimum CI strategy shows the accuracy of the theoretical BER formula in (4.9). In the following four scenarios, Bob's error performance is compared with Eve's according to different CI strategies that change relative to the relationship between N and L. In the simulations, the scenarios where N = 32 and L = 4, N = 32 and L = 8, N = 128 and L = 4, N = 128 and L = 8 are assumed. It is assumed that Alice and Bob have an identical lookup table
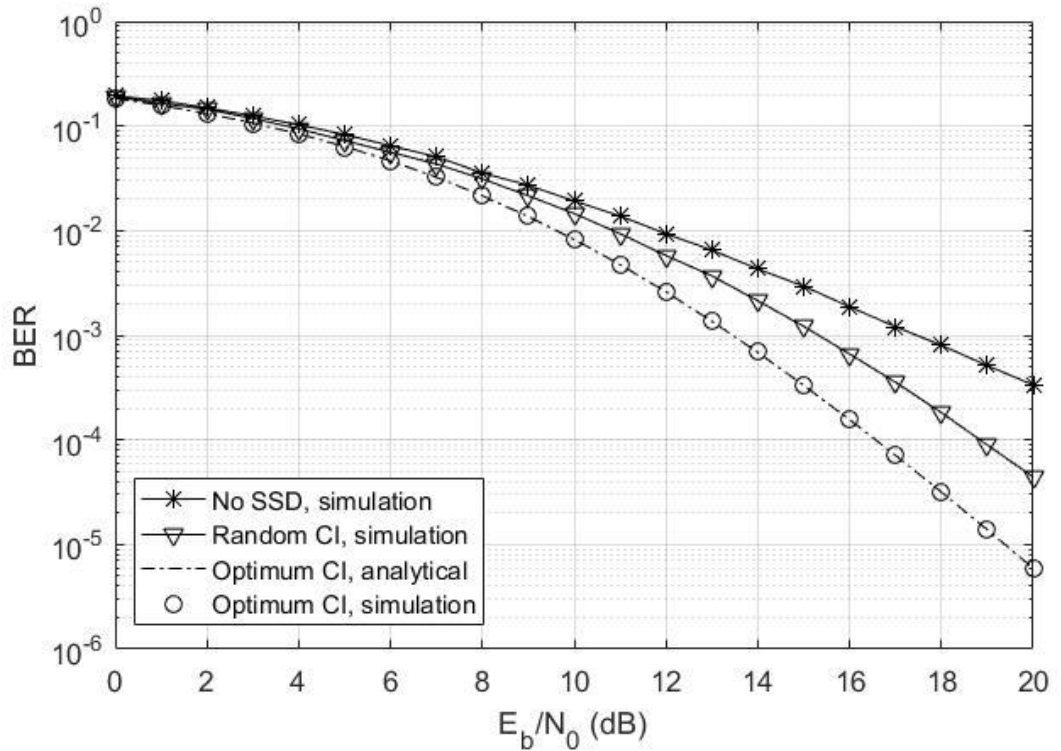
Figure 4.3 BER comparison of the relevant models for N = 32 and L = 4.

including indices to the different CI strategies making $H_{1,k}$ and $H_{1,m}$ ($H_{2,k}$ and $H_{2,m}$) uncorrelated. For the considered scenarios, there are multiple such CI strategies. Hence, Bob performs a comparison among these strategies and sends back the index of the strategy minimizing the instantaneous BER to the transmitter. This process requires a low-rate (only a few bits) feedback channel from Bob to Alice. In addition, it is demonstrated how the proposed model affects Eve's performance under two conditions. First, it is assumed that Eve has the knowledge of the values of N and L but does not know which interleaving strategy Alice is employing. Therefore, Eve randomly chooses one of the appropriate deinterleaving strategies that make the correlation between $H_{1,k}$ and $H_{1,m}$ ($H_{2,k}$ and $H_{2,m}$) equal to zero. Later, as a worst-case scenario, it is considered that Eve knows the values of N, L and even has the ability to intercept the feedback information sent from Eve to Alice. Thus, Eve can adjust her deinterleaving strategy to match exactly with Alice's interleaving strategy.

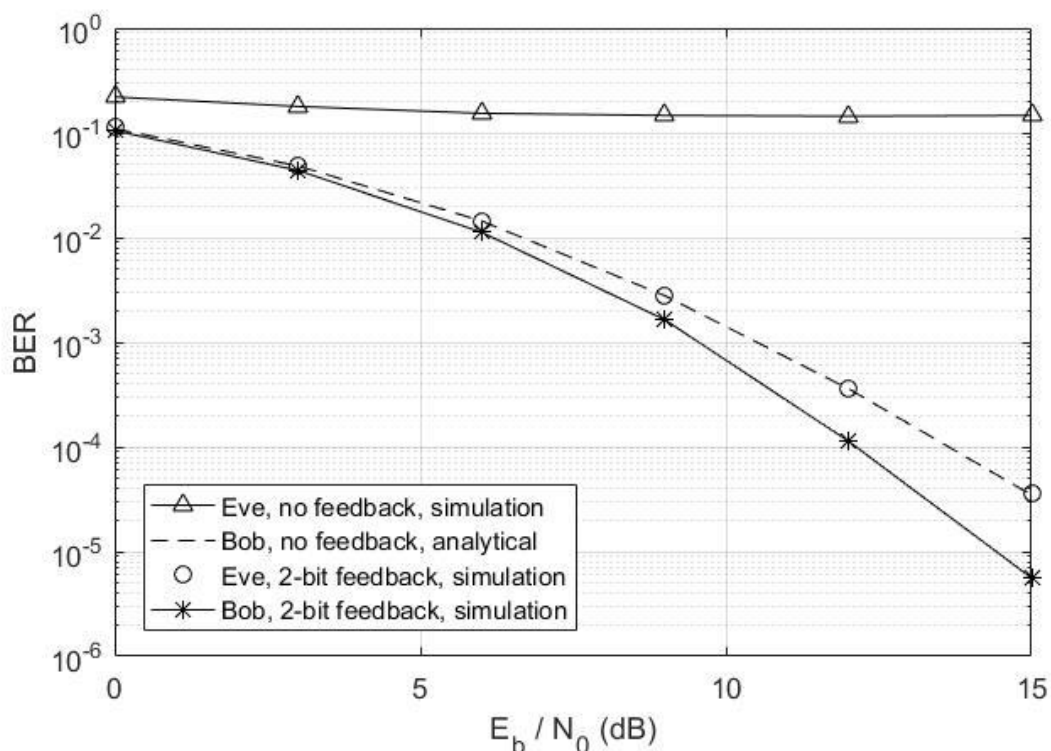In the first scenario, Bob's and Eve's performances for N = 32 and L = 4 are compared in Figure 4.4.

Figure 4.4 BER comparison of the legitimate user Bob and the illegitimate user Eve for N=32 and L=4.

There are three CI strategies making $H_{1,k}$ and $H_{1,m}$ ($H_{2,k}$ and $H_{2,m}$) uncorrelated in this case. These are represented by three different (k-m) values given by: 8, 16, and 24. The receiver uses a $\lceil \log_2 3 \rceil = 2$ bits feedback channel to inform the transmitter about the appropriate strategy that should be used. In Figure 4.4, it is definitely obvious that Eve's performance is totally ruined when she has no feedback information that shows that the communication link between the transmitter and legitimate user is secure. In addition, it can clearly be seen that even under the worst-case where Eve captures the feedback information, the proposed approach still provides a significant error performance advantage in favor of the legitimate user. For this worst-case, Bob has an approximate 1.63 dB gain lead over Eve at a BER of 10^{-4} with the CI strategy. The reason behind this can be explained as follows: The system decides on which strategy to use according to Bob's channel-dependent feedback. Even though Eve knows the strategy of Bob, it may not be the optimum strategy to use with her own channel. In fact, the probability that the strategy of Bob is the optimum strategy for Eve is equal

to 1/3. In this sense, the curve corresponding to Eve's performance when she has the feedback information also represents Bob's error performance with no instantaneous feedback. This is justified by the strong match between the analytical results and Eve's performance with the feedback information.

In the second case, Bob's and Eve's performances for N = 32 and L = 8 are demonstrated in Figure 4.5.

Figure 4.5 BER comparison of the legitimate user Bob and the illegitimate user Eve for N=32 and L=8.

There exist seven values of (k-m) that make $H_{1,k}$ and $H_{1,m}$ ($H_{2,k}$ and $H_{2,m}$) uncorrelated: 4, 8, 12, 16, 20, 24, and 28. However, (k-m) = 20 is excluded, as it leads to the same instantaneous BER with (k-m) = 12. The feedback channel needed for this scenario is $\lceil \log_2 6 \rceil = 3$ bits. In Figure 4.5, it can be clearly seen that Eve's performance is completely deteriorated without the feedback information that enables a secure communication link between Alice and Bob that prevents Eve to detect the transmitted data in a correct fashion. It is also demonstrated that Bob benefits a much higher gain than Eve under the worst circumstance. Bob has an approximate 2 dB advantage over

Eve for a BER of 10^{-4}. Finally, the theoretical curve of Bob that uses no feedback totally matches the performance of Eve with 3 bits feedback as expected. In Figure 4.6, Bob's and Eve's performances under the conditions N = 128 and L = 4 are compared.
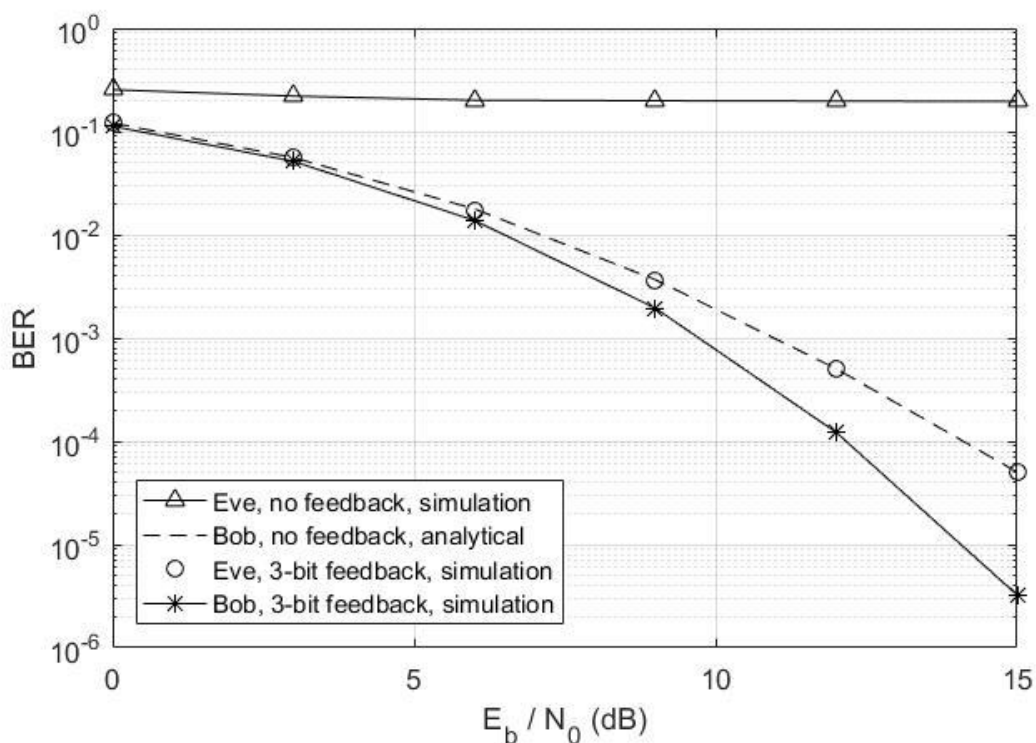

Figure 4.6 BER comparison of the legitimate user Bob and the illegitimate user Eve for N=128 and L=4.

There are three values of (k-m) that make $H_{1,k}$ and $H_{1,m}$ ($H_{2,k}$ and $H_{2,m}$) uncorrelated: 32, 64, and 96. The receiver needs a $\lceil \log_2 3 \rceil = 2$ bits feedback channel in this case. In Figure 4.6, it is definitely obvious that Eve's performance is totally ruined with the lack of feedback information showing that the communication link between the transmitter and legitimate user is secure. Furthermore, it is clear that under the worst-case security assumption, the proposed interleaving strategy favors the legitimate user heavily. Bob leads over Eve with an approximate 1.56 dB gain at a BER of 10^{-4}. The strong match between the theoretical curve of Bob that uses no feedback and the performance of Eve with 2 bits feedback is once again observed. Bob's and Eve's performances for the parameters N = 128 and L = 8 are studied in Figure 4.7.
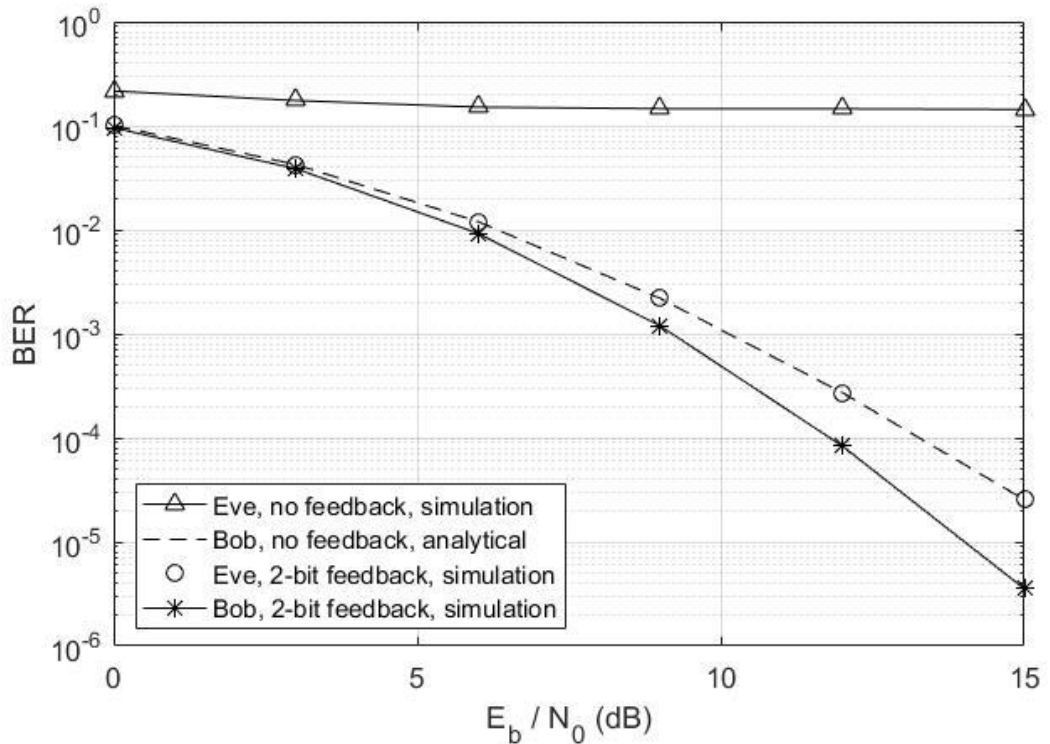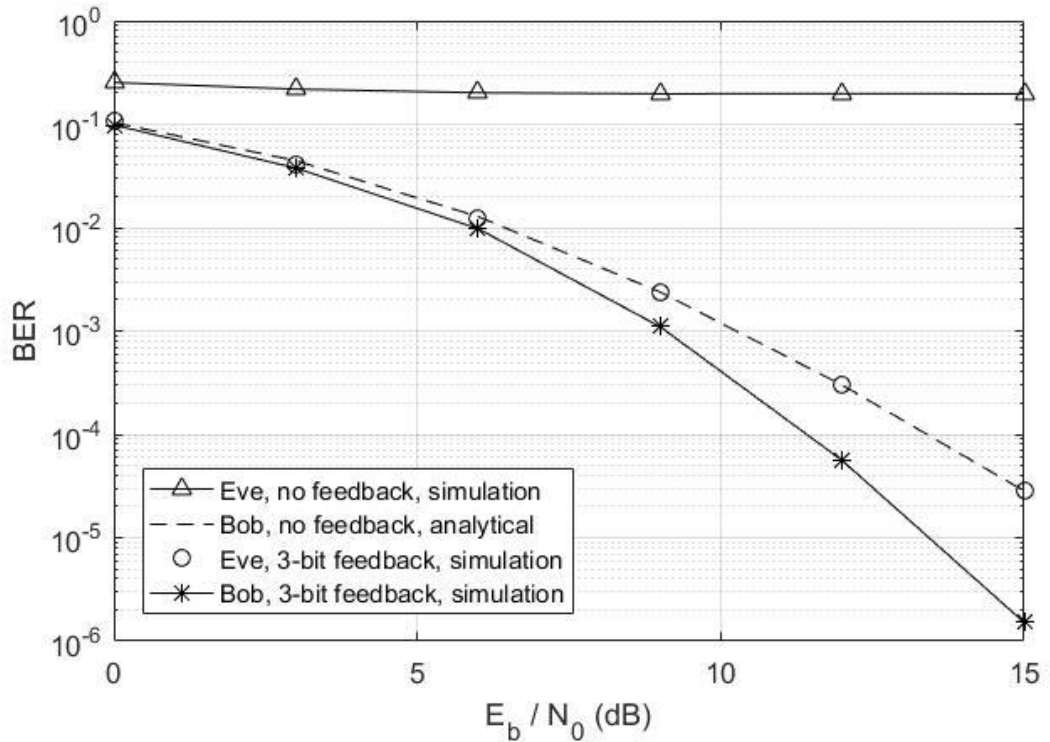
Figure 4.7 BER comparison of the legitimate user Bob and the illegitimate user Eve for N=128 and L=8.

Seven values of (k-m) make $H_{1,k}$ and $H_{1,m}$ ($H_{2,k}$ and $H_{2,m}$) uncorrelated: 16, 32, 48, 64, 80, 96, and 112. As before, (k-m) = 80 is excluded because that it results with the same instantaneous BER with (k-m) = 48. The feedback channel required is also $\lceil \log_2 6 \rceil$=3 bits. In Figure 4.7, it is definitely obvious that Eve's performance is entirely demolished demonstrating that the communication link between the transmitter and legitimate user is reliable. It can also be clearly seen that Bob has a much higher gain than Eve even when Eve captures the feedback information. For a BER of 10^{-4}, Bob possesses an approximate 2 dB gain lead over Eve. Lastly, it is one more time clear that the theoretical curve of Bob that uses no feedback and the performance of Eve with 3 bits feedback yield the same result.

As a practical impairment, the receiver is assumed to have an erroneous CSI for the final scenario. In this sense, the imperfection in CSI is modeled as follows:

$$\hat{h}_{v,l} = \varphi h_{v,l} + \sqrt{1-\varphi^2} e_{v,l} \tag{4.10}$$

where $h_{v,l}$ denotes the actual channel coefficient regarding the lth path between the vth transmit antenna and the receive antenna (l= 1, 2, …, L and v = 1, 2) [113]. Also, $e_{v,l}$ shows the associated CEE. The two complex random variables $h_{v,l}$ and $e_{v,l}$ are IID zero-mean complex Gaussian random variables with a variance value equal to one. The variable φ represents the correlation coefficient between $h_{v,l}$ and $e_{v,l}$. It is an indicator of how accurate the channel estimation is. In Figure 4.8, the proposed model with and without CI are compared under CEE for N = 32, L = 4 and φ=0.99.
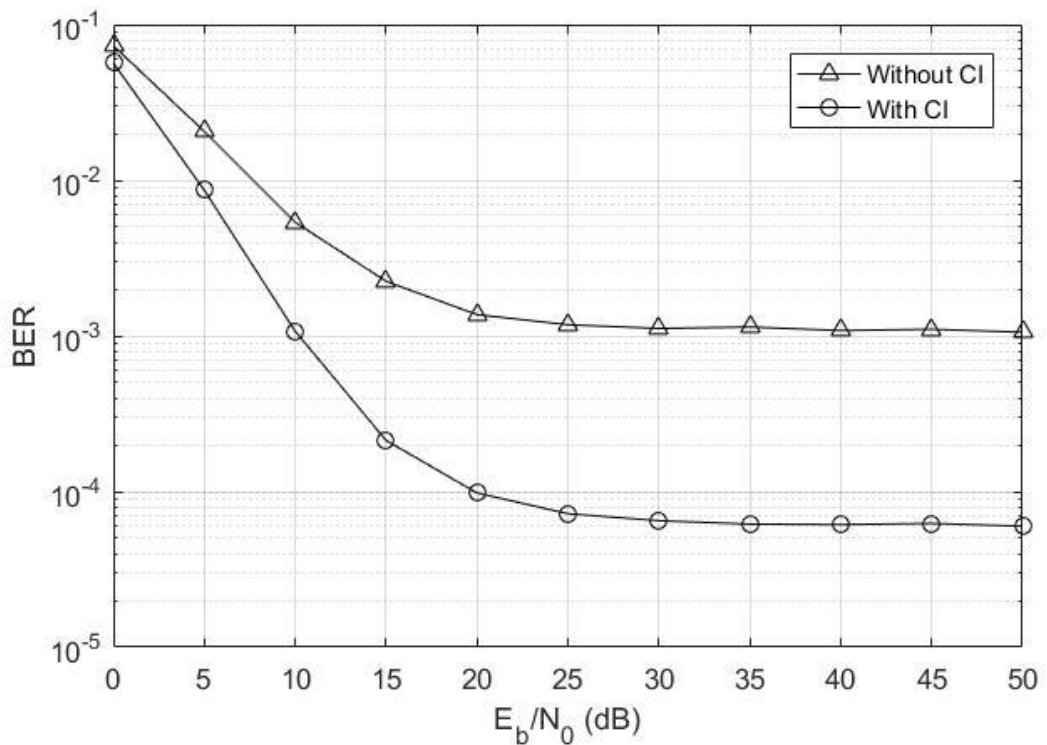
Figure 4.8 BER comparison of the proposed model with and without CI under CEE for N = 32, L = 4, and φ = 0.99.

It is clearly noticed that addition of CI to the system significantly lowers the error floor introduced by the CEE. The model without CI has an error floor at around 10^{-3} where the one with CI achieves an error floor of about 6×10^{-5}. This implies that even very slight CEE has a huge negative impact on the performance of the original system and this issue can be considerably solved by utilizing CI. Thus, CI highly increases the immunity of a system against CEEs.

4.4.2 Scenarios under Nakagami-m fading channel model

In this section, Bob's error performance is compared with Eve's according to different CI strategies that change relative to the relationship between N and L under Nakagami-m fading channel, in order to demonstrate how the suggested technique can improve the PLS.

In the first scenario, Bob's and Eve's performances for N = 32 and L = 4 are compared. There are three CI strategies making $H_{1,k}$ and $H_{1,m}$ ($H_{2,k}$ and $H_{2,m}$) uncorrelated in this case. These are represented by three different (k-m) values given by: 8, 16, and 24. The receiver uses a $\lceil \log_2 3 \rceil$=2 bits feedback channel to inform the transmitter about the appropriate strategy that should be used. In the second case, Bob's and Eve's performances for N = 32 and L = 8 are demonstrated. There exist seven values of (k-m) that make $H_{1,k}$ and $H_{1,m}$ ($H_{2,k}$ and $H_{2,m}$) uncorrelated: 4, 8, 12, 16, 20, 24, and 28. However, (k-m) = 20 is excluded, as it leads to the same instantaneous BER with (k-m) = 12. The feedback channel needed for this scenario is $\lceil \log_2 6 \rceil$=3 bits. In the third scenario Bob's and Eve's performances under the conditions N = 256 and L = 4 are compared. There are three values of (k-m) that make $H_{1,k}$ and $H_{1,m}$ ($H_{2,k}$ and $H_{2,m}$) uncorrelated: 64, 128 and 192. The receiver needs a $\lceil \log_2 3 \rceil$=2 bits feedback channel in this case. What is more, two analyses where the Nakagami-m shaping factor m = 2 and m = 3 are realized for all scenarios.

It is definitely obvious from the results obtained of the figures that Eve's performance is totally ruined when she has no feedback information that shows that the communication link between the transmitter and legitimate user is secure. The reason behind is that even the illegitimate user Eve has the critical knowledge of sub-carriers N and channel path numbers L it has to choose one of the possible CI strategies randomly, which leads to a totally detoriated and unreliable tapping. In addition, it can clearly be seen that even under the worst-case where Eve captures the feedback information, the proposed approach still provides a significant error performance advantage in favor of the legitimate user. Even under this worst-case, Bob has respectively an approximate 1 dB for Figure 4.9, 1.3 dB for Figure 4.10 and 1.3 dB for Figure 4.11 gain lead over Eve at a BER of 10^{-3} with the CI strategy. The reason behind
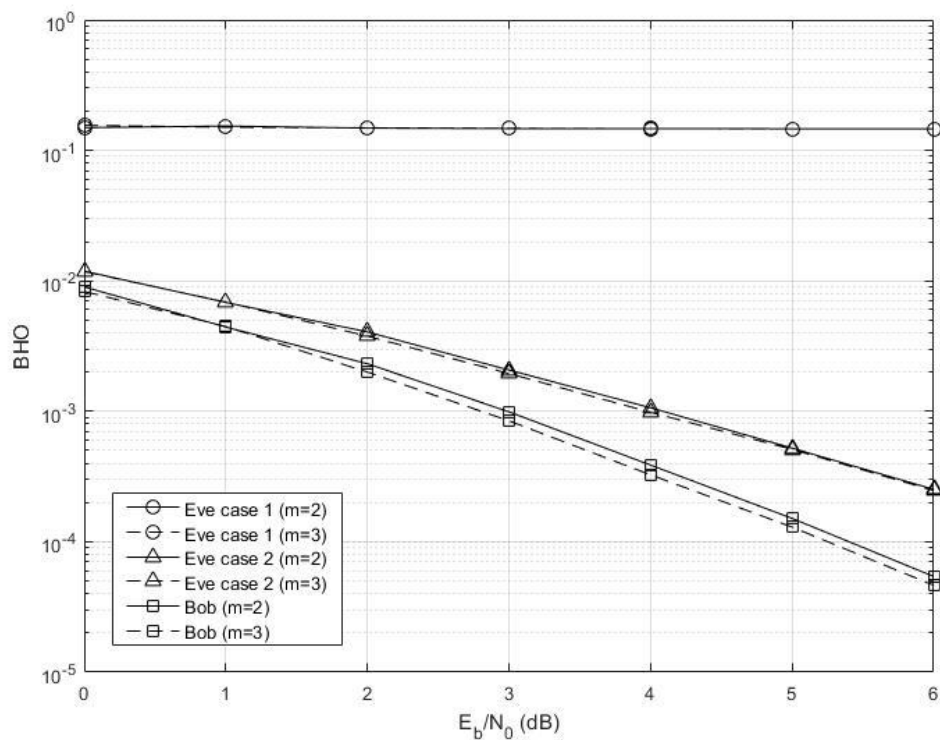
Figure 4.9 The BER comparison of Bob and Eve for N = 32 and L = 4.
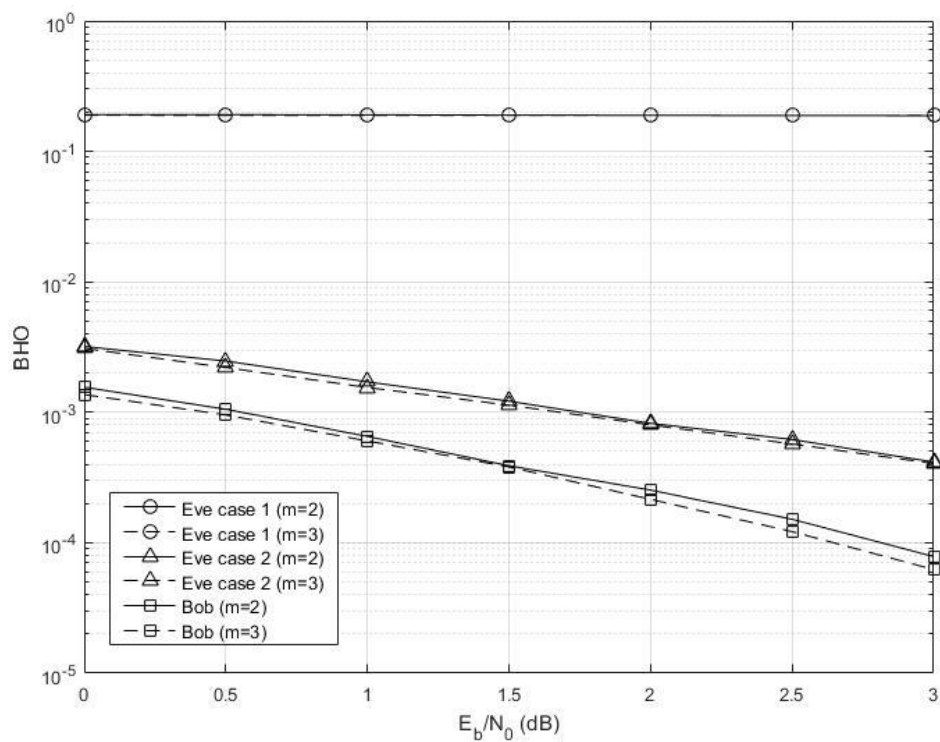
Figure 4.10 The BER comparison of Bob and Eve for N = 32 and L = 8.
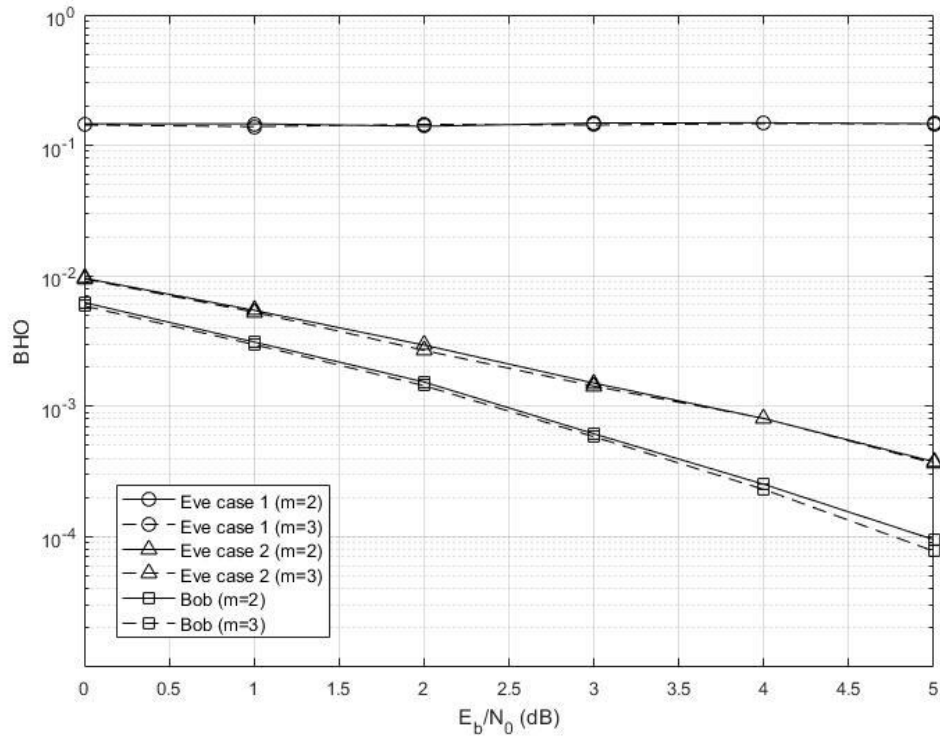
Figure 4.11 The BER comparison of Bob and Eve for N = 256 and L = 4.

this can be explained as follows: The system decides on which strategy to use according to Bob's channel-dependent feedback. Even though Eve knows the strategy of Bob, it may not be the optimum strategy to use with her own channel. In conclusion, it is demonstrated that the proposed technique can enhance PLS by either completely distorting Eve or by providing a much better error performance for the legitimate user compared with the illegitimate one.

By observing the results of the previous PLS scenarios, the error performance gains can be directly translated for the secrecy capacity metric as well, since both secrecy capacity and error rate are functions of resulting signal-to-noise ratios (SNR) at the receivers. Assuming that the channel capacity for the legitimate user is given by:

$$C_{leg}=E\left\{\sum_{k=0}^{N-1}\log_2\left(1+\zeta_k^{leg}\right)\right\} \tag{4.11}$$

and similarly for the eavesdropper it is shown as:

$$C_{eve}=E\left\{\sum_{k=0}^{N-1}\log_2\left(1+\zeta_k^{eve}\right)\right\} \tag{4.12}$$

then, the secrecy capacity for the studied network scheme can be written as:

$$C_s = C_{leg} - C_{eve}. \tag{4.13}$$

Here, ζ_k^{leg} and ζ_k^{eve} respectively denote the resulting SNR value at the kth subcarrier for the legitimate user and eavesdropper. Under the original Alamouti OFDM approach with no CI, it is straightforward to show that $C_s=0$ as long as the channel matrices for both the legitimate user and the eavesdropper have identical statistics. With the proposed scheme on the other hand, ζ_k^{leg} can be obtained by using the decision variables. We can write:

$$\zeta_k^{leg} = \left(|H_{1,k}|^2 + |H_{2,k}|^2 + |H_{1,m}|^2 + |H_{2,m}|^2 \right) \frac{E_b}{2N_0} \tag{4.14}$$

where $|H_{a,b}|^2$ represents the squared channel gain from the ath transmit antenna to the legitimate receiver on the bth subcarrier. On the other hand, as the eavesdropper does not know the CI strategy employed by the transmitter, she randomly chooses a CI strategy to form the decision variables. Regarding that the CI process is applied only on Q components, it is highly probable that Eve combines different symbols I and Q components to form a certain decision variable. In other words, the signal power at Eve comes from I component only, whereas Q component's contribution acts as noise. As a result, we can write:

$$\zeta_k^{eve} = \left(|H_{1,k}|^2 + |H_{2,k}|^2 \right) \frac{E_b/2}{N_0+N_k} \tag{4.15}$$

where N_k is the noise power due to the Q component. By substituting ζ_k^{leg} and ζ_k^{eve} into (4.11) and (4.12) respectively and taking the corresponding averages, it is clear that a positive C_s is obtained under the proposed technique.

4.5. Conclusion

In this chapter, a model that significantly improves the PLS of Alamouti OFDM systems with the help of SSD and CI strategy arranged according to the channel properties between a transmitter and an authorized user is proposed. The main

objective of the chapter is to enhance the PLS by ensuring that the legitimate user will always have a better error performance than an unauthorized user. Regarding different scenarios, appropriate CI strategies that make the correlation coefficients between the subcarrier gains affecting I and Q components of the transmitted modulated symbols equal to zero are utilized. An exact closed-form BER expression of the legitimate user under a frequency selective Rayleigh fading channel is derived and shown to be totally compatible with the simulation results. The numerical results demonstrate that the error performance of a standard Alamouti OFDM system can be highly enhanced with the addition of subcarrier coordinate interleaved SSD. It has also been shown that the approach improves the PLS by providing more immunity against unwanted eavesdropping. The model degrades the error performance of an unauthorized eavesdropper as much as it enhances the legitimate receiver's. Even in the situation where the unauthorized user somehow captures the CI strategy by intercepting the feedback channel, the error rate of the eavesdropper still turns out to be higher than the legitimate receiver. The reason for this is as follows: the CI approaches that the system uses are dependent on the main communication link between the transmitter and the authorized user. Hence, the proposed system enables a positive secrecy capacity unlike the original Alamouti OFDM approach that has zero secrecy capacity. It has also been demonstrated that the proposed scheme is beneficial in terms of resistance against channel estimation errors at the legitimate receiver. The approach induces only a non-significant increase in complexity and does not require extra bandwidth or time resources. Also, it can be shown that the inclusion of the CI strategies presented in the chapter does not alter peak-to-average-power ratio in the original Alamouti OFDM system.

For future work, the presented model can be utilized with other modulation techniques with modulation levels higher than two. The optimum rotation angles for these modulation schemes can be derived. In addition, the performance of the proposed model can be investigated by adopting minimum mean-squared-error or other types of equalizers instead of ZF.

CHAPTER 5

PERFORMANCE OF MMSE BEAMFORMING WITH TIME AND SPATIAL COORDINATE INTERLEAVING

This chapter is based on [31], where minimum mean square error (MMSE) beamforming (BF) schemes utilizing various number of transmit antennas with signal space diversity (SSD) are incorporated. Coordinate interleaving (CI) is performed in the spatial and time domains. The system has no channel state information (CSI) at the transmitter and imperfect CSI is assumed at the receiver in order to study the benefit of SSD under channel estimation errors. A parallel transmission takes place between the transmitter and the receiver, where MMSE BF is performed according to the erroneously estimated CSI. It is demonstrated that by using time or spatial CI, it is possible to highly improve the error performance of a MMSE BF system without the need of extra bandwidth, time slots or significant complexity increment. Different CI strategies used in this chapter present alternative solutions for different system design criteria in terms of error performance and latency.

5.1 Introduction

It is well known that the channel capacity of a single user multiple-input multiple-output (MIMO) communication system that uses N transmit and M receive antennas can be linearly increased by min(N,M) under specific conditions [2]. Minimum mean square error (MMSE) beamforming (BF) is a low complexity technique that can highly improve the bit error rate (BER) performance of a MIMO system [114,115]. The spatial multiplexing gain of an NxM (N≤M) MIMO MMSE-BF system that uses parallel data transmission at the transmitter is equal to N. Thanks to its advantages for both single and multiple users scenarios, MIMO MMSE systems are included in modern communication standards such as IEEE 802.11n and IEEE 802.16e.

In order to improve the error performance of a communication system under fading channels without the requirement of additional bandwidth or time slots, signal space diversity (SSD) is commonly used [18,53]. SSD has two steps to be performed with

systems that employ two-dimensional modulation schemes with constant envelope. The first step is to rotate the signal constellation diagram with a specific rotation angle that results in unique in-phase (I) and quadrature (Q) coordinates for each point in the signal constellation diagram. Following that, the second step is to apply coordinate interleaving (CI) so that the I and Q coordinates of a transmitted symbol experience independent fading coefficients in the channel [13]. The second step is performed usually by using CI techniques in the time domain [14,68]. Under this case the interleaving depth however, should not be smaller than the channel coherence time, which can be disadvantageous for latency-sensitive systems. An alternative technique for MIMO schemes is to apply CI in the spatial domain [58,63]. MIMO and SSD are combined with component interleaved orthogonal design, which is a type of space-time block codes and uses single symbol maximum likelihood (ML) detection property in [58]. Zero-forcing BF technique is utilized with SSD in [62].

In this chapter, SSD is introduced to a MMSE BF system by applying CI both at time and spatial domains. The error performance of the system is investigated under slow and flat Rayleigh fading channels by utilizing rotated binary phase shift keying (BPSK) and quadrature phase shift keying (QPSK) modulations. Such a system is studied in [116] with the assumption of no channel state information (CSI) at the transmitter and perfectly estimated CSI at the receiver. It is demonstrated that with the incorporation of SSD, it is possible to obtain a significant error performance improvement with only a negligible complexity increment and even a decrement in complexity for some special cases. In [117], an MMSE-BF BPSK system with an even number of transmit antennas and spatial CI is analyzed and tested under imperfect CSI at the receiver. It is shown that even slight channel estimation errors affect the system performance very badly and SSD is a significantly beneficial technique to cope with this problem. In this chapter, the approach in [117] is extended for BPSK MMSE-BF systems with an odd number of transmit antennas and QPSK MMSE-BF systems. Time CI is applied along with spatial CI. It is demonstrated that both time and spatial CI techniques are highly capable of handling the error performance degradation effect of channel estimation errors. While time CI is the best solution in terms of BER improvement, it may not be suitable for delay-sensitive systems. Spatial CI does not have the problem of latency and its performance is dependent on the interleaving

strategy used. Thus, the results of the chapter can offer solutions for different system design criteria.

5.2 System Model

In this chapter, a single-user NxM MIMO system ($2 \leq N \leq M$) that transmits N streams simultaneously in a parallel fashion from the transmitter is assumed. The complex baseband received signal vector can be written as

$$\mathbf{y} = \mathbf{Hx} + \mathbf{n} \tag{5.1}$$

where $\mathbf{H}$ represents the MxN channel matrix and the ith row and k^{th} column element of $\mathbf{H}$ corresponds to the fading coefficient between the kth transmit and i^{th} receive antennas. Additionally, $\mathbf{x}=[x_1 \; x_2 \; ... \; x_N]^T \in \mathbb{C}^{N \times 1}$ and $\mathbf{n} \in \mathbb{C}^{M \times 1}$ demonstrate the transmitted baseband vector signal ($x_i \in \{1,2,...,N\}$ represents the transmitted baseband signal from the ith transmit antenna) and additive white Gaussian noise (AWGN) vector at the receiver, respectively. The equation $E\{\mathbf{nn}^H\} = N_0 \mathbf{I}$ is true, where $\mathbf{I}$ and N_0 represent the identity matrix and the single sided power spectral density of AWGN that corresponds to each receive antenna, respectively. A slow and flat Rayleigh fading channel and uncorrelated antennas are considered. In this manner, the elements of $\mathbf{H}$ are considered as independent and identically distributed (IID) zero-mean complex Gaussian random variables that satisfy the equation $E\{|\mathbf{H}_{ik}|^2\}=1$ for any pair of i and k. It is assumed that there is no information of CSI at the transmitter and the receiver cannot estimate the CSI perfectly. The erroneous CSI of the receiver is modeled as

$$\mathbf{H} = \rho\widetilde{\mathbf{H}} + \sqrt{1-\rho^2}\mathbf{E} \tag{5.2}$$

where, $\widetilde{\mathbf{H}}$ is the receiver's estimation of channel matrix and $\mathbf{E}$ is the error contained within this estimation [113]. $\widetilde{\mathbf{H}}$ and $\mathbf{E}$ matrices are uncorrelated and each of their elements are IID zero-mean complex Gaussian random variables. In addition, for any i and k pair $E\{|\widetilde{\mathbf{H}}_{ik}|^2\}=E\{|\mathbf{E}_{ik}|^2\}=1$ equation is true. Also, ρ ($0 < \rho < 1$) is proportional to the correlation coefficient between the ith ($i \in \{1,2,...,N\}$) columns of actual ($\mathbf{H}$) and estimated ($\widetilde{\mathbf{H}}$) channel matrices. It is assumed that the channel does not change its

characteristics during a transmission period and changes independently from one transmission to another. N independently modulated signals ($s_i = s_{iI} + js_{iQ}$ for $i \in \{1,2,...,N\}$) are transmitted simultaneously in a parallel fashion, where I and Q sub-indices represent the I and Q coordinate components of a symbol. Transmitted symbols are mapped according to an $\pi/4$ anti-clockwise rotated BPSK (regarding the optimum rotation angle given in [69]) or a $\pi/6$ anti-clockwise rotated QPSK (regarding the rotation angle study done in [27]) constellation diagram (where the signal points on the diagram have equal probability) and hold the equation $|s_i|^2 = E_b$ where E_b is the energy per bit for BPSK and $|s_i|^2 = E_s$ where E_s is the energy per symbol for QPSK. The proposed system block diagram is given at Figure 5.1.
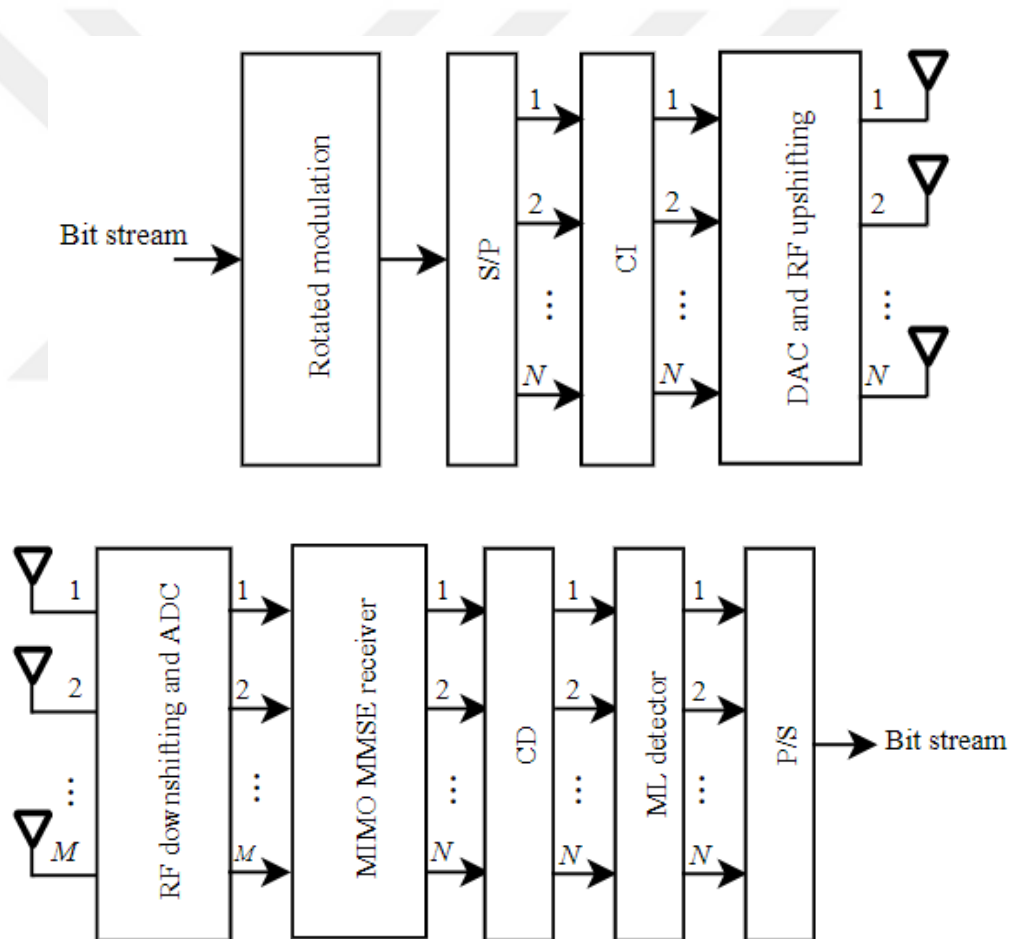

Figure 5.1 Block diagram of the system model

Here, after the rotated modulation and serial-to-parallel (S/P) transformation, CI takes place. For time CI, I and Q components of a symbol are transmitted in different time slots. With the time interleaving strategy x_i is equal to

$$x_i = s_{iI} + j s_{iQ}^{(\tau)}, \text{ for } i \in \{1,2,...,N\} \tag{5.3}$$

where $s_{iQ}^{(\tau)}$ symbolizes the ith modulated symbol at the τth transmission time, i.e., only Q components are interleaved in time domain. It is assumed that the interleaving depth (a function of τ) is greater than the coherence time of the channel. It can be seen that time CI has a disadvantage in terms of latency, as it needs two transmission periods instead of one. On contrast, for spatial CI, the I and Q components of a symbol should be sent from different antennas within the same transmission period. Two distinct CI strategies for spatial interleaving with both even and odd number of transmit antennas is used. For strategy 1 with even number of transmit antennas, x_i is defined as [117]

$$x_i = \begin{cases} s_{iI} + j s_{(i+1)I}, & \text{for } i \in \{1,3,5,...,N-1\}, \\ s_{(i-1)Q} + j s_{iQ}, & \text{for } i \in \{2,4,6,...,N\}. \end{cases} \tag{5.4}$$

For strategy 2 with even number of transmit antennas, x_i is given as

$$x_i = \begin{cases} s_{iI} + j s_{(i+1)Q}, & \text{for } i \in \{1,3,5,...,N-1\}, \\ s_{iI} + j s_{(i-1)Q}, & \text{for } i \in \{2,4,6,...,N\}. \end{cases} \tag{5.5}$$

Similarly, for scenarios with odd number of transmit antennas and spatial interleaving, two CI approaches are utilized. Strategy 1 for an odd number of transmit antennas is demonstrated as

$$x_i = \begin{cases} s_{iI} + j s_{(i+1)I}, & \text{for } i \in \{1,3,5,...,N-2\}, \\ s_{(i-1)Q} + j s_{iQ}, & \text{for } i \in \{2,4,6,...,N-3\}, \\ s_{(i-1)Q} + j s_{(i+1)Q}, & \text{for } i = N-1, \\ s_{iI} + j s_{(i-1)Q}, & \text{for } i = N. \end{cases} \tag{5.6}$$

Strategy 2 for an odd number of transmit antennas is on the other hand defined as

$$x_i = \begin{cases} s_{1I} + j s_{NQ}, & \text{for } i=1, \\ s_{iI} + j s_{(i+1)Q}, & \text{for } i \in \{2,3,4,...,N-1\}, \\ s_{NI} + j s_{1Q}, & \text{for } i=N. \end{cases} \tag{5.7}$$

The baseband vector signal $\mathbf{x}$ is transmitted after digital-to-analog conversion (DAC) and radio-frequency (RF) upshifting operations. Following RF downshifting and analog-to-digital (ADC) conversion, the baseband vector signal $\mathbf{y}$ is formed at the receiver. Subsequently, MMSE BF is performed on this signal by multiplying $\mathbf{y}$ with a specific $\mathbf{R} \in \mathbb{C}^{N \times M}$ matrix from left. $\mathbf{R}$ matrix is selected in such a way that the mean square error between $\mathbf{x}$ and $\mathbf{Ry}$ is minimized; $\mathbf{R} = \arg \min_{\mathbf{R}} \mathrm{E}\{\|\mathbf{Ry\text{-}x}\|^2\}$. It is demonstrated in [118] that $\mathbf{R} = \left[\rho^2 \mathbf{P} \widetilde{\mathbf{H}}^H \widetilde{\mathbf{H}} + \left((1\text{-}\rho^2) N E_b + N_0 \right) \mathbf{I} \right]^{-1} \rho \mathbf{P} \widetilde{\mathbf{H}}^H$, where $\mathbf{P} = \mathrm{E}\{\mathbf{xx}^H\}$ and $\mathrm{tr}(\mathbf{P}) = N E_b$ for BPSK ($\mathrm{tr}(\mathbf{P}) = N E_s$ for QPSK) where $\mathrm{tr}(.)$ shows the matrix trace operation. Using the approach in [116], for the $\pi/4$ anti-clockwise rotated BPSK scheme with an even number of transmit antennas, it can be demonstrated that $\mathbf{P}$ matrix has a block diagonal structure for the CI strategy 1 given in (5.4). For $\mathbf{B} = E_b \begin{bmatrix} 1 & 1 \\ 1 & 1 \end{bmatrix}$, it can be written [114]

$$\mathbf{P} = \begin{bmatrix} \mathbf{B} & \mathbf{0} & \ldots & \mathbf{0} \\ \mathbf{0} & \mathbf{B} & \ldots & \mathbf{0} \\ \vdots & \vdots & \ddots & \vdots \\ \mathbf{0} & \mathbf{0} & \ldots & \mathbf{B} \end{bmatrix}. \tag{5.8}$$

On the other hand, for the scenarios with an even number of transmit antennas and rotated BPSK, if spatial CI strategy 2 given in (5.5) or time CI is used the $\mathbf{P}$ matrix is diagonal and equals to $E_b \mathbf{I}$.

For $\pi/4$ anti-clockwise rotated BPSK scheme with the CI strategy 1 given in (5.6), it can be shown that $\mathbf{P}$ matrix is equal to

$$\mathbf{P} = \mathbf{C} \,, \tag{5.9}$$

$$\mathbf{P} = E_b \begin{bmatrix} 1 & 1 & 0 & 0 & 0 \\ 1 & 1 & 0 & 0 & 0 \\ 0 & 0 & & & \\ 0 & 0 & & \mathbf{C}/E_b & \\ 0 & 0 & & & \end{bmatrix}, \tag{5.10}$$

$$\mathbf{P} = E_b \begin{bmatrix} 1 & 1 & 0 & 0 & 0 & 0 & 0 \\ 1 & 1 & 0 & 0 & 0 & 0 & 0 \\ 0 & 0 & 1 & 1 & 0 & 0 & 0 \\ 0 & 0 & 1 & 1 & 0 & 0 & 0 \\ 0 & 0 & 0 & 0 & & & \\ 0 & 0 & 0 & 0 & & \mathbf{C}/E_b & \\ 0 & 0 & 0 & 0 & & & \end{bmatrix}, \tag{5.11}$$

for N=3, N=5 and N=7, respectively, where

$$\mathbf{C} = E_b \begin{bmatrix} 1 & \frac{1}{2} & \frac{1}{2} \\ \frac{1}{2} & 1 & \frac{j}{2} \\ \frac{1}{2} & -\frac{j}{2} & 1 \end{bmatrix}. \tag{5.12}$$

For $\pi/4$ anti-clockwise rotated BPSK scheme with the CI strategy 2 given in (5.7), it can be shown that $\mathbf{P}$ matrix is equal to

$$\mathbf{P} = \mathbf{D}, \tag{5.13}$$

$$\mathbf{P} = E_b \begin{bmatrix} 1 & 0 & 0 & 0 & 0 \\ 0 & 1 & 0 & 0 & 0 \\ 0 & 0 & & & \\ 0 & 0 & & \mathbf{D}/E_b & \\ 0 & 0 & & & \end{bmatrix}, \tag{5.14}$$

$$\mathbf{P} = E_b \begin{bmatrix} 1 & 0 & 0 & 0 & 0 & 0 & 0 \\ 0 & 1 & 0 & 0 & 0 & 0 & 0 \\ 0 & 0 & 1 & 0 & 0 & 0 & 0 \\ 0 & 0 & 0 & 1 & 0 & 0 & 0 \\ 0 & 0 & 0 & 0 & & & \\ 0 & 0 & 0 & 0 & & \mathbf{D}/E_b & \\ 0 & 0 & 0 & 0 & & & \end{bmatrix} \tag{5.15}$$

for N=3, N=5 and N=7, respectively, where

$$\mathbf{D} = E_b \begin{bmatrix} 1 & \frac{j}{2} & \frac{-j}{2} \\ \frac{-j}{2} & 1 & \frac{j}{2} \\ \frac{j}{2} & -\frac{j}{2} & 1 \end{bmatrix}. \tag{5.16}$$

Additionally, with time CI, a diagonal $\mathbf{P}$ matrix as $E_b\mathbf{I}$ and $E_s\mathbf{I}$ for BPSK and QPSK exists, respectively. Also, for both time and spatial CI with QPSK, the $\mathbf{P}$ matrix can be shown to be $E_s\mathbf{I}$.

Suppose that the kth diagonal element ($k \in \{1,2,...,N\}$) of $\mathbf{R\widetilde{H}}$ square matrix is represented by a_k. After applying maximal ratio combining technique on $\mathbf{Ry}$, $\mathbf{z} = [z_1\ z_2\ ...\ z_N]^T$ is obtained, where z_k is equal to the multiplication of a_k^* and the kth element of $\mathbf{Ry}$. Also, assume that the decision variable that the ML detector uses for the kth modulated symbol (s_k) is shown by g_k ($k \in \{1,2,...,N\}$). These decision variables are obtained by applying coordinate deinterleaving operation on the $\mathbf{z}$ vector according to the CI strategy at the transmitter. If we are to assume the I and Q components of s_k are transmitted from β. and λ. transmit antennas, respectively, it can be written that $g_k = \rho|a_\beta|^2 s_{kI} + j\rho|a_\lambda|^2 s_{kQ} + \varsigma_k + \upsilon_k$. Here, ς_k and υ_k represents the inter-symbol interference and AWGN that affects s_k, respectively. When the ML detector decides for the kth modulated symbol, I and Q components of each signal point in the signal constellation are scaled by $\rho|a_\beta|^2$ and $\rho|a_\lambda|^2$, respectively. Finally, the signal point that is closest to g_k in the signal constellation is declared as the decided result and the estimated bit stream is obtained by parallel-to-serial (P/S) transformation.

5.3. Simulation Results

In this section, the proposed MIMO MMSE system and the original MIMO MMSE system are compared in terms of BER for $\rho = 0.99$. The proposed schemes use rotated BPSK or QPSK constellation diagrams and the MMSE BF matrices can be obtained by replacing the suitable $\mathbf{P}$ matrix according to the CI strategy used. Figures 5.2, 5.3, 5.4 and 5.5 compare these systems under different numbers of antennas and CI strategies.

It can be clearly seen that in situations where channel estimation error exists, communication systems' error performances are inevitably limited by an error floor. This problem arises even in cases where ρ has a very big value (which means quite accurate channel estimation). It is demonstrated that the original MIMO MMSE schemes without CI suffer from this problem in the worst way in all scenarios. The

proposed method significantly lowers the error floor of the original scheme no matter what CI strategy is used. Because of the totally uncorrelated transmission of a symbol's I and Q components, time CI yields the best error performance in all cases. There is no correlation between the fading coefficients affecting I and Q components of a symbol with time CI, as the receiver applies MMSE BF in two different time slots separated more than channel coherence time. Regarding spatial CI, it is demonstrated that strategy 1 leads to performances that are either equal to or be seen that for the N=2, M=3 case strategy 1 yields a slightly better improvement of the error floor than strategy 2. However, for the scenario with N=3, M=3 the error performances of strategies 1 and 2 are the same. In Figure 5.3, it can be seen that with spatial CI, strategy 1 is much more beneficial than strategy 2 for both N=4, M=5 and N=5, M=5 cases. In Figure 5.4 and Figure 5.5, the results demonstrate that for spatial CI, using strategy 1 or 2 present the same result. Thus, it can be deduced that the performance of spatial CI is dependent on the interleaving strategy being used.
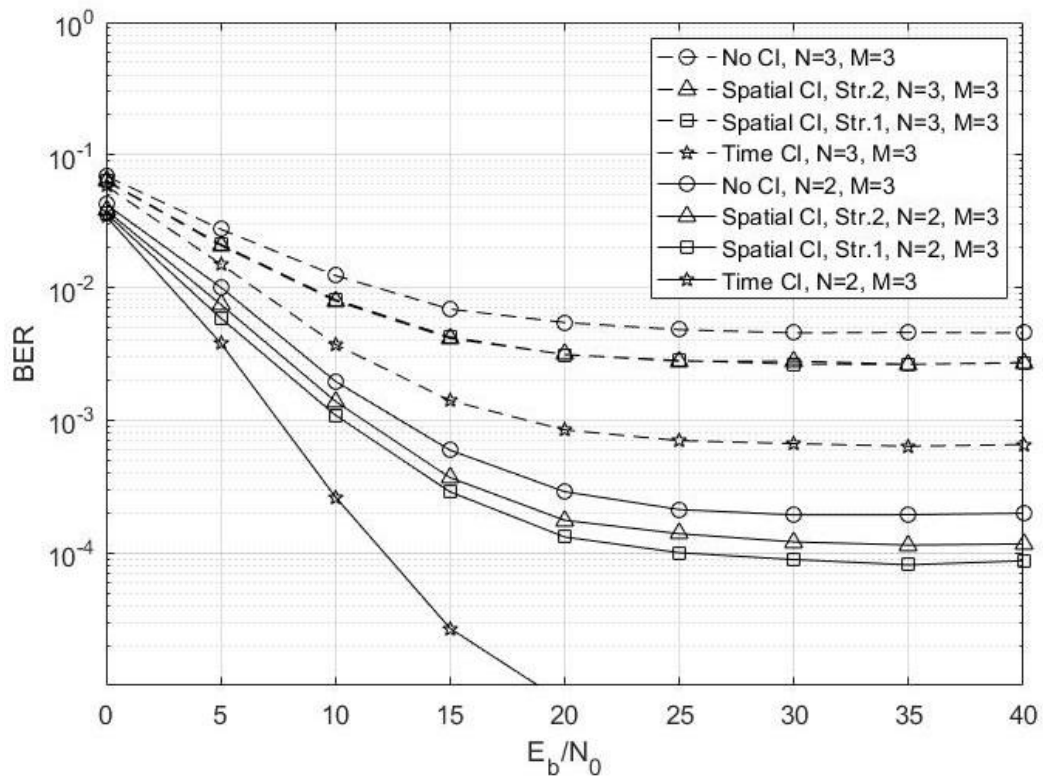

Figure 5.2 BER performances of BPSK schemes with N = 2, M = 3 and N = 3, M = 3 for ρ = 0.99.
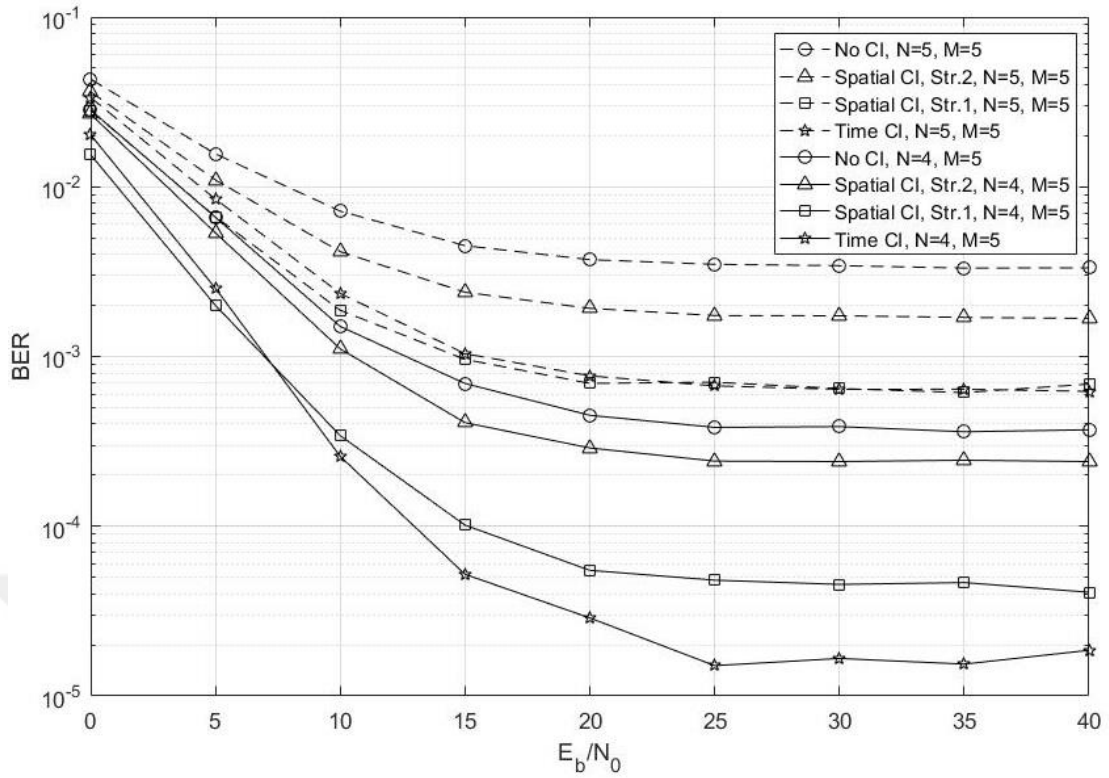
Figure 5.3 BER performances of BPSK schemes with N = 4, M = 5 and N = 5, M = 5 for ρ = 0.99.
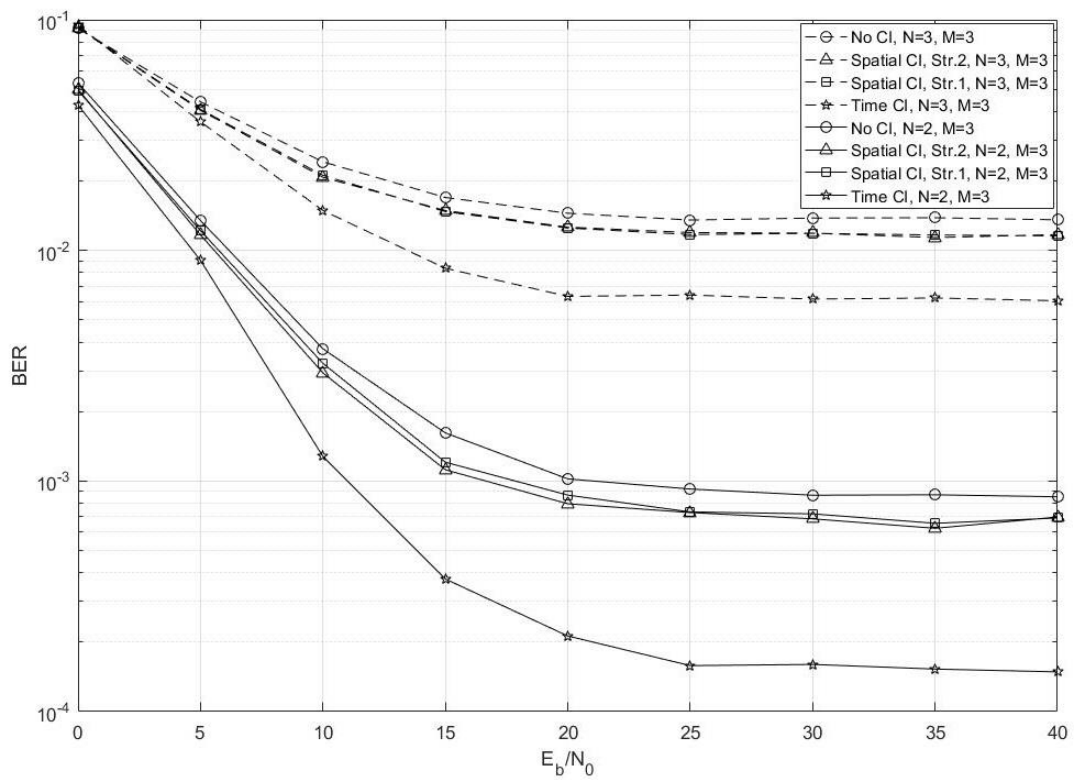
Figure 5.4 BER performances of QPSK schemes with N = 2, M = 3 and N = 3, M = 3 for ρ = 0.99.
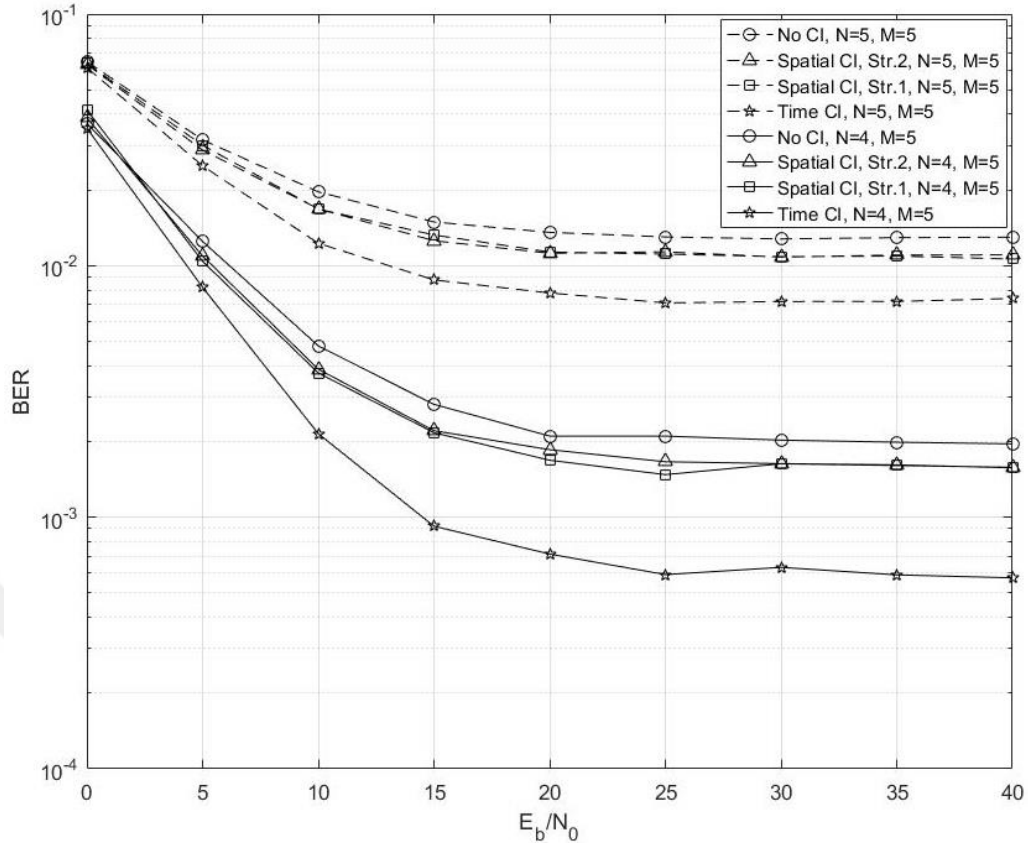
Figure 5.5 BER performances of QPSK schemes with N = 4, M = 5 and N = 5, M = 5 for ρ = 0.99.

5.4 Conclusion

In this chapter, the error performance of a MMSE BF receiver combined with SSD is studied where there is no CSI at the transmitter and erroneous CSI exists at the receiver. It is shown that under a slow and flat Rayleigh fading channel and with BPSK and QPSK modulations, the error floor of the system can be significantly improved by SSD without the need for additional bandwidth or time slots. Time CI provides the best performance improvement, although it may cause problem for latency sensitive systems. Spatial CI strategies offer different error floor performances depending on the interleaving strategy being used. As a result, the chapter proves that the immunity against channel estimation errors for a MMSE BF system can be highly increased with SSD and the CI strategy can be implemented according to the design criteria.

CHAPTER 6

DISCUSSION AND CONCLUSION

In this thesis, multiple antenna systems are combined with SSD and implemented into various system models in order to enhance the performance. With these applications, multiple antenna systems with SSD are investigated from a wide perspective. In order to deal with the ever increasing user numbers and the demand for faster, more reliable and more quality communication services, telecommunication engineers are always on the search for new ideas which some of them can be really groundbreaking. Utilization of multiple antennas instead of single antennas is one of them. By increasing the antenna number at a communication system more potential for higher data rates and better quality with less errors is achieved. Another important technique that achieved popularity after its introduction is SSD. This method enables to improve the error performance of a system with very little sacrifice from complexity and no extra need for resources. Thus, the joint usage of multiple antennas and SSD can lead to huge performance improvements and it is shown in this thesis to be true for many applications. In Chapter 2, the fundamental insight theory of the thesis subjects, such as wireless channels, physical layer security, OFDM, multiple-antenna systems and SSD are presented. In Chapter 3, zero-forcing receive beamforming with signal space diversity systems are studied under different interleaving techniques. It has been shown that with the incorporation of SSD the error performance of a system can be highly improved especially with time interleaving method. Spatial method also provides some increment and it does not have latency problem which can be problematic for sensitive systems. With the FPGA implementation of the system, it has been shown that SSD brings in a non-significant extra complexity. Also, zero-forcing MIMO systems with SSD are studied under transmit antenna correlation in this chapter. It has been shown that SSD can provide significant performance leaps despite the negative effects of transmit antenna correlation. In addition, it has been demonstrated that different spatial correlation types have various amounts of impact on the system. In Chapter 4, the physical layer security of an Alamouti OFDM system is enhanced by the help of SSD. It is demonstrated that, with suitable strategies that

are designed to make the correlation coefficients between subcarrier channel gains as minimum as possible, it is possible to improve the PLS of a network, thus to provide a reliable and secure communication enviroment. The PLS of a network under Nakagami-m fading channels is also shown to be advanced with the addition of SSD in this chapter. It has been clearly exhibited that, by using proper subcarrier coordinate interleaving strategies, it is possible to make the coefficients between the subcarrier channel gains equal to zero. Also, it is demonstrated that, an eavesdropper will perform worse than a legitimate user even if she captures the strategy used via the main communication channel. Finally in Chapter 5, the performance of MMSE beamforming is studied under different coordinate interleaving techniques of SSD. It has been shown that utilization of SSD with either time or spatial coordinate interleaving significantly improves the performance of MMSE beamforming systems even under the case where channel estimation errors exist at the receiver. In conclusion, the various studies done and results obtained in this thesis prove that the combination of multiple-antenna systems and SSD has a huge potential to be used within the system models that are proposed in the thesis and also is a very promising idea for future studies and applications.

The proposed techniques in this thesis can also be applied for different studies and can be extended into various new ideas. In order to shed light on some potential future work ideas, some of the suggestions that can be proposed are:

[1] In the thesis, the coordinate interleaving step has been realized for time, spatial and subcarrier domains. This technique can be extended to other domains that diversity can be achieved such as polarization and antenna angle.

[2] Throughout the thesis work, modulations with a maximum of two dimensions has been used. The proposed techniques here can be further developed for modulation schemes with dimenisons higher than two, and further be generalized. The optimum rotation angles that are suitable for these schemes can be found and CI strategies can be adapted accordingly. The theoretical error probability expressions can also be derived.

[3] In the thesis, the effect of transmit antenna correlation has been examined for the proposed scheme. This work can be extended for models with no transmit

antenna correlation and the existence of receive antenna correlation. To take one step further, the case where correlation exists for both transmit and receive antennas can be examined.

[4] Throughout the thesis, Alamouti STBC has been implemented into SSD system models. Different diversity techniques and STBC structures other than Alamouti model can be incorporated with SSD and the error performance can be improved even further.

[5] In the thesis, the physical layer security has been provided with the help of SSD and subcarrier CI. The same experimentation can be repeated with observing different secrecy metrics. The graphs for these metrics can be obtained in order to prove the strength of the proposed model in terms of security.

[6] Throughout the thesis, OFDM with cyclic prefix has been used against the effects of frequency selective channels. Other forms of OFDM, such as polynomial cancellation coded OFDM (PCC-OFDM) can be considered to use alongside with multiple-antenna SSD systems. PCC-OFDM can help to improve the robustness against deteriorating effects of wireless channels like time and frequency offsets.

[7] The hardware implemetation of the proposed schemes in the the thesis is always a welcoming idea for researchers. Either with FPGAs or experimental set-ups it is possible to examine the performance of the proposed models in realistic conditions and compare them with the simulated results that are given in the thesis.

REFERENCES

[1]   Driessen, P. F. & Foschini, G. J. On the capacity formula for multiple input-multiple output wireless channels: A geometric interpretation. IEEE Trans. Comm., 47 (2), 173-176. 1999

[2]   Telatar, E. Capacity of multi-antenna gaussian channels. European Trans. Telecomm., 10 (6), 585-595. 1999

[3]   Hampton, J. R. Introduction to MIMO Communications (1st Ed.). Cambridge University Press. 2014

[4]   Perahia, E. IEEE 802.11n development: History, process, and technology. IEEE Comm. Mag., 46 (7), 48 – 55. 2008

[5]   Eklund, C., Marks, R. B., Stanwood, K. L. & Wang, S. IEEE standard 802.16: a technical overview of the WirelessMAN/sup TM/ air interface for broadband wireless access. IEEE Comm. Mag., 40 (6), 98-107. 2002

[6]   Budigere, K., Panchakarla, N., Chemmagate, B. & Roy, S. LTE: Long term evolution of 3GPP. 2010

[7]   Rysavy Research/5G Americas, LTE to 5G cellular and broadband innovation. 2017

[8]   Farhan, K. A. & Speidel, J. Advances in MIMO techniques for mobile communications - A survey. Int. J. Comm., Network System Sciences, 3 (3), 213-252. 2010

[9]   Yang, S. & Hanzo, L. Fifty years of MIMO detection: The road to large-scale MIMOs. IEEE Comm. Surveys & Tutorials, 17 (4), 1941-1988. 2015

[10]   Zheng, K., Zhao, L., Mei, J., Shao, B., Xiang, W. & Hanzo, L. Survey of large scale MIMO systems. IEEE Comm. Surveys & Tutorials, 17 (3), 1738-1760. 2015

[11]   Busari, S. A., Huq, K. M. S., Mumtaz, S., Dai, L. & Rodriguez, J. Millimeter-wave massive MIMO communication for future wireless systems: A survey. IEEE Comm. Surveys & Tutorials, 20 (2), 836-869. 2018

[12]   Shaikh, A. & Kaur, M. J. Comprehensive survey of massive MIMO for 5G communications. Advances Science Eng. Tech. Int. Conf. Dubai, United Arab Emirates, 1-5. 2019

[13]   Taricco, G. & Viterbo, E. Performance of component interleaved signal sets for fading channels. Electr. Lett., 32 (13), 1170-1172. 1996

[14]   Boutros, J. & Viterbo, E. Signal space diversity: A power and bandwidth-efficient technique for the Rayleigh fading channel. IEEE Trans. Inf. Theory, 44 (4), 1453-1467. 1998

[15]   Slimane, S. B. An improved PSK scheme for fading channels. IEEE Trans. Veh. Tech., 47 (2), 703-710. 1998

[16]   Schober, R., Lampe, L. H. J., Gerstacker, W. H. & Pasupathy, S. Modulation diversity for frequency-selective channels. IEEE Trans. Inf. Theory, 49 (9), 2268-2276. 2003

[17]   Kiyani, N. F. & Weber, J. H. Iterative demodulation and decoding for rotated MPSK constellations with convolutional coding and signal space diversity. IEEE Veh. Tech. Conf., 1712-1716. 2007

[18]   Tran, N. H., Nguyen, H. H. & Le-Ngoc, T. Performance of BICM-ID with signal space diversity. IEEE Trans. Wireless Comm., 6 (5), 1732-1742. 2007

[19]   Tran, N. H., Nguyen, H. H. & Le-Ngoc, T. Bit-interleaved coded OFDM with signal space diversity: Subcarrier grouping and rotation matrix design. IEEE Trans. Signal Processing, 55 (3), 1137-1149. 2007

[20]   Kiyani, N. F., Rizvi, U. H., Weber, J. H. & Janssen, G. J. M. Optimized rotations for LDPC-coded MPSK constellations with signal space diversity. IEEE Wireless Comm. Networking Conf., Kowloon, 677-681. 2007

[21]   Hwang, S. U., Choi, J., Jeon, S., Ryu, H. J. & Seo, J. Performance evaluation of MIMO-OFDM with signal space diversity over frequency selective channels. IEEE Int. Symp. Broadband Multimedia Systems Broadcasting, Bilbao, 1-5. 2009

[22]   Zhang, W., Xia, X. & Ching, P. C. High-rate full-diversity space–time–frequency codes for broadband MIMO block-fading channels. IEEE Trans. Comm., 55 (1), 25-34. 2007

[23]   Zhang, W., Xia, X. & Letaief, K. B. Space-time/frequency coding for MIMO-OFDM in next generation broadband wireless systems. IEEE Wireless Comm. 14 (3), 32-43. 2007

[24]   Wu, Z. & Gao, X. An efficient MIMO scheme with signal space diversity for future mobile communications. EURASIP J. Wireless Comm. Networking, 2015 (1), 1-18. 2015

[25]   Jeon, S., Kyung, I. & Kim, M. Component-interleaved receive MRC with rotated constellation for signal space diversity. IEEE 70th Veh. Tech. Conf. Fall, Anchorage, AK, 1-6. 2009

[26]   Su, W., Safar, Z. & Liu, K. J. R. Full-rate full-diversity space-frequency codes with optimum coding advantage. IEEE Trans. Inf. Theory, 51 (1), 229-249. 2005

[27]   Reşat, M. A., Çiçek, A., Özyurt, S. & Çavuş, E. Analysis and FPGA implementation of zero-forcing receive beamforming with signal space diversity under different interleaving techniques. J. Circuits, Systems & Computers, 29 (1). 2020

[28]   Reşat, M. A. & Özyurt, S. Performance of zero-forcing MIMO systems with signal space diversity under transmit antenna correlation. 10th Int. Conf. Electrical & Electronics Eng., Bursa, Turkey, 700-704. 2017

[29]   Reşat, M. A., Karakoç, M. C. & Özyurt, S. Improving physical layer security in Alamouti OFDM systems with subcarrier coordinate interleaving. IET Communications. Submitted

[30]   Reşat, M. A., Karakoç, M. C. & Özyurt, S. Alamouti DFBÇ sistemlerinde fiziksel katman güvenliğinin Nakagami-m sönümlemeli kanallar üzerinde iyileştirilmesi. 28. IEEE Sinyal İşleme ve İletişim Uygulamaları Kurultayı. Submitted

[31]   Reşat, M. A. & Özyurt, S. Performance of MMSE beamforming with time and spatial coordinate interleaving. 11th Int. Conf. Electrical & Electronics Eng., Bursa, Turkey. 2019

[32]   Proakis, J., G. & Salehi, M. Communication Systems Engineering (2nd Ed.) Pearson. 2001

[33]   Goldsmith, A. Wireless communications (1st Ed.). Cambridge University Press. 2005

[34]   Abdelkader, S. Channel estimation and signal-space diversity for vector-valued transmissions. Ph. D. Thesis, University of Ulm. 2007

[35] Boutros, J., Viterbo, E., Rastello, C. & Belore, J. Good lattice constellations for both Rayleigh fading and Gaussian channels. IEEE Trans. Inf. Theory, 42 (2), 502-518. 1996

[36] Saeed, A., Xu, H. & Quazi, T. Alamouti space-time block coded hierarchical modulation with signal sapce diversity and MRC reception in Nakagami-m fading channels. IET Comm, 8 (4), 516-524. 2014

[37] Paruk, Z. & Xu, H. Performance analysis and simplified detection for two-dimensional signal space diversity with MRC reception. SAIEE Africa Research J., 104 (3), 97-106. 2013

[38] Kiyani, N. F. Wireless communication systems using signal space diversity. M. Sc. Thesis, University of Gavle. 2009

[39] Ahmadzadeh, S. A. Signal space cooperative communication. IEEE Trans. Wireless Comm., 6 (4), 1266-1271. 2010

[40] Schlegel, C. & Costello Jr., D. J. Bandwidth efficient coding for fading channels: Code construction and performance analysis. IEEE J. Select. Areas Comm., 7 (9), 1356-1368. 1989

[41] Essop, A. Signal space diversity with and without Alamouti transmit diversity using generalised selection combining. M. Sc. Thesis, University of Kwa-Zulu Natal. 2015

[42] Salehi, M. & Proakis, J. G. Digital communications (5th Ed.) San Diego, USA: McGraw - Hill Higher Education. 2007

[43] Xu, K. Antennas selection for MIMO systems over Rayleigh fading channels. 1110th Int. Conf. Comm., Circuits Systems, Chengdu, China, 185-189. 2004

[44] Cho, Y. S., Kim, J., Yang, W. Y. & Kang, C. G. MIMO-OFDM wireless communications with MATLAB. Wiley-IEEE Press (1st Ed.). 2010

[45] Hamamreh, J. M., Furqan, H. M. & Arslan, H. Classifications and applications of physical layer security techniques for confidentiality: A comprehensive survey. IEEE Comm. Surveys & Tutorials, 21 (2), 1773-1828. 2019

[46] Boelcskei, H., Gesbert, D., Papadias, C. B. & et al. Space-time wireless systems: From array processing to MIMO communications. Cambridge University Press. 2008

[47]   Kaviani, S., Krzymien, W. A. User selection for multiple-antenna broadcast channel with zero-forcing beamforming. Proc. IEEE Global Comm. Conf., New Orleans, 1-5. 2008

[48]   Monzingo, R. A., Miller, T. W. Introduction to adaptive arrays. NY: Wiley. 1980

[49]   Gerlach, D., Paulraj, A. Adaptive transmitting antenna arrays with feedback. IEEE Signal Processing Lett., 1, 150-152. 1994

[50]   Haustein, T., von Helmolt, C., Jorswieck, E. & et al. Performance of MIMO systems with channel inversion. Proc. IEEE Veh. Tech. Conf., Birmingham, 35-39. 2002

[51]   Joham, M., Utschick, W. & Nossek, J. A. Linear transmit processing in MIMO communications systems. IEEE Trans. Signal Processing, 53, 2700-2712. 2005

[52]   Wiesel, A., Eldar, Y. C. & Shamai, S. Zero-forcing precoding and generalized inverses. IEEE Trans. Signal Processing, 56 4409-4418. 2008

[53]   Boulle, K., Belfiore, J. C. Modulation scheme designed for Rayleigh fading channel. Proc. CISS. 1992

[54]   Srinivas, K. V., Koilpillai, R. D., Bhashyam, S. & et al. Co-ordinate interleaved spatial multiplexing with channel state information. IEEE Trans. Wireless Comm., 8, 2755-2762. 2009

[55]   Gao, X. & Wu, Z. Precoded spatial multiplexing MIMO system with spatial component interleaver. EURASIP J. Wireless Comm. Networking. 2016

[56]   Yılmaz, A., Kucur, O. Performance analysis of modulation diversity with OSTBC transmission over Nakagami-m fading channels. AEU-Int. J. Electronics Comm., 68, 59-63. 2014

[57]   Kim, J., Lee, I. Coded layered space-time transmission with signal space diversity in OFDM systems. Proc. IEEE Global Comm. Conf., St. Louis, 3866-3870. 2005

[58]   Khan, M. Z. A., Rajan, B. S. Single-symbol maximum likelihood decodable linear STBCs. IEEE Trans. Inf. Theory, 52, 2062-2091. 2006

[59]   Lee, H., Andrews, J. G., Heath, R. W. & et al. The performance of space-time block codes from coordinate interleaved orthogonal designs over Nakagami-m fading channels. IEEE Trans. Comm., 57, 653-664. 2009

[60]   Lee, H. & Paulraj, A. MIMO systems based on modulation diversity. IEEE Trans. Comm., 58, 3405-3409. 2010

[61]   Li, Y. & Salehi, M. Coded MIMO systems with modulation diversity for block-fading channels. Proc. Inf. Sciences and Systems Conf., Princeton. 2012

[62]   Özyurt, S. & Kucur, O. Zero-forcing beamforming with signal space diversity. IEEE Trans. Veh. Tech., 67, 812-816. 2018

[63]   Özyurt, S. & Kucur, O. Performance analysis of maximal ratio combining with transmit antenna selection and signal space diversity under exponential antenna correlation. IET Comm., 12, 612-619. 2018

[64]   Essop, A. & Xu, H. Symbol error rate of generalized selection combining with signal space diversity in Rayleigh fading channels. SAIEE Africa Research J., 106, 201-211. 2015

[65]   Deepti, M., Srinivas, K. V. & Koilpillai, R. D. A new space-time signaling scheme for MIMO-OFDM systems with limited feedback. Proc. IEEE Tencon Conf., Hyderabad, 1-5. 2008

[66]   Deepti, M. & Koilpillai, R. D. A new diagonally layered spatial multiplexing scheme with limited feedback. National Conf. Comm., Chennai, 1-5. 2010

[67]   Wu, Z. & Gao, X. An efficient practical MIMO-OFDM scheme with coded modulation diversity for future wireless communications. Wireless Personal Comm., 91, 487-508. 2016

[68]   Vishnu, A. & Bhashyam, S. Co-ordinate interleaved amplify-and-forward relaying with a multi-antenna relay. Proc. National Conf. Comm., Mumbai, 1-6. 2015

[69]   Özyurt, S. & Kucur, O. Performance of zero-forcing receive beamforming with signal space diversity over Rayleigh fading channels. Proc. Advances Wireless Optical Comm., Riga, 147-151. 2017

[70]   Tse, D. & Viswanath, P. Fundamentals of wireless communication, Cambridge University Press. 2005

[71]   Abramowitz, M., Stegun, I. A. Handbook of mathematical functions with formulas, graphs, and mathematical tables. New York, NY, USA: Dover. 1972

[72]   Simon, M. K. & Alouini, M. S. Digital communication over fading channels: A unified approach to performance analysis, John Wiley & Sons. 2000

[73]   Mukherjee, A., Fakoorian, S., Huang, J. & et al. Principles of physical layer security in multiuser wireless networks: a survey. IEEE Comm. Surveys & Tutorials, 16 (3), 1550-1573. 2014

[74]   Poor, V. & Schaefer, R. Wireless physical layer security. Proc. National Academy Sciences USA, 114 (1), 19-26. 2016

[75]   Wu, Y., Khisti, A., Xiao, C. & et al. A survey of physical layer security techniques for 5G wireless networks and challenges ahead. IEEE J. Sel. Areas Comm., 36 (4), 679-695. 2018

[76]   Barros J. & Rodrigues, M. Secrecy capacity of wireless channels. Proc. IEEE Int. Symp. Inf. Theory, Seattle, WA, 356-360. 2006

[77]   Li, Z., Yates, R. & Trappe, W. Secrecy capacity of independent parallel channels. Proc. Allerton Conf. Comm., Control, Comp., Allerton Park, IL, 1-18. 2006

[78]   Li, Z., Yates, R. & Trappe, W. Secret communication with a fading eavesdropper channel. Proc. IEEE Int. Symp. Inf. Theory, Nice, France, 1296-1300. 2007

[79]   Gopala, P., Lai, L. & Gamal, H. On the secrecy capacity of fading channels. IEEE Trans. Inf. Theory, 54 (10), 4687-4698. 2008

[80]   Liang, Y., Poor, H. & Shamai, S. Secure communication over fading channels. IEEE Trans. Inf. Theory, 54 (6), 2470-2492. 2008

[81]   Jeon, H., Kim, N., Choi, J. & et al. Bounds on secrecy capacity over correlated ergodic fading channels at high SNR. IEEE Trans. Inf. Theory, 57 (4), 1975-1982. 2010

[82]   Hero, A. Secure space-time communication. IEEE Trans. Inf. Theory, 49 (12), 3235-3249. 2003

[83]   Parada, P. & Blahut, R. Secrecy capacity of SIMO and slow fading channels. Proc. IEEE Int. Symp. Inf. Theory, Adelaide, Australia, 2152-2155. 2005

[84]   Li, Z., Trappe, W. & Yates, R. Secret communication via multi-antenna transmission. Proc. 41st Conf. Inf. Sciences Systems, Baltimore, MD, 1-6. 2007

[85]   Khisti, A. & Wornell, G. The MIMOME channel. Proc. Allerton Conf. Comm., Contr., Comp., Monticello, IL, 1-8. 2007

[86]   Liu, T. & Shamai, S. A note on the secrecy capacity of the multiple-antenna wiretap channel. IEEE Trans. Inf. Theory, 55 (6), 2547-2553. 2009

[87]   Shafiee, S. & Ulukus, S. Towards the secrecy capacity of the Gaussian MIMO wire-tap channel: the 2-2-1 channel. IEEE Trans. Inf. Theory, 55 (9), 4033-4039. 2009

[88] Li, J. On ergodic secrecy rate for Gaussian MISO wiretap channels. IEEE Trans. Wireless Comm., 10 (4), 1176-1187. 2011

[89] Oggier, F. & Hassibi, B. The secrecy capacity of the MIMO wiretap channel. IEEE Trans. Inf. Theory, 57 (8), 4961-4972. 2011

[90] Agrawal, D., Tarokh, V., Naguib, A. & et al. Space-time coded OFDM for high data-rate wireless communication over wideband channels. 48th IEEE Veh. Tech. Conf., Ottawa, Canada, 2232-2236. 1998

[91] Mudulodu, S. & Paulraj, A. A transmit diversity scheme for frequency selective fading channels. IEEE Global Telecomm. Conf., San Francisco, CA, 1089-1093. 2000

[92] Lu, B. & Wang, X. Space-time code design in OFDM systems. IEEE Global Telecomm. Conf., San Francisco, CA, 1000–1004. 2000

[93] Li, Z. & Xia, X. An Alamouti coded OFDM transmission for cooperative systems robust to both timing errors and frequency offsets. IEEE Trans. Wireless Comm., 7 (5), 1839-1844. 2008

[94] Kim, J., Heath, R. & Powers, E. Receiver designs for Alamouti coded OFDM systems in fast fading channels. IEEE Trans. Wireless Comm., 4 (2), 550-559. 2005

[95] Ha, J., Mody, A., Sung, J. & et al. LDPC coded OFDM with Alamouti/SVD diversity technique. Wireless Personal Comm., 23 (1), 183-194. 2002

[96] Eldemerdash, Y., Dobre, O. & Liao, B. Blind identification of SM and Alamouti STBC-OFDM signals. IEEE Trans. Wireless Comm., 14 (2), 972-982. 2015

[97] Marey, M., Samir, M. & Ahmed, M. Joint estimation of transmitter and receiver IQ imbalance with ML detection for Alamouti OFDM systems. IEEE Trans. Veh. Tech., 62 (6), 2847-2853. 2013

[98] Shu, F., Wu, X., Hu, J. & et al. Secure and precise wireless transmission for random-subcarrier-selection-based directional modulation transmit antenna array. IEEE J. Sel. Areas Comm., 36 (4), 890-904. 2018

[99] Shen, T., Zhang, S., Chen, R. & et al. Two practical random-subcarrier-selection methods for secure precise wireless transmisions. IEEE Trans. Veh. Tech., 68 (9), 9018-9028. 2019

[100] Wu, C., Lan, P., Yeh, P. & et al. Practical physical layer security schemes for MIMO-OFDM systems using precoding matrix indices. IEEE J. Sel. Areas Comm., 31 (9), 1687-1700. 2013

[101] Romero-Zurita, N., Ghogho, M. & McLernon, D. Physical layer security of MIMO–OFDM systems by beamforming and artificial noise generation. Physical Comm., 4 (4), 313-321. 2011

[102] Akitaya, T., Asano S. & Saba, T. Time-domain artificial noise generation technique using time-domain and frequency-domain processing for physical layer security in MIMO-OFDM systems. IEEE Int. Conf. Comm. Workshop, Sydney, NSW, 807-812. 2014

[103] Kim, Y. & Kaveh, M. Coordinate-interleaved space-time coding with rotated constellation. 57th IEEE Semiannual Veh. Tech. Conf., Jeju, South Korea, 732-735. 2003

[104] Jung, T. & Cheun, K. Design of concatenated space-time block codes using signal space diversity and the Alamouti scheme. IEEE Int. Symp. Inf. Theory, Yokohama, Japan, 124. 2003

[105] Jeony, S., Lee, J., Kyung, I. & et al. Component-interleaved Alamouti coding with rotated constellations for signal space diversity. IEEE Int. Symp. Broadband Multimedia Systems & Broadcasting, Shanghai, China, 1-6. 2010

[106] Han, C., Hashimoto, T. & Suehiro, N. Constellation-rotated vector OFDM and its performance analysis over Rayleigh fading channels. IEEE Trans. Comm., 58 (3), 828-838. 2010

[107] Liu, Z., Xin, Y. & Giannakis, G. Linear constellation precoding for OFDM with maximum multipath diversity and coding gains. IEEE Trans. Comm., 51 (3), 416-427. 2003

[108] Zhu, X. & Xue, J. On the correlation of subcarriers in grouped linear constellation precoding OFDM systems over frequency selective fading. Proc. IEEE Veh. Tech. Conf., Melbourne, Australia, 1431-1435. 2006

[109] Özyurt, S. & Kucur, O. Performance of OFDM with signal space diversity using subcarrier coordinate interleaving. IEEE Trans. Veh. Tech., 67 (10), 10134-10138. 2018

[110]   Li, H., Wang, X. & Zou, Y. Dynamic subcarrier coordinate interleaving for eavesdropping prevention in OFDM systems. IEEE Comm. Lett., 18 (6), 1059-1062. 2014

[111]   Li, H., Wang, X. & Tang, H. Compensation of imperfect channel reciprocity through MMSE prediction for physical-layer confidentiality enhancement. Proc. Int. Conf. Military Comm. Inf. Sys., Brussels, Belgium, 1-6. 2016

[112]   Yusuf, M. & Arslan, H. On signal space diversity: an adaptive interleaver for enhancing physical layer security in frequency selective fading channels. Physical Comm., 24, 154-160. 2017

[113]   Yoo, T. & Goldsmith, A. Capacity of fading MIMO channels with channel estimation error. Proc. IEEE Int. Conf. Comm., Paris, France, 808-813. 2004

[114]   H. V., Poor & S., Verdu. Probability of error in MMSE multiuser detection. IEEE Trans. Inf. Theory, 43 (3), 858-871. 1997

[115]   A., Zanella, M., Chiani & M. Z., Win. MMSE reception and successive interference cancellation for MIMO systems with high spectral efficiency. IEEE Trans. Wireless Comm., 4 (3), 1244-1253. 2005

[116]   S., Özyurt, M., Öztürk & E., Çavuş. A low complexity MIMO MMSE receiver with performance enhancement via coordinate interleaving. Submitted

[117]   S., Özyurt. Performance of MIMO MMSE receiver with signal space diversity under channel estimation errors. 27th Signal Processing Comm. Applications Conf., Sivas, Turkey, 1-4. 2019
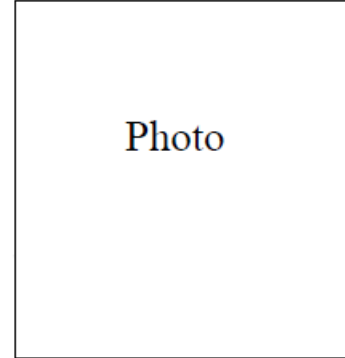
CURRICULUM VITAE

PERSONAL INFORMATION

Name Surname : Mustafa Anıl REŞAT

Place of Birth : Altındağ - Ankara

Date of Birth : 01.09.1988

Phone : +905374555118

E-mail : maresat@ybu.edu.tr

EDUCATION

High School : TED Ankara College Foundation Private High School (Sep. 2002 - Jun. 2005)

Bachelor : TOBB University of Economics and Technology - Electrical and Electronics Engineering Department (Sep. 2005 - Jan. 2010)

M.Sc. Degree : Gazi University - Electrical and Electronics Engineering Department (Sep. 2010 - Jun. 2013)

Ph.D. Degree : Ankara Yıldırım Beyazıt University - Electronics and Communication Engineering Department (Feb. 2014 - Feb. 2020)

WORK EXPERIENCE

Intern :

- Aremsan Generator Company (Jul. 2007 - Aug. 2007)

- Nuriş Electrical & Welding Machines Manufacturing and Trading Company (Jul. 2008 - Aug. 2008)

- Arçelik Company Dishwasher Plant (Jul. 2009 - Aug.2009)

Research Assist. : Ankara Yıldırım Beyazıt University - Electrical and Electronics Engineering Department (Feb. 2014 - Present)

TOPICS OF INTEREST

- Wireless communications

 - Multiple-input multiple-output

- Orthogonal frequency division multiplexing

- Physical layer security

- Signal processing for telecommunication systems

PUBLICATIONS

International Journal Papers

[1]   Genç, F. & Reşat, M. A., Savaşçıhabeş, A. & Ertuğ, Ö. On the comparative performance analysis of turbo-coded non-ideal single-carrier and multi-carrier waveforms over wideband Vogler-Hoffmeyer HF channels. Radioeng. J., 23 (3). 2014

[2]   Reşat, M. A. & Ertuğ, Ö. On the performance analysis of SC-FDMA uplink communication systems using multiple-CFO synchronization with null-subcarriers. Semantic Scholar Comp. Sci. 2013

International Conference Papers

[3]   Reşat, M. A., & Ertuğ, Ö. On the comparative performance analysis of GFDMA and SC-FDMA systems under multiple CFO synchronization using null sub-carriers. 22nd Int. Conf. Software, Telecomm. Comp. Networks, Split, 241-246. 2014

[4]   Reşat, M. A. & Ertuğ, Ö. Comparison of the performance analyses of SC-FDMA and GFDMA systems under null sub-carriers based multiple carrier frequency offset synchronization. 22nd Signal Processing Comm. App. Conf., Trabzon, Turkey, 1355-1358. 2014

[5]   Reşat, M. A., Gökçimen, H. İ. & Arıöz, U. A comparative analysis on cepstrum, linear predictive coding and particle filtering based formant estimation methods. 22nd Signal Processing and Comm. App. Conf., Trabzon, Turkey, 365-368. 2014

National Conference Papers

[6]   Reşat, M. A. & Ertuğ, Ö. SC-FDMA ve GFDMA sistemlerinin sıfır alt-taşıyıcılar tabanlı çoklu taşıyıcı frekansı ötelenmesi senkronizasyonu altında performans analizlerinin karşılaştırılması. Union Radio-Scientifique Internationale - Turkey VII. Scientific Congr., Elazığ, Turkey. 2014

[7]   Reşat, M. A. & Ertuğ, Ö. Sıfır alt-taşıyıcılı çoklu-CFO senkronizasyonu kullanan SC-FDMA yukarı-hat iletişim sistemlerinin performans analizi. ASELSAN Comm. Inf. Tech. Workshop, Ankara, Turkey. 2013

Thesis

[8]   Reşat, M. A. Multi-antenna communication systems with signal space diversity. Ph.D. Thesis, Ankara Yıldırım Beyazıt Uni., Grad. School Natural Sci., Electronics Comm. Eng. Dep. 2020

[9]   Reşat, M. A. Performance analysis of uplink SC-FDMA systems with multiple-CFO synchronization using null subcarriers. M.Sc. Thesis, Gazi Uni., Grad. School Natural Applied Sci., Electrical Electronics Eng. Dep. 2013

PROJECTS

[1]   An Experimental Channel Coded MIMO-OFDM Communication System at 0.24 THz for NLOS Indoor Applications. Project Asst., TÜBİTAK 1001, Project No: 115E336. Aug. 2015 - Present

[2]   Physical Layer Algorithms for Military Frequency-Hopping HF-Band Radio Links. Project Asst., Subcontract R&D Project, ASELSAN Inc. - Comm. Inf. Tech. Division, Code: HBT-IA-2011-025. Jul. 2011 - Jul. 2012

[3]   Compact Multimode Microstrip Antenna Arrays and Associated Signal Processing for MIMO Communications. Project Asst., ESF-COST Action-IC0803-RFCSET: RF Microwave Comm. Subsystems Emerging Wireless Tech., Code: TÜBİTAK-EEEAG-#108E025. Jul. 2008 - Jul. 2011

PUBLICATIONS INCLUDED AS PART OF THE THESIS

International Journal Papers

[1]   Reşat, M. A., Çiçek, A., Özyurt, S. & Çavuş, E. Analysis and FPGA implementation of zero-forcing receive beamforming with signal space diversity under different interleaving techniques. J. Circuits, Systems & Computers, 29 (1). 2020

[2]   Reşat, M. A., Karakoç, M. C. & Özyurt, S. Improving physical layer security in Alamouti OFDM systems with subcarrier coordinate interleaving. IET Communications. Submitted

International Conference Papers

[3]   Reşat, M. A. & Özyurt, S. Performance of MMSE beamforming with time and spatial coordinate interleaving. 11th Int. Conf. Electrical & Electronics Eng., Bursa, Turkey. 2019

[4]   Reşat, M. A. & Özyurt, S. Performance of zero-forcing MIMO systems with signal space diversity under transmit antenna correlation. 10th Int. Conf. Electrical & Electronics Eng., Bursa, Turkey, 700-704. 2017

National Conference Papers

[5]   Reşat, M. A., Karakoç, M. C. & Özyurt, S. Alamouti DFBÇ sistemlerinde fiziksel katman güvenliğinin Nakagami-m sönümlemeli kanallar üzerinde iyileştirilmesi. 28. IEEE Sinyal İşleme ve İletişim Uygulamaları Kurultayı. Submitted